BUILDING ENERGY MODELING FOR GREEN ARCHITECTURE AND INTELLIGENT DASHBOARD APPLICATIONS

by

Justin DeBlois

B.S. in Mechanical Engineering, University of Massachusetts, 2008

Submitted to the Graduate Faculty of

Swanson School of Engineering in partial fulfillment

of the requirements for the degree of

PhD in Mechanical Engineering

University of Pittsburgh

2013

UNIVERSITY OF PITTSBURGH

SWANSON SCHOOL OF ENGINEERING

This dissertation was presented

by

Justin DeBlois

It was defended on

November 11, 2013

and approved by

Melissa M. Bilec, Ph.D., Assistant Professor
Department of Civil and Environmental Engineering

Minking K. Chyu, Ph.D., Professor
Department of Mechanical Engineering and Materials Science

Akex K. Jones, Ph.D., Associate Professor
Department of Electrical and Computer Engineering

Mark Kimber, Ph.D., Assistant Professor
Department of Mechanical Engineering and Materials Science

Dissertation Director: Laura A. Schaefer, Ph.D., Professor
Department of Mechanical Engineering and Materials Science

BUILDING ENERGY MODELING FOR GREEN ARCHITECTURE AND INTELLIGENT DASHBOARD APPLICATIONS

Justin DeBlois, PhD

University of Pittsburgh, 2013

Buildings are responsible for 40% of the carbon emissions in the United States. Energy efficiency in this sector is key to reducing overall greenhouse gas emissions. This work studied the passive technique called the roof solar chimney for reducing the cooling load in homes architecturally. Three models of the chimney were created: a zonal building energy model, computational fluid dynamics model, and numerical analytic model. The study estimated the error introduced to the building energy model (BEM) through key assumptions, and then used a sensitivity analysis to examine the impact on the model outputs. The conclusion was that the error in the building energy model is small enough to use it for building simulation reliably. Further studies simulated the roof solar chimney in a whole building, integrated into one side of the roof. Comparisons were made between high and low efficiency constructions, and three ventilation strategies. The results showed that in four US climates, the roof solar chimney results in significant cooling load energy savings of up to 90%. After developing this new method for the small scale representation of a passive architecture technique in BEM, the study expanded the scope to address a fundamental issue in modeling - the implementation of the uncertainty from and improvement of occupant behavior. This is believed to be one of the weakest links in

both accurate modeling and proper, energy efficient building operation. A calibrated model of the Mascaro Center for Sustainable Innovation's LEED Gold, 3,400 m^2 building was created. Then algorithms were developed for integration to the building's dashboard application that show the occupant the energy savings for a variety of behaviors in real time. An approach using neural networks to act on real-time building automation system data was found to be the most accurate and efficient way to predict the current energy savings for each scenario. A stochastic study examined the impact of the representation of unpredictable occupancy patterns on model results. Combined, these studies inform modelers and researchers on frameworks for simulating holistically designed architecture and improving the interaction between models and building occupants, in residential and commercial settings.

TABLE OF CONTENTS

LIST OF TABLES

LIST OF FIGURES

1.0 INTRODUCTION

1.1 MOTIVATION

Residential and commercial buildings account for 22% and 18% of the total energy consumption in the United States, respectively [1]. Eighty percent of this energy comes from fossil fuels, so reducing consumption at the point of use is an immediate and effective way to reduce greenhouse gas emissions and mitigate climate change [2]. In buildings, these reductions can occur through efficiency improvements to the buildings themselves and behavioral changes by occupants.

This work studies novel building energy modeling (BEM) applications for both residential and commercial buildings in order to target the vast majority of the building sector. BEM methodology is expanded to allow for the examination of a new passive cooling technique for homes by creating a modeling technique for the roof solar chimney (RSC), evaluating its uncertainty, and studying its application in a house. Then, a framework is built for further expanding BEM to educate commercial building occupants on green, energy efficient behavior, and the use of simulations to show the energy-savings potential of this technology. Conversely, the effect of uncertainty in occupancy prediction on BEM model results is examined with stochastic simulations.

Figure 1 shows the relation between the three main research directions. There is a central focus on expanding the scope of uses for BEM for both residential and commercial buildings. The RSC simulation shares a push toward expanding the technical capabilities and validation of models with the stochastic occupancy studies. The RSC modeling and the development of savings estimation algorithms share an objective of using BEM to educate occupants. The two MCSI studies, the stochastic occupancy studies and the development of savings algorithms share a focus of studying the two-directional relationship between occupant behavior and building energy modeling.

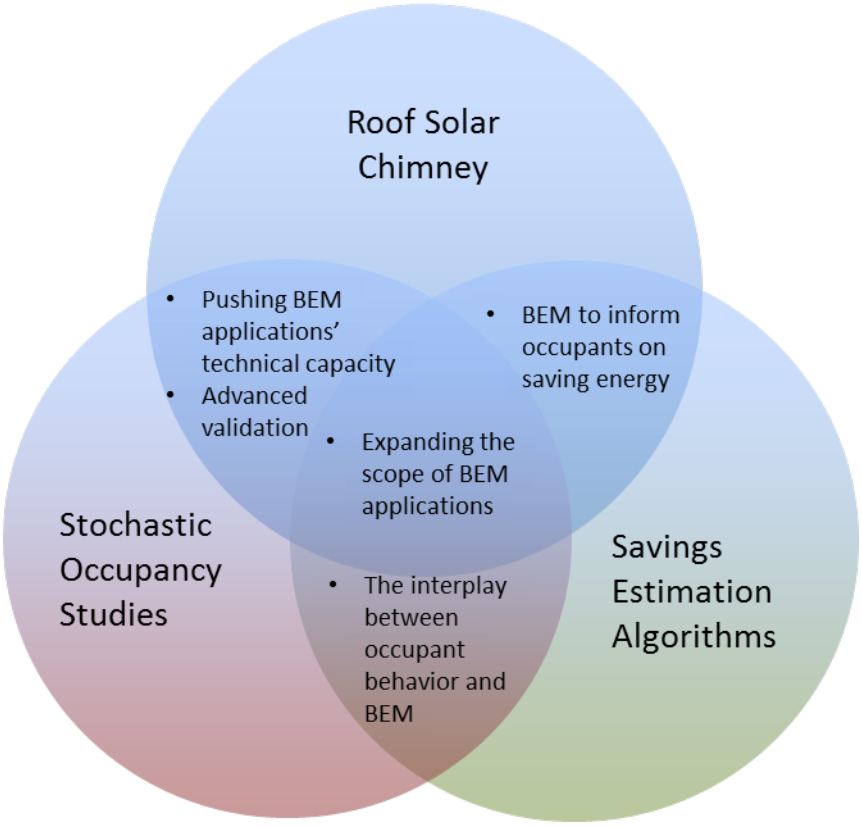

Figure 1: Venn diagram of the three primary BEM studies

1.1.1 Energy Consumption and Natural Ventilation

Despite the recent downturn in the housing market, the US Census Bureau reports the construction of 496,000 single family homes in 2010, and 198,000 in the first half of 2011 [3]. Of these, 89% were detached units. In the United States, the residential sector accounts for 22.1 quadrillion Btus of energy consumption per year, or 22.5% of the total. Heating and cooling of homes accounts for approximately one third of their primary energy use [4]. Improving efficiency in this sector significantly reduces consumption of non-renewable fuels and mitigates the associated climate and societal problems.

In detached homes in the United States, electricity is the largest energy source, and the US Energy Information Administration (EIA) found that in 2009, over 100 million homes used air conditioning. The prevalence of air conditioning ranges from 98% in the warmer South to 91% in the Midwest, 86% in the Northeast, and 65% in the West. The majority of houses use central air conditioning, and central air conditioning runs all summer in over one third of the homes in each region, and in 67% of homes in the South [5]. In 2005, the latest year for which data was available, homes used 25.6 quadrillion Btu ($7.5*10^6$ GWh), with 20% of their total electricity for air conditioning [4].

The energy consumption due to air conditioning systems can be reduced through the design or renovation of homes. This work seeks, through simulation, to explore the potential of a simple advanced natural ventilation method for cooling. The roof solar chimney is an air channel built into a roof surface, to collect heat and induce a buoyancy flow of air from the interior of the channel to the exterior of the house. When the surface is opaque, as in the case of this study, the concept can also be referred to as a ventilated roof. First, modeling methods for a roof solar chimney are explored, calibrated, and numerically validated. Next, control and comfort are

addressed, and the methods are compared to, and in conjunction with, contemporary high efficiency building techniques in four US climate zones.

1.1.2 Mascaro Center Occupant Behavior Studies

To further improve the energy performance of buildings and reduce waste, deterministic building modeling should both better account for occupant behaviors and aim to affect those behaviors related to energy use by informing building occupants about their choices and promoting thoughtful decision making.

Research and development efforts are increasing for stationary and mobile dashboard applications that inform building occupants of the current and historical energy consumption of their building. In order to show occupants how to make the most energy-conscious decisions at a given time, a prediction capability could be added to these applications. Depending on the time of day, state of the building, and weather, the optimal behaviors for occupants or the expected return for a given choice changes. This work explores a computational method, which is simple enough to be run on a mobile device, for creating real-time predictions for a number of optional occupant behavior and operational scenarios. To accomplish this, neural networks were trained using data from extensive runs of a calibrated building model.

The representation of occupancy and gains is the most prominent source of error in building models. Error in building energy modeling (BEM) can be seen as coming from four sources: the mathematical models of heat and mass transfer and their solutions, imperfections in the building and HVAC system definitions, weather variations, and user behavior and gains. While improvements have been made in reducing the first three error sources through more physically accurate modeling, little progress has been made in the fourth, occupancy [6]. Models

of existing buildings for predictive control, retro-commissioning or energy conservation measure evaluation are all subject to uncertainty due to the unpredictability of occupancy and the difficulty in obtaining reliable data. This work undertakes to study the uncertainty in building energy modeling and prediction for an existing building when there is a moderate degree of gains and occupancy data available. It uses the calibration case study of the Mascaro Center to examine the uncertainty created through the use of diversity schedules and explores the possibility of representing the occupancy and gains with stochastic methods. The Mascaro Center for Sustainable Innovation (MCSI) is a 3,400 m^2, LEED Gold, university building with open office, office, dry lab and wet lab spaces.

1.2 BUILDING ENERGY MODELING APPLICATIONS

Building energy modeling (BEM) is used as a tool to design and improve buildings. With simulation, heating ventilation and air conditioning (HVAC) designs and control strategies can be tested and improved. BEM is often used to predict the energy consumption of a building in the design stages, confirm that it meets energy code requirements, and to predict the energy or cost payback for retrofit energy conservation measures (ECMs). The BEM field is growing quickly in recent years, and physics-based, deterministic modeling of entire building systems has become widespread in the architectural and engineering fields. The models are increasingly accessible to non-technical building specialists such as architects, but the amount of time and expert knowledge currently required to effectively use them makes them unavailable to building occupants and residential building designers.

The literature on the simulation of building systems goes back several decades, with a rapid increase in interest and development in the 1980s, after the energy crisis of the previous decade and recent advancements in computer technology [7]. EnergyPlus is currently the primary DOE supported simulation program, and has been under development by national labs and research groups since 1996 [8]. ESP-r is widely used in research and consulting in Europe, developed in the Energy Systems Research Unit at the University of Strathclyde. For computational fluid dynamics simulations of ventilation and natural ventilation, ANSYS Fluent is commonly used.

1.2.1 ESP-r

ESP-r was used for the zonal modeling of the roof solar chimney. ESP-r is well validated and is used both in research and industry [9]. ESP-r solves a thermal network and an air-flow network simultaneously [10]. The heat transfer and zonal airflow network capabilities have been validated in different building types, but the zones are not typically used for small flow channels.

For heat transfer calculations, ESP-r uses a constant volume and finite difference approach. Each zone represents a constant volume of air at a single temperature. Each air volume is bordered by multiple surfaces. Conduction is modeled with a finite difference approach by placing multiple nodes through the thickness of each solid surface. A heat balance is then created for each node, balancing the radiation, convection and conduction heat transfer, and thermal mass [11]. The heat balance for a solid construction node is the following:

$$\rho c_p \frac{\partial T}{\partial t} = -\frac{\partial q''}{\partial x} + q''_{plant} \tag{1.1}$$

where ρ is the material density, c_p is the specific heat, T is the temperature, q" is the conduction heat flux in the x direction, perpendicular to the layer, and $q"_{plant}$ is the heat injected to the layer by a plant system. For an air node, the heat balance is the balance of the energy stored in the air of the zone and the convection into the zone, the advection from inter-zone air flow, the advection from infiltration (neglected in this case), and the plant heat source in the room:

$$\rho c_p V \frac{\partial T_a}{\partial t} = \sum_{S=1}^{N} h_{c,S} A_s \left(T_S - T_a\right) + \sum_{J=1}^{M} \dot{m}_{J \to a} c_p \left(T_J - T_a\right) + q_{conv,a} + q_{plant,a} \tag{1.2}$$

where V is the volume of the air in the zone, T_a is the temperature of the zone air, where a represents the current zone, $h_{c,S}$ is the surface convection coefficient for surface S from 1 to N, A_s is the area, and T_s is the temperature of that surface. The mass flow rate from airflow network node J to the current zone a, with J from 1 to M, is $\dot{m}_{J \to A}$. The convective heat transfer from gain sources in the room is $q_{conv,a}$, and $q_{plant,a}$ is the gain from plant components.

The airflow network is solved simultaneously with the heat transfer network. The nodes of the airflow network can be linked to the energy balance nodes of zones, integrating the heat and flow calculations. External boundary airflow nodes are created at different locations outside of external openings, at atmospheric pressure or at pressures influenced by the wind. Connections between nodes are created by the user to represent windows, doors and other openings. Each connection between two nodes, i and j, is represented by a power, quadratic or other law relating mass flow ($\dot{m}_{ij}$) and pressure drop between the nodes (ΔP_{ij}):

$$\dot{m}_{ij} = f\left(\Delta P_{ij}\right) \tag{1.3}$$

Buoyancy forces are calculated across each connection, using the node and connection heights defined by the user and the temperature difference between nodes. The flow network solver finds a pressure balance between the flow resistance and the pressure due to buoyancy,

wind, or plant components for all of the nodes in the network [10]. In general, the system of equations solved by the flow network solver simply represents a mass balance:

$$\sum_{J=1}^{n} f(\Delta P_{ij}) = 0 \tag{1.4}$$

For node i, the sum of mass flow rates in and out of the node to neighboring nodes j must be zero. A complete description of the fluid network includes pressure due to buoyancy forces and flows induced by plant components.

There are a number of other features of the program. A plant network can be defined, but only ideal plant components were used in this case in order to determine cooling load. Controls based on temperature, flow rate or other variables can be applied to plant and airflow components. Schedules can be used to define internal equipment, lighting and occupancy gains, as well as plant operation and flow components. Databases can be created for weather data and custom surface constructions or fenestration. Fictional surfaces, transparent with no thermal mass, can be used to divide a room into several zones in order to resolve temperature variations in the space. ESP-r is useful because it offers the functionality of commercial programs while maintaining a high level of user control in defining zones, boundary conditions, and airflow networks.

1.2.2 ANSYS Fluent

ANSYS Fluent was the computational fluid dynamics (CFD) package used to calibrate and verify the zonal model of the roof solar chimney. The basis for CFD is the numerical solution of a set of conservation equations for mass, momentum, and energy on a discretized grid. Equation 1.5 is mass conservation, or continuity:

$$\frac{\partial \rho}{\partial t} + \Delta \bullet (\rho \vec{v}) = S_m \tag{1.5}$$

where ρ is the density, $\vec{v}$ is the velocity, and S_m is a mass source term that equals zero for most single phase flows. Conservation of momentum can be expressed by Equation 1.6:

$$\frac{\partial}{\partial t}(\rho \vec{v}) + \Delta \bullet (\rho \vec{v} \vec{v}) = -\Delta p - \Delta \bullet (\bar{\bar{\tau}}) + \rho \vec{g} + \vec{F} \tag{1.6}$$

In this equation, p is the static pressure, $\bar{\bar{\tau}}$ is the stress tensor, $\vec{g}$ is the gravitational constant, and $\vec{F}$ is any external or user defined force. For flows that include heat transfer, the energy conservation equation is also included:

$$\frac{\partial}{\partial t}(\rho E) + \Delta \bullet (\vec{v}(\rho E + p)) = \Delta \bullet \left(k_{eff} \Delta T - \sum_j h_i \vec{J}_i + (\bar{\bar{\tau}}_{eff} \bullet \vec{v}) \right) + S_h \tag{1.7}$$

Conservation of energy involves k_{eff}, the effective conductivity of the fluid, the internal energy E, the enthalpy of species j, h_j, the diffusion flux of element j, $\vec{J_j}$, the effective stress tensor $\bar{\bar{\tau}}_{eff}$, and a volumetric energy source term, S_h. These conservation equations are discretized and solved simultaneously for each node on the grid. In addition to the CFD solver, ANSYS Fluent includes geometry creation and meshing modules.

1.2.3 Energy Plus

EnergyPlus was used for the Mascaro Center for Sustainable Innovation (MCSI) building energy model, and related studies. Like ESP-r, EnergyPlus's central simulation engine is a zone based heat balance. Zones are nodes representing geometric air spaces with a single air temperature. They are bounded by real and imaginary surfaces. Surfaces are simulated with a finite difference approach, with up to sixty nodes through the several construction layers of a wall.

The simulation engine also includes a building systems engine, which runs the simulation of the heating ventilation and air conditioning (HVAC) components. The simulation engine is designed to be integrated with native and custom made modules that add to the capabilities of the program. They provide detailed radiation calculations through windows, dynamic simulation of plant components, and airflow networks [12] for flow between zones or natural ventilation. Figure 2 shows the EnergyPlus structure.

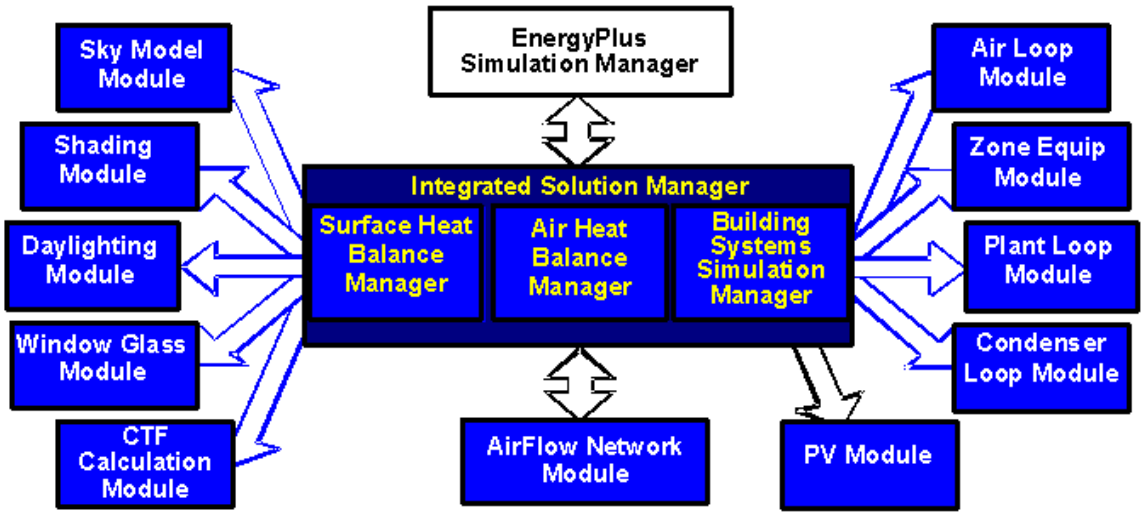

Figure 2: EnergyPlus program schematic [12]

EnergyPlus encourages developers to develop new modules for integration with the system. It is programmed in Fortran 90. It is free to commercial and non-commercial developers to use as a simulation engine for more user-friendly interfaces. EnergyPlus takes *.idf* text files as inputs, so a user interface helps visualize the geometry and plant diagrams, error check models, and perform repetitive tasks.

Each build of EnergyPlus has been tested and validated extensively. Analytical tests on the HVAC and building envelopes were conducted with the standards developed by the American Society of Heating, Refrigeration and Air Conditioning (ASHRAE) research projects 865 and 1052 [13]. Comparative tests have been done for ANSI/ASHRAE Standard 140-2011, among several others [14]. These tests mainly validate components of the EnergyPlus architecture in ideal conditions, but many studies have detailed the validation of real building models [15]. The DOE has traditionally developed documentation to aid in making user interfaces, but left graphical user interface programming to outside developers.

1.2.4 DesignBuilder and MLE+

DesignBuilder and MLE+ are both programs by outside developers to extend the capabilities of Energy Plus. DesignBuilder is a graphical user interface for EnergyPlus. DesignBuilder was used to create the initial iteration of the MCSI model, especially the detailed geometry model. It operates in a tree structure [16]. The structure is roughly: building, zone, surface, subsurface. HVAC systems are defined at the building level. Other settings such as gains, controls, occupancy, and construction materials are first defined at the highest level. These are the default, unless one is changed at a lower level. DesignBuilder can run the simulations with the embedded version of EnergyPlus or output an *.idf* file for more detailed editing by hand or with drop down menus in the EnergyPlus IdfEditor. The model was run in DesignBuilder for initial simulations, and was then exported for more detailed editing with IdfEditors and text editors.

MLE+, for Matlab Energy Plus, is a small program that sits between Energy Plus and Matlab [17]. It allows for the integration of the two programs on a time step level. It is especially useful for testing new controls structures using Simulink, but can be adapted for any purpose.

Input and output objects are created in the EnergyPlus .idf file. These can include schedules, control actuators and setpoints. A Matlab script reads the outputs from Energy Plus and computes new inputs for each time step. In this study, the program was used to simulate occupant behavior that is affected by the enhanced dashboard display.

1.3 THE ROOF SOLAR CHIMNEY

As energy modeling programs develop new capabilities for modeling ventilation and passive techniques, and the importance on energy efficiency becomes more recognized, passive heating and cooling concepts are increasingly being implemented in environmentally conscious new construction projects. Natural ventilation and free cooling are efficient ways to cool buildings and should be part of a well designed home's HVAC system, even when mechanical cooling is also required. As prescriptive energy code requirements have become stricter and homebuyers are increasingly concerned with their utility bills and carbon footprints, homes have become more efficient [18, 19]. Advanced window, insulation and sealing technologies are used to reduce the cooling load, while high efficiency centralized air systems improve occupant control and maintain precise ventilation levels. Advances have been made in active solar thermal technologies for satisfying both for heating and cooling demand [20, 21]. These trends, however, make it increasingly difficult to effectively use passive techniques to cool. With advancements in displacement ventilation efficiency and envelope improvements, the return on further incremental developments is decreasing. Passive techniques seem low tech and can be difficult to control and predict, but they have been shown to provide conditioning with no energy use and improve the occupants' perception of comfort.

One technique that shows promise and is the subject of numerous studies is the solar chimney [22]. For a residential application, a sloped rooftop solar chimney (RSC) is often the most practical configuration and has been the subject of previous studies [23]. The RSC induces natural ventilation by using the roof to collect solar radiation and transferring the heat to the air in a sloped channel, thereby inducing an upward flow of air. The RSC also provides a path for buoyancy-induced ventilation when the temperature in the occupied space is higher than ambient. Therefore RSCs can be used to enhance free night cooling, a passive technique that has been shown to reduce the energy consumption of buildings in the existing stock [24]. RSCs can be built into the space between rafters under a residential roof, so they are easily integrated into building practices and even existing buildings.

In addition to passive conditioning, the growing "green" and "net zero energy" construction sector uses advanced insulation and renewable energy to achieve high efficiencies. Low energy houses are often carefully sealed for low air infiltration and highly insulated to prevent conduction heat transfer [25-27]. This strategy incrementally reduces the heating and cooling load required to condition the house. To achieve a net zero energy status, photovoltaic panels on the roof or another source of renewable energy generally produce the balance of the electricity consumed [28]. A survey of architects and building professionals shows that they favor the integration of photovoltaic panels into building facades to ease design and improve aesthetics [29]. RSCs may be an efficient way to remove unwanted heat gain in roof integrated photovoltaic systems by providing a pathway for convective cooling behind the panels.

To better design a RSC, the operation and dynamics of a whole house should be considered holistically. Solar chimneys have been simulated, experimentally tested and optimized extensively [30-32]. However, no implementation of an RSC in commonly used

building modeling software was found in the literature. Building modeling provides a framework for evaluating the occupant comfort and the energy consumption of homes, and can yield application specific performance predictions to inform design choices. Developing new strategies for representing custom architecture and design techniques is key to promoting the use of passive and holistic design. To make the RSC concept more accessible to home designers and builders, this work develops a technique for modeling an RSC in zonal building modeling software and evaluates the sensitivity of the model to inputs and assumptions. This is the first step in a larger research thrust towards responsive modeling which identifies and resolves key user and occupants needs. Detailed modeling is expanded for implementation in a whole building, before further exploring the interplay between these models and the building user.

1.4 OCCUPANCY AND PARAMETRIC MODELING

Apart from the study of natural ventilation and passive cooling, one major shortcoming of BEM is the treatment of building occupancy, occupant behavior, and internal gains. This work includes a Monte-Carlo study of the impact of the representation of, and uncertainty in, occupancy and gains schedules on model results. It also uses parametric modeling to simulate several energy saving scenarios. Several parametric studies have been published recently that relate to this project. Costa et al. used a calibrated model to study different operation strategies for building operation. They ran the model for several temperature set points and supply air temperatures to compare energy use intensity (EUI) and thermal comfort [33]. De Wilde et al. used parametric analysis to estimate the changes in building performance over time due to deterioration of the construction materials and HVAC systems. They used a gamma process stochastic model to

represent the quality of components over time. The results included margins of error representing the uncertainty in predicting component deterioration [34].

Work by Hoes et al. explored the sensitivity of BEM results to the level of complexity of models for occupant behavior. These models included both occupant presence and interaction with the building such as daylighting and window operation. Hoes et al. suggested that parametric sensitivity analysis be used to determine which parameters require the most detail and complexity in the model [35]. They noted that building type is critical to the adoption of appropriate occupancy models. For example, a museum or auditorium experiences large variations in occupancy throughout the day but little user interaction, while an office building may have steady occupancy but users who actively control shading and natural ventilation.

Another parametric study by Wang et al. confirmed that the difference between real and modeled occupant behavior and building operation are the most important sources of uncertainty in a case study building. The parameter space included ten different annual weather files and several building operation parameters which were divided into good, average, and poor operation. A Monte Carlo analysis showed that the energy use distribution has a log-normal distribution and uncertainties from -20% to 42% at an 80% confidence level [36].

Combined, these studies indicate that modeling the real occupant presence and behavior is the limiting factor in BEM predictions. They take a static approach in the sense that they attempt to predict the long term performance of a building with limited preliminary knowledge. They then find the uncertainty due to the limitations of that knowledge by making assumptions for and estimations of the uncertainty in the inputs.

1.5 PREDICTIVE MODELING

In addition to representing occupant behavior accurately in building models, it is important to inform occupants, using modeling results, on the most energy efficient behaviors and interventions they can make in the building environment. In this study, the approach of predictive modeling was used as a first attempt to make real-time predictions of the effectiveness and energy savings of a number of occupant behaviors. Most of the predictive modeling literature is in the field of model predictive control. Model predictive control (MPC) is building control with an algorithm that optimizes control settings by minimizing a cost function such as the energy consumption combined with the occupant discomfort over the next few hours. To evaluate the cost function, the current state of the building must be known and a building model must be defined that can be run quickly for those initial conditions. Four main types of models have been used for short-term prediction and MPC: lumped capacitance and an analog circuit, a deterministic model such as EnergyPlus, machine learning, and responsive HVAC models.

The neural network approach was taken by Kwok et al. to estimate the cooling load of a building in real time. They used external weather and current occupancy level by area and total rate as inputs [37, 38]. This method seemed to effectively predict the very short term cooling load, but is not capable of making hypothetical predictions because it is based solely on patterns in measured data.

Ostendorp et al. used EnergyPlus as part of an optimization scheme that ran once per day to determine the best schedule for opening windows. The study assumed that the weather and gains for the upcoming day could be predicted. Then rule extraction with regression was conducted on the optimized results to develop three alternative algorithms that create window operation schedules for an office based on the current and previous states of certain components.

The results showed that the simplified algorithms for optimizing operations were up to 90% as effective as the optimal one [39].

Oldewurtel et al. developed and validated a comprehensive resistance-capacitance model of a single room for MPC and included a measure of uncertainty in their study. The MPC algorithms evaluated uncertainty due to weather prediction by using a stochastic weather prediction based on forecasts and their uncertainty compared to real weather data, while gains prediction was not mentioned [40]. Platt et al. modeled a single zone with a combination of a resistance capacitance model for heat transfer in the building, and energy and mass balance equations representing the HVAC system. They then used a genetic algorithm to predict the zone air temperature up to two hours in advance based on the zone model, external temperature and supply air [41]. Goyal et al. created a lumped parameter model for a multi-zone building, which has a high order and is computationally intensive. Then order reduction techniques were used to simplify the model for use in MPC [42]. These studies relied on highly specialized custom modeling to create models that could run in real time. In this case the advantages of using EnergyPlus or another commercial program are lost, and models developed as part of building design, commissioning or measure evaluation can't be used.

The literature review showed that to date, the only reliable, accurate method for real-time modeling of a building is co-simulation. This work found that an approach using neural networks could accurately assess the performance of several energy saving scenarios in real time, with much less computational intensity.

1.6 NEURAL NETWORKS IN BUILDING MODELING APPLICATIONS

Artificial neural networks were used to create real-time prediction algorithms for energy savings. This is an original use of neural networks; however, they have been used extensively in the building modeling literature for other purposes. They were primarily used for finding energy requirements, predicting air temperatures and thermal comfort, and analyzing or optimizing HVAC systems and controls [43]. Neural networks were used to predict real-time energy consumption and comfort, where those metrics were not directly measureable [44]. Similarly, another group trained them to compute the thermal comfort metric of predicted mean vote (PMV) for use in predictive modeling and the optimization of controls [45]. Neural networks were shown to successfully predict the real-time cooling load from a few weather variables and building states [38]. Another approach used them with environmental variables and an electricity meter as a proxy for occupancy to compute the cooling energy consumption [46]. One study set up a neural network-based system to analyze the applicability of day lighting to a proposed design, showing them to be more accurate than multi-variable regression [47]. Neural networks provide a low-computation, but often high-accuracy, approximation to complex models.

1.7 SUMMARY

The residential and commercial building sectors are primary consumers of energy and emitters of greenhouse gases, among other pollutants. There is a great opportunity to reduce pollution and the consumption of fossil fuels by improving efficiency in these sectors. This work expands the study of building modeling to new concepts, in ways that expand our knowledge both of BEM

and of efficient building design and operation. Chapter 2 is a study of the roof solar chimney, a passive cooling technique, for residential buildings. A new modeling technique was developed and validated, and the uncertainty due to several sources of error was explored. Further, the model was put into practice by modeling a whole building to explore controls, quantify annual performance, and compare to other energy efficient construction methods.

A primary source of uncertainty in the typical use of building modeling tools, not considered in the previous study, is the treatment of occupancy and occupant behavior. To explore these effects this research is extended beyond the residential sector and into the commercial sector, where occupant behavior might be expected to have an even larger impact, and a highly calibrated model was developed of the Mascaro Center, as discussed in Chapter 3. A set of Monte Carlo simulations explored the effect of natural variations in occupancy and gains on model outputs and model calibration.

In Chapter 4, methods for using the building model to influence occupant behavior are discussed. The calibrated model was used to develop algorithms that could be applied in a dashboard application to inform the user, a building occupant, on the real-time energy impact of a number of altered occupant behaviors. The first attempt at developing these algorithms took a nearest neighbor search approach, searching model results for time steps that were similar to the current state of the building. When that approach was found to lack accuracy, neural networks were used to fit model data to a number of building and weather state variables. This method was shown to be more accurate, and easily applicable in the context of a mobile application. A user interface was developed, and the operation of the system in the hands of an occupant was simulated by using co-simulation. Finally, Chapter 5 summarizes the key conclusions of the studies and proposes future work for both the residential and commercial modeling studies.

2.0 MODELING A ROOF SOLAR CHIMNEY

2.1 ZONAL CHIMNEY MODEL

Studies of solar chimneys and RSCs use a variety of computational fluid dynamics, numerical, experimental, and analytical approaches, but experimental quantification of the performance of solar chimneys is the most common approach [22]. Several recent studies of RSCs evaluate the performance of the chimney separately from the rest of the house and use a few representative sets of outside conditions [32, 48-51]. They provide encouraging results and give insight into the optimal spacing and slope of the air channels. Thicknesses of 0.1 to 0.2 m are most commonly suggested, and an inclination of 45 degrees is within 10% of optimal for middle latitudes [48]. Hirunlabh et al. attempt to account for variations in seasonal performance by comparing slopes, configurations and the choice of convection coefficient correlation over a characteristic day from each of three seasons [31]. Maerefat et al. study the use of RSCs to assist passive ground source cooling and evaporative cooling systems by simulating worst case sets of ambient conditions [52, 53].

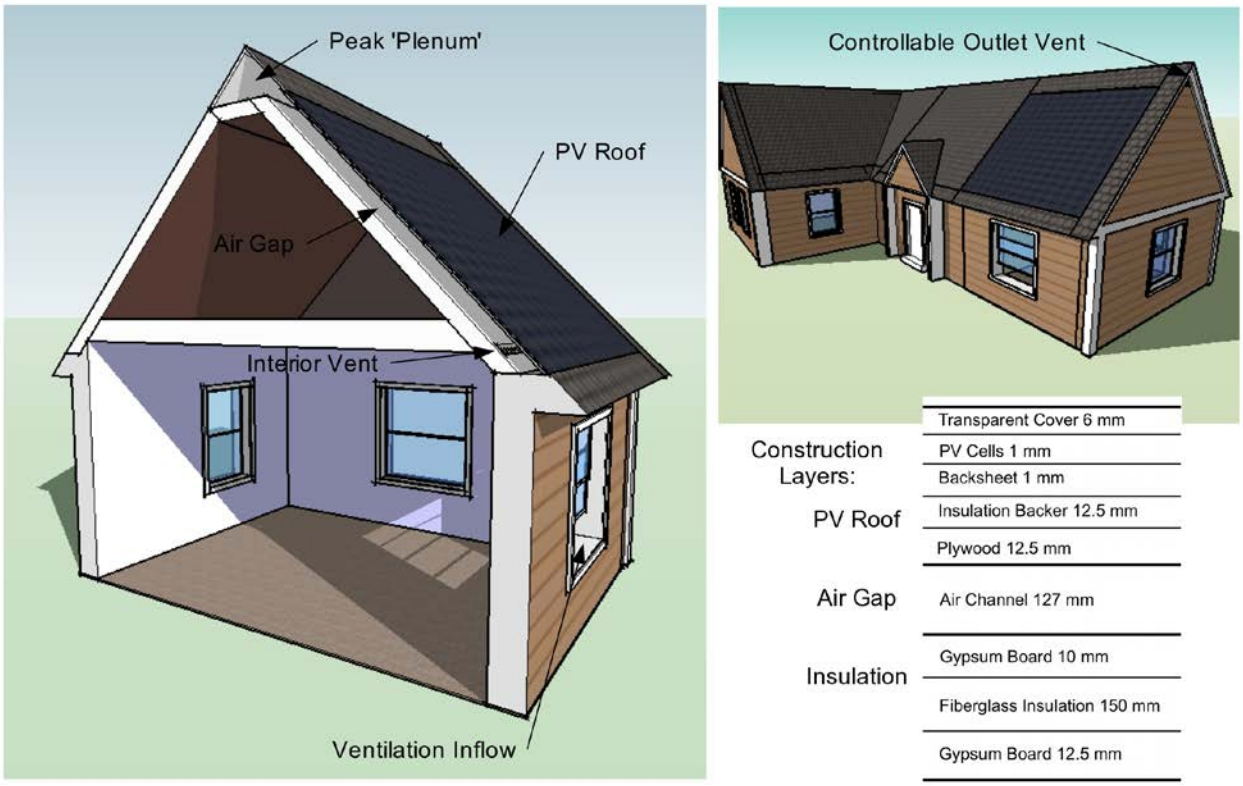

Figure 3: (left) Geometry of the roof solar chimney; (right) Materials and layer thicknesses

The RSC for this study is shown in Figure 3. The roof surface is a building integrated photovoltaic array applied to plywood. There is a 0.127 m air gap with insulating layers below. The vertical height of the channel is 2.6 m, and the slope is 45 degrees. Air flows in from a vent near the ceiling of a generic room in the house, and out into a plenum located in the peak of the house. The plenum is passively vented to the outside through a vertical external wall at one end. The design is easily controllable, using the vent in the peak of the house to prevent back-flow. Apart from the roof integrated PV panels, the house looks identical to one with a traditional roof. Using a plenum in the peak of the house allows a large area of the roof to be exposed to flow while protecting the RSC outlet from wind and the elements. The following assumptions were made for modeling:

- Heat conduction is one dimensional;
- For radiation view-factor calculations, the air gap is wide and long compared to the depth, and surfaces are diffuse grey;
- The dynamics of the airflow are fast compared to building temperature dynamics;
- The channel is smooth and rectangular;
- The density of the air is a function of temperature only, and the air does not participate in radiation heat transfer;
- All other material properties are independent of temperature;
- Leakage and infiltration are negligible;
- Energy conversion to electricity by the PV can be left out of heat transfer calculations at this stage in the study; and
- The effect of wind can be neglected and the panels face directly south.

The RSC model was implemented in a comprehensive building modeling software package so the assumptions related to wind, infiltration, energy conversion and panel azimuth can be changed easily, but they were not varied in this study.

The focus of this work was to explore the dynamics of the RSC in the Pittsburgh, PA, climate as it provides cooling in the summer weather. The RSC is an excellent case study of a small scale modeling issue which must be integrated with a larger model in order to fully understand the impacts on thermal comfort and energy consumption, from an occupant's perspective. The simulation pushes the boundaries of BEM software to become responsive to holistic ventilation design which cannot be packaged as a simulation module, and represent its impact on the building occupant as part of a larger building.

Three models were created. A mathematical model of the chimney was created for a sensitivity analysis. A model of the RSC and adjacent rooms was created in the building energy modeling program ESP-r, for broader scope dynamic simulation and in order to determine boundary conditions for the mathematical model. A CFD model of the air gap was created with ANSYS Fluent, and used to calibrate the flow loss coefficients and study the natural convection from the surfaces of the RSC. Figure 4 summarizes the flow of information between the models.

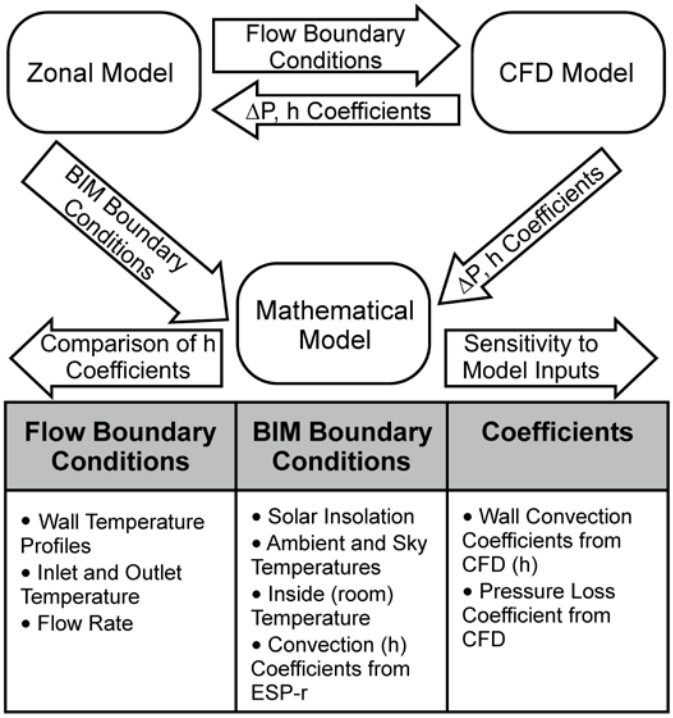

Figure 4: RSC Model information flow chart

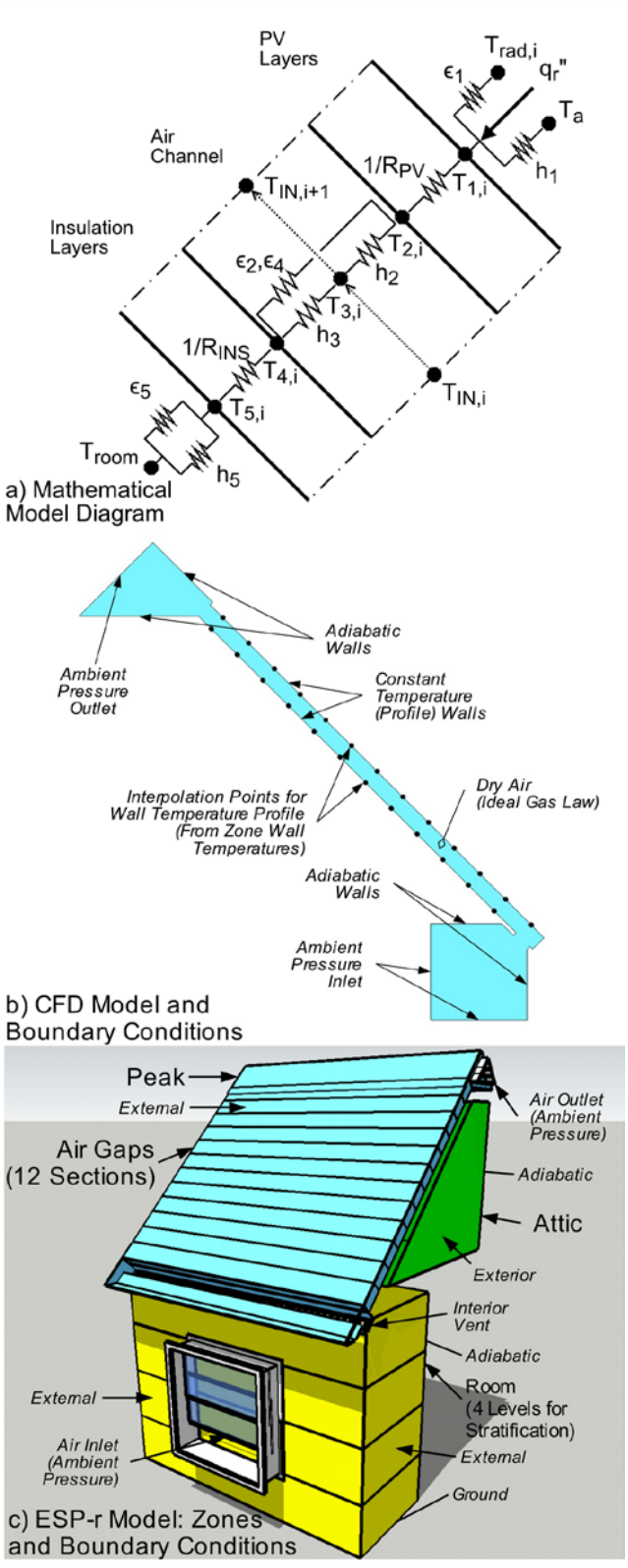

Figure 5: Boundary Conditions and diagrams for the mathematical, CFD and zonal models of the RSC

A week in the summer was simulated and the boundary conditions from sample time steps were divided into three localities for the sensitivity analysis: nighttime free cooling flow, daytime buoyant flow, and daytime convective flow. For each, several design parameters and ambient conditions were included in a sensitivity analysis on the ventilation flow rate. The effect of the variation in the convection coefficient on the results of the building simulation, such as the ventilation rate, heat conduction into the attic, and roof surface temperature was also examined in detail.

2.1.1 Mathematical Model

The mathematical model consisted of a heat balance for nodes at each surface and in each zone, and a pressure-based airflow balance. Figure 5a shows the node placement of a single segment of the thermal network. The heat balance included 13 such sections. The airflow network included buoyancy forces and losses in the channel, at the inlet and at the outlet, balanced over all of the nodes.

The design and boundary conditions of the mathematical model corresponded to the zonal model. The dimensions and discretization matched that of the zonal model, with 12 channel sections and an inlet section. The ambient temperature, effective radiant temperature, and solar insolation from the weather data were external boundary conditions for the mathematical model. These were constant temperature and constant heat flux conditions, respectively. The room temperature was the internal temperature boundary condition and the initial temperature for the airflow. The air pressure outside the chimney inlet and outlet were assumed to be ambient, because the mathematical model did not take into account the resistance to flow of the peak vent and the window. An examination of the results of the zonal model

showed that these pressure drops are relatively small parts of the flow resistance. Mathematical model inputs included material properties, the internal temperature, ambient conditions and the convective heat transfer coefficients.

For chimney section i from i = 0 to 12, the heat balance for the outer surface of the PV, node 1, was:

$$\varepsilon_1\sigma\left(T_{1,j}{}^4 - T_{r,i}{}^4\right) + h_{1,i}\left(T_{1,i} - T_a\right) + \frac{1}{R_{PV}}\left(T_{1,i} - T_{2,i}\right) = \varepsilon_1 q_r'' \tag{2.1}$$

where ε_1 is the PV panel emissivity, T_r is the outside equivalent radiant temperature, T_a is the ambient temperature, R_{PV} is the total thermal resistance of the roof surface layers, and q_r" is the solar radiation per unit area incident on the roof surface. The convective heat transfer coefficient for the external surface is h_1, from a correlation for natural convection on sloped surfaces used by the EnergyPlus building simulation program [12, 54]. The balance for node 2, the inner surface of the PV construction, was:

$$\frac{\sigma}{1/\varepsilon_2 + 1/\varepsilon_4 - 1}\left(T_{2,i}{}^4 - T_{4,i}{}^4\right) + h_{2,i}\left(T_{2,i} - T_{3,i}\right) + \frac{1}{R_{PV}}\left(T_{2,i} - T_{1,i}\right) = 0 \tag{2.2}$$

where ε_2 is the emissivity of the inside of the PV surface, ε_4 is the emissivity of the insulation outer surface, and h_2 is the convective heat transfer coefficient for the inside of the PV surface. The energy balance for the air space, node 3, was:

$$h_{2,i}\left(T_{3,i} - T_{2,i}\right) + h_{4,i}\left(T_{3,i} - T_{4,i}\right) = \frac{2}{L} c_p \dot{m}\left(T_{in,i} - T_{3,i}\right) \tag{2.3}$$

where h_4 is the convection coefficient from the insulation surface to the airflow, L is the length of the segment, c_p is the heat capacity of air, and m is the air mass flow rate. $T_{in,i}$ is the temperature of air entering the section i, and $T_{in,0}$ is the room air temperature T_{room}. For i from 0

to 11, $T_{in,i+1} = T_{in,i}+2*(T_{3,i}-T_{in,i})$ represented the linear increase in air temperature along each section. For node 4, the insulation surface, the energy balance was:

$$\frac{\sigma}{1/\varepsilon_2 + 1/\varepsilon_4 - 1}\left(T_{4,i}{}^4 - T_{2,i}\right) + h_{4,i}\left(T_{4,i} - T_{3,i}\right) + \frac{1}{R_{INS}}\left(T_{4,i} - T_{5,i}\right) = 0 \tag{2.4}$$

where R_{INS} is the combined thermal resistance of the insulation layers, and T_5 is the temperature of the inside surface of the insulation layers, facing the attic. The node 5 energy balance was:

$$\varepsilon_5\sigma\left(T_{5,i}{}^4 - T_{room}{}^4\right) + h_{5,i}\left(T_{5,i} - T_{room}\right) + \frac{1}{R_{INS}}\left(T_{5,i} - T_{4,i}\right) = 0 \tag{2.5}$$

where ε_5 is the emissivity of the inner insulation surface, and the attic is assumed to act as a black body at the internal room air temperature. The convection coefficient calculated for the attic's sloped ceiling is h_5.

The buoyancy pressure difference across the chimney was found by balancing the weight of a column of air inside the house against one outside:

$$\frac{\Delta P_b}{g} = -\rho_{T_{room}} H_{room} - \rho_{T_{plen}} H_{plen} - \sum_{i=0}^{12} \rho_{T_{3,i}} H_{segment} + \rho_{T_a} H_{house} \tag{2.6}$$

where ρ_T is the density of the air at temperature T. T_{plen} is the temperature of the air exiting segment 12 and entering the plenum. H_{room} is the vertical distance from the window to the chimney vent, $H_{segment}$ is the vertical height of each segment (0.2m), H_{plen} is the height from the exit of the chimney channel to the external plenum vent, and H_{house} is the total height from the window to the plenum vent. The pressure loss due to flow resistance, ΔP_r, was found by fitting a power law to the flow calibration data:

$$\Delta P_r = \left((1/.0857)\dot{m}\right)^{1/.5047} \tag{2.7}$$

The five heat balance equations were solved simultaneously for one section at a time, from i = 0 to 12. Then the buoyancy and resistance pressure differences were calculated, and the mass flow rate was adjusted:

$$\dot{m}^{(j+1)} = (1-.3)\dot{m}^{(j)} + .3 * .0857\left(\frac{\Delta P_b{}^{(j)} + \Delta P_r{}^{(j)}}{2}\right)^{.5047} \tag{2.8}$$

The thermal network was solved again for the new mass flow rate, and the process repeated until the buoyancy and resistance pressures converged.

2.1.2 Computational Fluid Dynamics Calibration

The CFD model was a two dimensional representation of the RSC air gap with small expanded domains at the entrance and exit, created in ANSYS Fluent (Figure 5b). The domain was smaller than the mathematical and zonal models because it only included the air gap and the inner surfaces of the channel walls, leaving out the construction layers and the larger peak and room zones. The boundary conditions matched those of the mathematical and zonal model as closely as possible.

This model was a higher order representation of airflow in the thirteen gap zones where the computation of convective heat transfer was important. The surfaces that corresponded to the walls of the peak and room zones were treated as adiabatic walls and the mass flow rate at the inlet was taken from the larger zonal model. Temperature boundary conditions for the walls of the chimney were profiles with inverse distance interpolation between thirteen points corresponding to the thirteen surfaces in the zonal model. The CFD model was two dimensional, because the air channel was symmetric with an aspect ratio of over 30.

The CFD model was a more physically accurate model of heat transfer and fluid flow than the heat transfer correlation and pressure-based network used in ESP-r. To further reduce error, care was taken in the choice of boundary conditions and a number of simulation configurations were run for comparison (Table 1).

The model used a steady state assumption and temporally constant temperature boundary conditions for the walls because the time constant of the airflow was about 30 seconds while the temperatures of the building components changed over hours. Meanwhile, the time-step of the zonal model being verified was at least 30 seconds, so a steady state CFD model was sufficient to represent a given time step. A constant heat flux boundary condition for the surfaces, although easier to experimentally verify, was believed to be less appropriate for this application because the heat fluxes through the surfaces can change more quickly than the temperatures of the surfaces - for example when the air temperature in the gap changes or a cloud blocks the solar insolation.

The inlet and outlet were at atmospheric pressure because the results of the zonal model showed that the pressure difference between the room and attic was minimal and the flow was mainly buoyant or convective. The inlet temperature and outlet backflow air temperatures were defined using the data from the zonal model, which included a larger domain and reflected the thermal state of the entire house section.

Table 1: CFD results for alternative choices of material and turbulence models

Configuration Change	Wall Heat Flux (W)	Percent Difference
None	128.8	n/a
Boussinesq approximation	129.9	0.77%
k-ε standard turbulence model	125.7	-2.37%
k-ε realizable turbulence model	125.1	2.76%
k-ω turbulence model	130.5	0.77%
k-ω SST turbulence model	128.2	-0.39%
Transition k-kl-ω turbulence model	132.5	1.57%
Without "full buoyancy effects"	128.8	0.00%
Without "full thermal effects"	128.8	0.00%

The pressure-based solver was used in Fluent, with the RNG k-ε turbulence treatment and enhanced wall treatment. The RNG method accounts for small-scale effects in a larger flow field, such as natural convection near the wall of a channel. The model took turbulence into account by using two further conservation equations for the turbulent kinetic energy, k, and the turbulent dissipation, ε. Table 1 shows that when compared with other methods of turbulence calculation, the results differed by up to 2.8%. The RNG method was believed to be the best choice because it accounts for small scale effects better than the standard k-ε model, but the flow did not involve high shear or separation, which realizable k-ε excels at. The results matched the k-ω and k-ω SST turbulence models closely. Within the RNG model, the full thermal effects and full buoyancy effects options were activated due to the nature of the flow, but these had a negligible quantitative impact on the results. The turbulence constants used in the RNG k-ε method are

derived directly from the RNG procedure, so are not a source of error [55]. One constant, universally applicable in RNG calculations, has been determined experimentally. A more complete discussion of Fluent's treatment of turbulence in natural ventilation simulation, including mathematical representations, can be found in Cable et al. [56].

Wall functions are important for the simulation of convective flow. Fluent's enhanced wall treatment improves the accuracy for heat transfer across an interface, as in natural convection, by blending laminar (linear) and turbulent (logarithmic) laws based on the cell location within the boundary layer. Therefore, a smooth transition exists in velocity in cells across the edge of the boundary layer. The heat transfer is less dependent on the grid, because the treatment is more versatile. On the other hand, the standard wall treatment works best with the either the first cell centroid well outside of the boundary layer, or an extremely fine mesh within the boundary layer [57]. Using the standard wall treatment with the current grid gave significantly different results due to the results becoming grid dependent. However, as Figure 6 shows, the results of the model with enhanced wall treatment were not dependent on the grid. It was found that with standard wall treatment, the results with standard treatment converged towards the enhanced results as the cell size decreased beyond the point of computational feasibility.

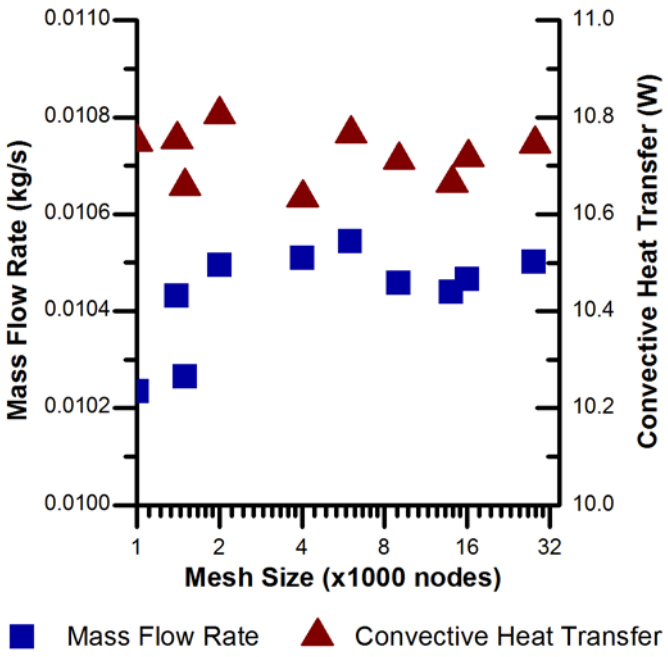

Figure 6: Convergence for the heat transfer and mass flow rates as the CFD mesh is refined

Air density was calculated with the ideal gas law at each solver iteration. The Boussinesq approximation is often used with this type of simulation for ease in convergence, but the ideal gas law is a more accurate way to calculate of density because it does not approximate a linear relationship between density and temperature, or neglect pressure. The difference in results between the methods was found to be less than 1%, however.

A mesh with approximately 14,000 nodes was used for the simulations. This mesh was highly inflated along the heat transfer surfaces with 10 nodes placed within the boundary layer, the maximum aspect ratio kept to approximately 20, and the transition ratio at the edge of inflation below 3:1. Mesh independence was confirmed for this configuration, as shown in Figure 6. The figure shows that as the level of refinement was increased beyond 14,000 nodes up to 77,000 nodes, the calculated heat transfer and air mass flow rate converge to steady values with a small amount of continued variance of less than 1%.

2.1.3 Zonal Model

The building energy modeling program ESP-r was used for the zonal modeling part of this study. A symmetric slice of a house including an RSC was modeled in order to simulate the building components directly affecting the chimney in addition to the chimney itself (Figure 5c). The model included the plenum zone, an attic zone below the chimney, and a portion of a room below the chimney divided into four levels to capture temperature stratification. The room had a 2x1 meter window.

The surface temperatures were expected to vary along the length of the air channel, as the temperature of the air flowing through the gap increased along the length. The gap was therefore discretized, creating a zonal model of the RSC. A zonal approach to modeling a vertical solar chimney has been numerically and experimentally validated in previous studies [58, 59]. The zones in the flow channel were separated by fictional surfaces with no thermal mass. These surfaces have no thermal mass but can change temperature, absorbing long-wave radiation as a blackbody and then re-emitting it to the adjacent zone based on the temperature reached by the surface. As heated surfaces, they can also convect heat to the air node. To avoid this problem, the radiation view-factors were modified so that the fictional surfaces do not receive heat from the insulation or PV surfaces, as in the case of infinite parallel plates. Convection from the fictional surfaces was confirmed to be negligible.

External surface boundary conditions were the external conditions of heat flux from solar insolation data, radiation loss to the sky and ground, and natural convection to the ambient air temperature. A standard ground temperature profile was used for a temperature boundary condition for conduction into the floor surface. The model only included one corner section of a larger house, so the North and West-facing surfaces are adiabatic. The air entered through a

window at about one meter in height, at ambient temperature and pressure, and exited through a vent in the peak (6m) to the ambient conditions. To evaluate the thermal comfort and get a more complete prediction of the performance of the design, the whole house would need to be modeled.

Three major sources of potential inaccuracy were identified for further study: heat convection, airflow resistance, and discretization. The discretization was tested for convergence, and attempts were made to calibrate the heat convection coefficient and airflow resistance with the ESP-r interface using results from the CFD model.

2.1.3.1 Discretization Convergence

A convergence study was carried out for the solar chimney, with an entrance segment (0.28m long) and from 1 to 18 channel segments (3.39 to 0.19m long). Twelve channel segments was determined to be an appropriate balance between accuracy and complexity, with an average difference of 2.9% between 12 and 18 segments over a simulation of several days. Figure 7 shows convergence for a sample time-step of natural convection dominated flow, as well as the average absolute error for each model compared to the maximum of 18 segments.

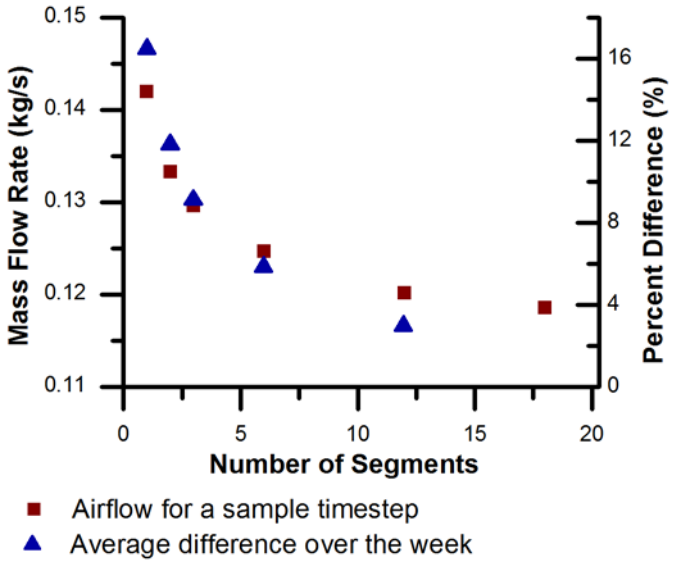

Figure 7: Convergence of the mass flow rate in the RSC as the number of segments is increased

2.1.3.2 Flow Resistance Calibration

The connection between each channel segment was a "general flow conduit," which is characterized by ESP-r with length, area, roughness, and dynamic loss coefficient. The connection from the room to the first segment was a "common orifice flow" component, which requires an opening area and discharge coefficient from the user. The lengths and areas were calculated from the geometry of the channel segment and opening vent, and the roughness was assumed to be zero. The dynamic loss coefficient and discharge factor were determined with the use of computational fluid dynamics. The flow resistance of the entrance to the channel can have a very significant effect on the induced mass flow rate [50].

The dynamic loss factor was first determined by simulating flow through the channel without opening effects; the pressure opening at each end was normal to flow and the same width as the channel. The dynamic loss coefficient was calibrated so that the mass flow in the ESP-r

model and CFD model matched over a range of pressure differences. Then the entire air channel, including the opening with its 90 degree 'turn,' was simulated in Fluent for a varying pressure drop. The opening discharge coefficient in the ESP-r model was calibrated from this data. Figure 8 shows the calibration results.

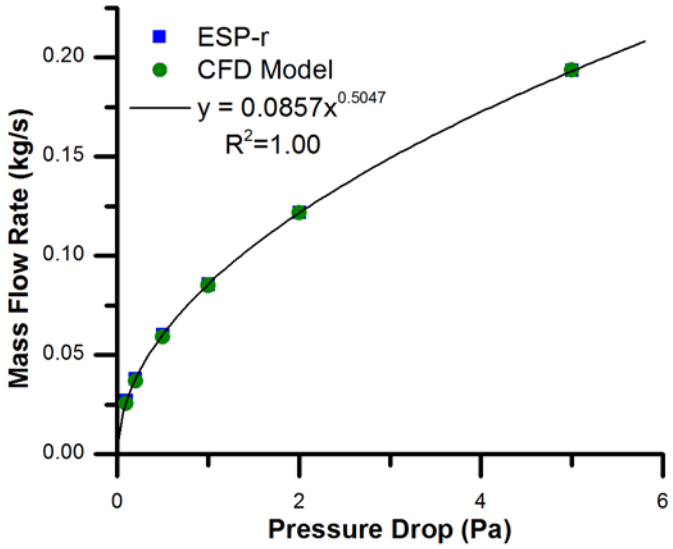

Figure 8: Calibration of the ESP-r loss coefficients for flow through the channel using CFD

2.1.3.3 Convection Coefficient Calibration

A primary shortcoming of building energy modeling software, especially relating to the prediction of passive heating and cooling techniques, is the treatment of convection coefficients. CFD can calculate convective heat transfer with accuracy, but no building simulation tool has fully integrated CFD into a fluid flow and heat transfer network [11]. ESP-r offers several options for the treatment of convection coefficients. The Bar-Cohen and Rohsenow correlation for natural convection was used because it is intended for predicting convection in flows between heated vertical parallel plates. This is a correlation for the dimensionless Nusselt number, which

represents the ratio of convective heat transfer to conductive heat transfer over a surface. The Nusselt number (Nu) is correlated with a function of the Rayleigh number (Ra), the dimensionless number representing the amount of convection heat transfer in a fluid. The correlation is as follows, with the channel depth (b), and the length (L) [60]:

$$\overline{Nu_b} = \left[\frac{567}{\left[Ra_b (b/L)\right]^2} + \frac{2.87}{\left[Ra_b (b/L)\right]^{1/2}} \right]^{-1/2} \tag{2.9}$$

The Nusselt number gives the convective heat transfer coefficient with the relationship Nu = hL/k, where h is the convective heat transfer coefficient, L is the characteristic length and k is the conductivity of the solid. The Rayleigh number is calculated using:

$$Ra = \frac{g\beta}{\nu\alpha}(T_s - T_\infty)x^3 \tag{2.10}$$

where g is gravitational acceleration, β is the thermal expansion coefficient of air, ν is the kinematic viscosity of air, α is the thermal diffusivity of air, T_s is the surface temperature, T_∞ is the zone air temperature, and x is the characteristic length of the surface.

When the Bar-Cohen and Rohsenow correlation is selected, the user can influence the magnitude of the convection coefficient through the user interface only indirectly with the settings for the width and height of the channel. In an attempt to adjust for the angle of the RSC, the input for height was calibrated using another CFD study. The calibration was for a time-step from a typical sunny summer day, and the height input was adjusted with an iterative process until both the rate of heat transfer and the surface temperature profiles in the ESP-r and Fluent models converged. The Bar-Cohen and Rohsenow correlation is for natural convection flow only, and therefore has poor accuracy when there is buoyant flow due to a high room air temperature, or at night. The associated uncertainty is examined further in Section 2.1.4.

2.1.4 Sensitivity Testing and Uncertainty

A simulation for August 5 through 12 in the Pittsburgh, PA, climate area is shown in Figure 9. This week was selected to be typical for the climate and one for which the RSC provides ventilation in a wide range of ambient conditions. The dynamic simulation shows that the flow rate is highest when the temperature in the room is much higher than the ambient temperature, and not necessarily when the solar insolation is highest. The RSC acts as a natural conduit for free cooling at night and in the day. During the hottest days, the mass flow rate falls, but the room temperature stays well below the ambient. A control mechanism will be needed to prevent backflow, possibly implemented with differential pressure sensors at the outlet vent. At night and in the morning there is more flow, exhausting the heat from the room and drawing cooler air through the window.

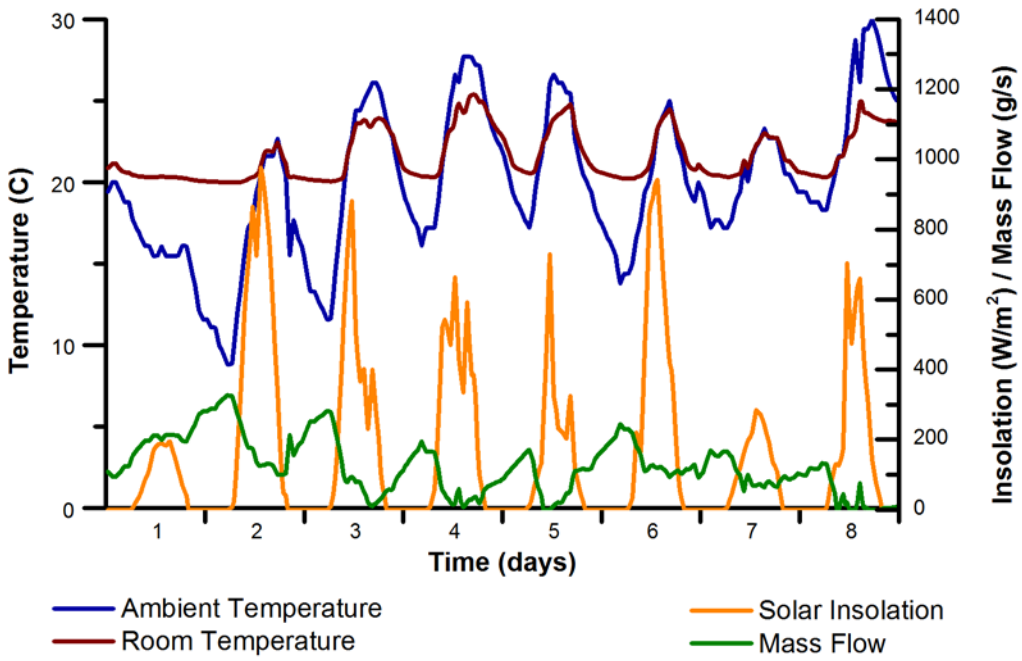

Figure 9: RSC simulation from August 5 through August 12 under Pittsburgh, PA, climatic conditions

Two sample days were chosen for analysis: the 6th and the 8th of August. There were forty-five hourly data points during which there was ventilation flow. A summary of the data is shown in Table 2. The points can be divided into three modes of operation of the RSC. The first is night cooling, which is driven by a temperature difference between the inlet and outlet of the chimney. In this mode, the temperatures of the chimney walls are often lower than the air temperature, so the flow is opposed to the natural convection flow direction. The second is natural convection flow, during time-steps when there is significant solar radiation and the internal to external temperature difference is zero or slightly negative. The third is daytime buoyant flow for mixed convective and buoyant flow, which often occurs in the morning or evening when the outside temperature falls, but solar radiation is still significant or the chimney surfaces retain heat.

The division of points between these modes is subjective, but it is based on the temperature difference between inlet and outlet and the amount of solar radiation. Points with positive flow and significant positive difference between inlet and outlet were considered buoyant, and divided between daytime buoyant and night free cooling based on the amount of solar radiation. The level of temperature difference in inlet to outlet for a distinction between the modes was determined based on a sensitivity analysis – the level at which convective coefficient becomes relatively unimportant to the flow.

Table 2: Data point statistics for the three flow modes

	Points	Avg. Insolation (W/m^2)	Avg. Outside T (C)	Avg. Inside T (C)	Avg. Mass Flow (kg/s)	Avg. Error in h	Error Standard Deviation
Night Free Cooling	18	0.7	14.8	20.4	0.0537	-34.4%	23.0%
Convection Flow	8	398.6	23.7	23.1	0.0187	1.7%	9.7%
Buoyant Daytime	19	353.6	15.8	20.2	0.0498	-24.9%	13.7%

For each data point, the surface temperatures for each segment, inlet temperature, mass flow rate and ambient boundary conditions were passed to the CFD model. The heat transfer coefficients from the CFD results were compared to the coefficients calculated by ESP-r to determine the average error, where error is calculated as if the numerical (CFD) result is the true coefficient.

The results show a high level of error in the heat transfer coefficient for the buoyant flow modes, to which the Bar-Cohen and Rohsenow correlation does not apply. In order to understand the impact of this uncertainty in the heat transfer coefficient on the results of a building simulation, the steady state mathematical model was run for each data point. First, it was solved for the heat transfer coefficient profiles and ambient conditions from the building model. Then it was run for the same conditions with the convection coefficients for each segment predicted by the CFD model. The resulting difference in outputs is shown in Figure 10.

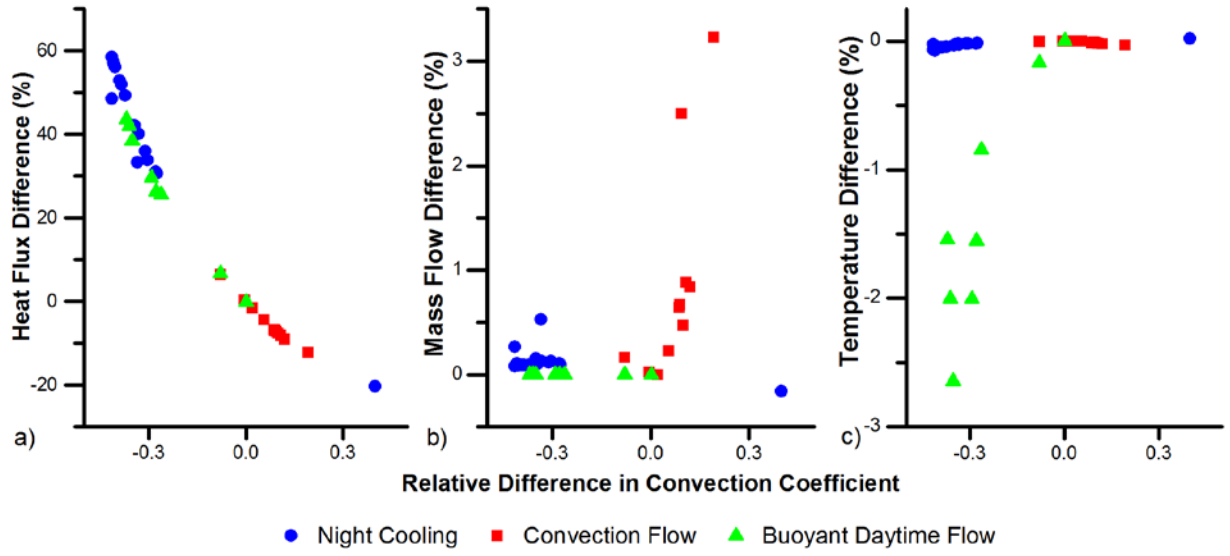

Figure 10: Uncertainty plots for (a) lateral heat flux through the insulation layer to the attic, (b) ventilation mass airflow rate, and (c) PV surface temperature

Figure 10a shows that the rate of heat flow through the insulation surface into the attic is highly dependent on the convection coefficient during the night cooling and buoyant daytime flow modes. In natural convection flow there is less sensitivity to uncertainty in the convection coefficient because the uncertainty in the coefficient is lower, while the airflow rate is generally smaller and radiation heat transfer is a larger portion of the heat transfer through the surface. The mass flow rate, in Figure 10b, has a maximum difference of 3.5% in the natural convection mode. The mass flow rate is much more dependent on the heat transfer coefficient in natural convection flows, but the uncertainty in the coefficient is smaller because the Bar-Cohen and Rohsenow correlation applies well to those conditions. The flow rate is not sensitive to uncertainty in the convection coefficient when there is a significant buoyancy induced flow from temperature difference, as in the nighttime and buoyant daytime modes. Figure 10c shows that for the night cooling and natural convection flow modes, the PV surface temperature is not

sensitive to the convective heat transfer coefficient. It is most sensitive to the convection coefficient in the buoyant daytime flow mode because there is a high airflow rate and a large difference between the channel air temperature and PV temperature, so the magnitude of convection heat transfer is higher. The difference in surface temperature is below 3% for all of the data points.

Local sensitivity analyses of the mass flow rate were done for each mode of RSC operation using the steady-state mathematical model, as shown in Figure 11. Each analysis used the average conditions of the flow mode as the center point, and standard deviations were determined from the respective data sets. The data points for the inlet to outlet temperature difference, radiant sky temperature, solar radiation, and convective heat transfer coefficient were adjusted over +/- 2 standard deviations. The flow loss coefficient and the thermal resistance of the PV surface were adjusted over a range of 20%.

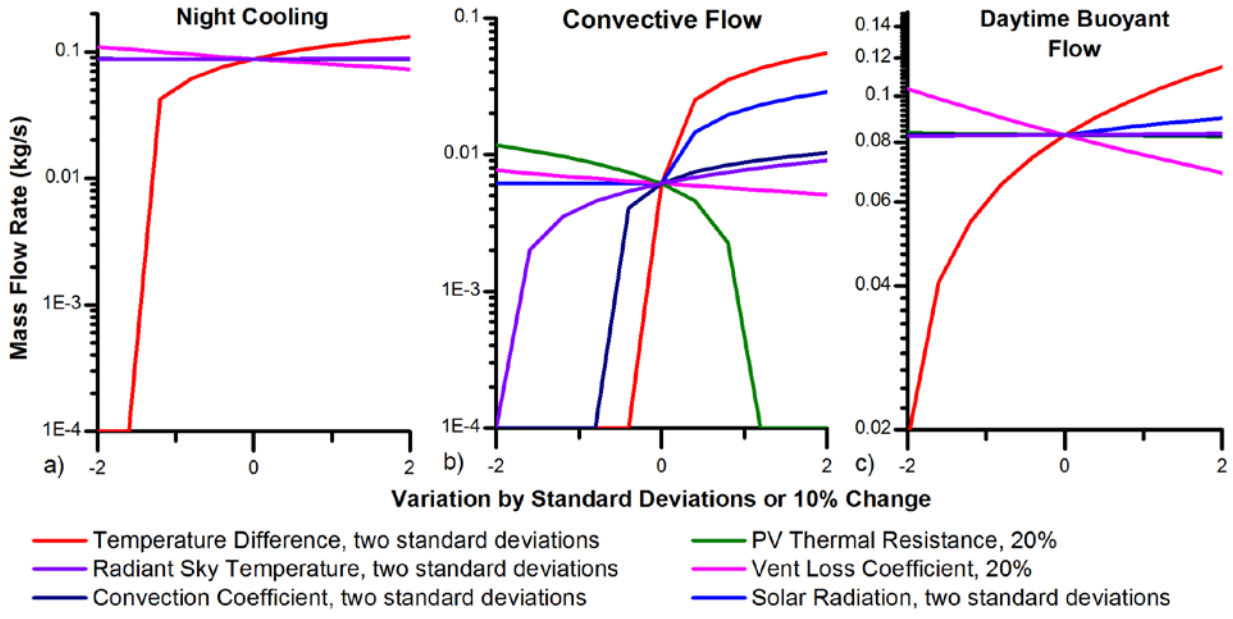

Figure 11: Local sensitivity analysis for (a) night cooling, (b) natural convection flow, (c) daytime (mixed) buoyant flow

The results (Figure 11) show that for all three modes, the flow rate is most sensitive to the interior versus ambient temperature difference. For night cooling operation the only other important variable is the loss coefficient through the RSC, while in mixed daytime flow the solar insolation is also a factor. The convective flow mode has a lower flow rate for a more delicately balanced set of conditions. For example, relatively small changes in the thermal resistance of the PV layers, effective radiant sky temperature, temperature difference, or convection coefficient can reduce the flow to zero. The solar radiation is also a significant input, and a decrease in the radiation turns the flow into one that is no longer convective, but driven by the slight difference in temperatures for the center point. The results at this locality are less sensitive to the vent loss coefficient, relative to the other parameters.

2.2 WHOLE HOUSE MODELING

Following the development of a reliable modeling technique for a RSC section, a home was designed utilizing the technique for whole building simulations. In the preliminary modeling, the RSC was found to act as a channel for stack ventilation more often than as a solar chimney, and this was considered in the geometry and controls design.

During periods of high solar insolation, the absorptive surface of a ventilated roof heats up and air flow is induced by natural convection. RSCs often use a transparent outer layer and absorptive inner layer, while the outer layer in consideration here is comprised of photovoltaic panels applied to plywood. Therefore, the roof is opaque and much of the cooling potential is found to come from buoyancy induced night ventilation, so the term ‘ventilated roof’ can be used. The roof for this study was designed with an external surface of building integrated

photovoltaic panels (BIPV). PV panels are highly absorptive, creating both the challenge of removing the heat that builds up during the day and an opportunity to use this heat to induce ventilation, making them ideal for a ventilated roof.

The configuration studied here draws air through inlets in the ceilings of the rooms below it. The outlets flow into a plenum in the peak of the house. The plenum is vented outside at each end of the house. This configuration is shown in more detail in Figure 3. For the ventilation to best cool the whole house, flow between rooms must be facilitated. This is achieved with vents in the interior walls, near the floor and ceiling. These vents allow air to circulate between rooms due to temperature stratification, as well as due to pressure differentials caused by wind. In the case of typical single sided ventilation, the actual air flow through windows is limited and difficult to predict even when there is significant wind. Simply allowing cross ventilation has been shown to greatly improve the effectiveness and predictability of natural ventilation [61, 62].

Natural ventilation and solar chimneys have been studied extensively with experimental, analytical, and numerical approaches [63-65]. However, no published work has simulated one in the context of a larger house, with the added complexity and design considerations that entails. Aboulnaga et al. used an analytical approach to simulate a RSC with a ventilation inlet subject to wind pressure [23]. The flow rate was predicted parametrically for different wind speeds, solar insolation values, and dimensions. Maerefat et al. modeled a small house using a roof solar chimney in conjunction with an earth to air heat exchanger and evaporative cooling to preheat ventilation air [52, 53]. The techniques were shown to be effective for sets of ambient conditions representative of each season. The ventilated roof was studied numerically and experimentally in a commercial building context by Susanti et al. [66]. With a simple resistive thermal model, this study showed that the use of an outer layer of sheet metal to create a double skin roof on a

factory building could either significantly reduce air conditioning energy use in a conditioned space or improve comfort in an unconditioned space throughout the summer. Biwole et al. examined the heat transfer in a double skin roof, running parametric variations while holding the inlet and outlet air temperature constant [32]. In general, the operation of this passive technique in the context of a larger building has not been considered. In experimental and numerical work, inlet and outlet temperatures typically remain fixed at a small difference, and solar insolation is only changed parametrically. The present study seeks to simulate the ventilated roof as part of the whole building to identify performance characteristics and potential savings.

2.2.1 Building Model

A generic, single story, three bedroom, detached home was simulated. The home was 184 m^2. The building was 'L' shaped and the 1-1 pitch roof had two sections, with the longer one running east to west (Figure 12). The widest uninterrupted portion of the roof was south facing with building integrated PV; this roof section was ventilated. The occupied space was divided into four zones for thermal modeling: (1) the family zone, including a kitchen and living area; (2) the dining zone, with a dining room and study; (3) the bed zone, including two bedrooms; and (4) the bath zone, with two bathrooms, closets, and a spare bedroom. The ventilated roof drew air from the dining and bed zones (see Figure 13).

Figure 12: Isometric View - Baseline and Prototype Home

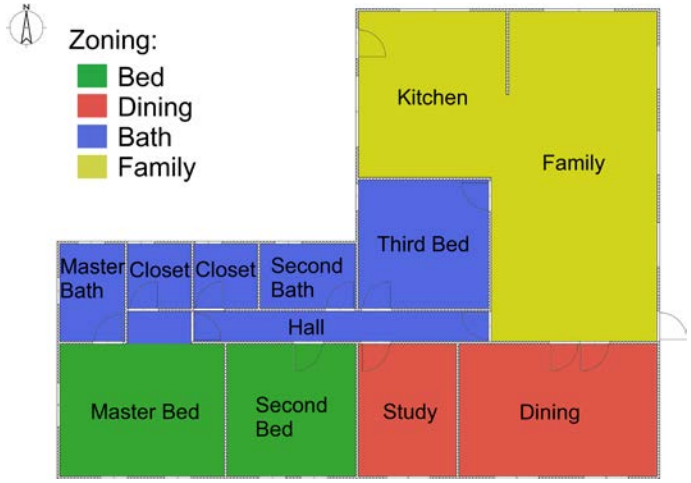

Figure 13: Room Layout and Zoning - Baseline and Prototype Home

The house was simulated for six cases (three ventilation configurations, operating at either regular or high efficiency levels) in each of four climates. Most of the parameters for the first of these, the Baseline case, were guided by the Building America House Simulation Protocols by the National Renewable Energy Laboratory (NREL), with exceptions in some parameters as described [67]. This report references IECC 2009 for constructions standards [68]. The gains and infiltration levels in the Baseline model matched those in the NREL Simulation Protocols as well, as described by Table 3. The standard specifies occupancy levels in hours per

week per person and total numbers of persons, and internal gains levels in total energy. Schedules were developed for each zone for each gain source according to behavioral assumptions for the zone type. For example, the Bed zone had higher lighting in the morning and evening and constant occupancy throughout the night, while the Dining zone had higher lighting and occupancy at meal times and during the weekend. Schedules were customized for this particular house, but the total gains match the standard. Fenestration was designed to provide adequate ventilation and views for the house layout, rather than according to the standard window-wall ratio.

Table 3: RSC model details and assumptions

	Bed	Dining	Bath	Family	Total
Floor area (m^2)	36	36	47	65	184
Occupancy gains (average sensible, latent kWh/day)[1,2,3]	1.29, 0.97	0.50, 0.38	0.62, 0.47	0.39, 0.29	2.81, 2.10
Lighting gains (average kWh/day)[1,3]	0.62	1.49	1.32	1.94	5.38
Equipment gains (average kWh/day)[1,3]	1.84	3.00	1.39	3.00	9.24
Fenestration area (m^2)	6.6	4.8	6	12.6	30
Infiltration area (m^2)[1]	0.0130	0.0130	0.0169	0.0234	0.0662

[1]According to DOE Building America House Simulation Protocols [67], High Efficiency cases have a 30% reduction in lighting gains, 15% reduction in equipment gains, and 50% reduction in infiltration area
[2]2.64 occupants, 16.5 hours/day/person
[3]Schedules (not shown) reflect custom home occupancy pattern

The Baseline model included only single sided ventilation, but airflow was calculated with an airflow network. The zones were connected by flow components representing the cracks below and above doors, but interzone flow was small. The network included infliltration flow to the exterior in addition to controlled window flow. Each zone was divided into three sections vertically to capture stratification in the air temperature. The windows opened to the middle section of each zone, and this section was also the one used for control of heating and cooling.

As mentioned previously, there was no plant model, because ideal control was employed to capture the cooling and heating load. The construction materials are described in Table 4. The most significant variation from the NREL Building Simulation Protocols and IECC 2009 standard was the use of high thermal mass exterior walls, accomplished by adding a thick layer of concrete block to the exterior constructions [67, 68].

The second case, the Cross Ventilated case, was designed to allow air flow between interior zones. This resulted in the wind driving flow through the house by taking advantage of the pressure differential between upwind and downwind exterior surfaces. In this airflow network there were open vents in the interior walls near the floor and ceiling, rather than simply small cracks around the doors. The third case, known as the Ventilated Roof case, included both cross ventilation and the operation of the chimney.

Often, when seeking energy savings, insulation, fenestration and efficiency are improved before considering more design-intensive, advanced passive techniques. To evaluate the effectiveness of this prioritization, all three of these cases were simulated as High Efficiency versions as well as using the base efficiency. High Efficiency cases employed triple pane low-e windows, improved exterior insulation, a 50% reduction in infiltration area, 30% reduction in lighting gains, and 15% reduction in equipment gains (Table 3 and Table 4).

Table 4: RSC constructions and insulation details

Component[1]	Layers: Base Case *(High Efficiency)*
Exterior walls	1. Weatherboard 12.5 mm 2. Glasswool 150 mm *(200 mm)* 3. Concrete block 152 mm 4. Air gap 50 mm 5. Gypsum board 12.5 mm 6. Plaster 3 mm U = 0.23 W/m^{2}K *(0.18 W/m^{2}K)*,
Interior walls	1. Gypsum 12.5 mm 2. Concrete block 125 mm 3. Gypsum 12.5 mm U = 2.28 W/m^{2}K
Windows	1,3: Double pane 5.7 mm 2: 8mm air gap *HE: (Triple pane low-e 5.7 mm, 12.7 mm air gaps)* U = 1.97 W/m^{2}K *(1.23 W/m^{2}K)*, SHGC = 0.64 *(.37)*
Floors	1. Gravel 2. Concrete 3. Air 120 mm 4. Chipboard 19 mm 5. Wilton 6mm U = 0.18 W/m^{2}K
Ceilings	1. Plaster 4mm 2. Gypsum board 12.5 mm 3. Glasswool insulation 299 mm U = 0.13 W/m^{2}K
Standard roof	1. Asphalt Shingles 12.5 mm 2. Plywood 19 mm U = 3.08 W/m^{2}K, Outer surface ε = 0.95,α = 0.95, ρ = 0.05
PV roof	1. Polymer cover 6mm 2. PV Cells 1 mm 3. PV Backsheet 1 mm 4. Insulation Backer 12.7 mm 5. Plywood 19 mm U = 1.394 W/m^{2}K Outer surface ε = 0.84, α = 0.84, ρ = 0.16 Inner surface ε = 0.9, α = 0.65, ρ = 0.35
Inner surface of flow channel	1. Gypsum 12.5mm 2. Polyurethane insulation 150mm 3. Gypsum 12.5 mm U = 0.189 W/m^{2}K Channel Surface ε = 0.9, α = 0.9, ρ = 0.1

2.2.2 Climate and Controls

Four climates were chosen for the simulation in order to discern patterns and differences in the performance of the six cases. The climates range from Pittsburgh, which is relatively cool and where many houses use window air conditioners, to Phoenix, with its hot, arid climate and more common 24/7 central air conditioning. The other two locations chosen were Albuquerque and Atlanta, two locations with cooling requirements in between those of Pittsburgh and Phoenix. Albuquerque, however, is a dry climate while Atlanta is a wet one. According to IECC climate zone nomenclature, Pittsburgh is 5A (moist), Albuquerque is 4B (dry), Atlanta is 3A (moist), and Phoenix is 2B (dry) [68]. Typical Meteorological Year 3 (TMY3) weather data from NREL was used for each location. For each location, TMY determines a typical week best representing the average conditions of that season. These weeks were used for a refined analysis of the performance characteristics of the ventilated roof base case. The seasonal typical week summary statistics are found in Table 5.

Table 5: RSC study climate summary data

Typical Weeks		Pittsburgh	Albuquerque	Atlanta	Phoenix
Spring	Dates	5/13 - 5/19	4/19 - 4/25	4/26 - 5/2	4/12 - 4/18
	DB Avg/High/Low (C)	15.7/32.7/0	13/24.4/3.3	16.5/25.6/2.8	22.6/33/13
	RH Avg %	67.6	35.3	71.0	24.3
	Insolation[1] kWh/day/m^2	5.62	9.14	6.99	10.26
Summer	Dates	7/22 - 7/28	8/10 - 8/16	8/24 - 8/30	8/24 - 8/30
	DB Avg/High/Low (C)	20.2/26/14	24.4/33.3/15.6	25.7/33.3/18.3	32.8/41/23
	RH Avg %	81.6	49.1	68.5	17.5
	Insolation[1] kWh/day/m^2	4.80	9.43	7.70	9.24
Fall	Dates	11/5 - 11/11	10/13 - 10/19	9/29 - 10/5	10/13 - 10/19
	DB Avg/High/Low (C)	7.2/19/-1	13.5/23.3/2.2	17.3/26.7/7.2	23.8/33/13
	RH Avg %	54.1	30.1	78.3	39.5
	Insolation[1] kWh/day/m^2	6.25	10.21	5.62	9.41
Winter	Dates	N/A	N/A	N/A	1/20 - 1/26
	DB Avg/High/Low (C)				12.7/24/4
	RH Avg %				45.8
	Insolation[1] kWh/day/m^2				8.30

[1]Insolation incident on solar roof

Recently much research attention has been given to adaptive thermal comfort. These works show that the temperature range that occupants find comfortable depends on the location, climate and outside weather. This is due to behavioral, physiological and cultural adaptations as well as the perception of acceptable discomfort. When occupants have a higher degree of control over temperature and ventilation, and in naturally ventilated spaces, the temperature range perceived as comfortable is wider. While there is no one temperature that all people will find comfortable, the ASHRAE standard 55-2010 characterizes the 80% acceptability upper and lower thermal comfort limits for naturally ventilated spaces in terms of the mean monthly outdoor air temperature, T_m (Equations 2.11 and 2.12, respectively). The monthly mean temperature is the average of the daily mean temperatures for the month, which are in turn the average of the daily high and low temperatures [69]. The heating setpoint, T_L, and cooling set-point, T_U, were defined by Equations 2.11 and 2.12:

$$T_U = 0.31 * (T_m) + 21.3 \quad (2.11)$$

$$T_L = 0.31 * (T_m) + 14.3 \quad (2.12)$$

All control set-points were implemented by month, because ASHRAE standards use monthly comfort temperatures. Heating and cooling controls were implemented as an ideal injection of heating or cooling energy into the air network point of each internal, first floor zone. This is an idealized model chosen to simply calculate the load required to maintain minimum comfort. The heating and cooling set-points are the 80% comfort limits described by ASHRAE. Windows were controlled (opened) according to three logic rules: the inside temperature was above a certain window operation set-point; the interior temperature was below the cooling set-point (mechanical cooling was not in operation); and the outside temperature was lower than the inside temperature. These rules and the specific window set-points were developed to: prevent overcooling from creating heating load at night; to prevent heat gain when mechanical cooling is in operation; and to prevent ventilation flow from bringing in warmer air, increasing the cooling load. As previously discussed, backflow through the ventilated roof was prevented by a pressure differential sensor across each vent from the peak plenum to the exterior. The only climate with a large heating load was Pittsburgh, and cooling does not operate during the heating season. Heating was outside the scope of this study, and is not included in the results. However, care was taken that the use of free cooling did not cause the interior temperature to fall below the heating set-point. The heating, cooling and window operation set-points are shown in Figure 14.

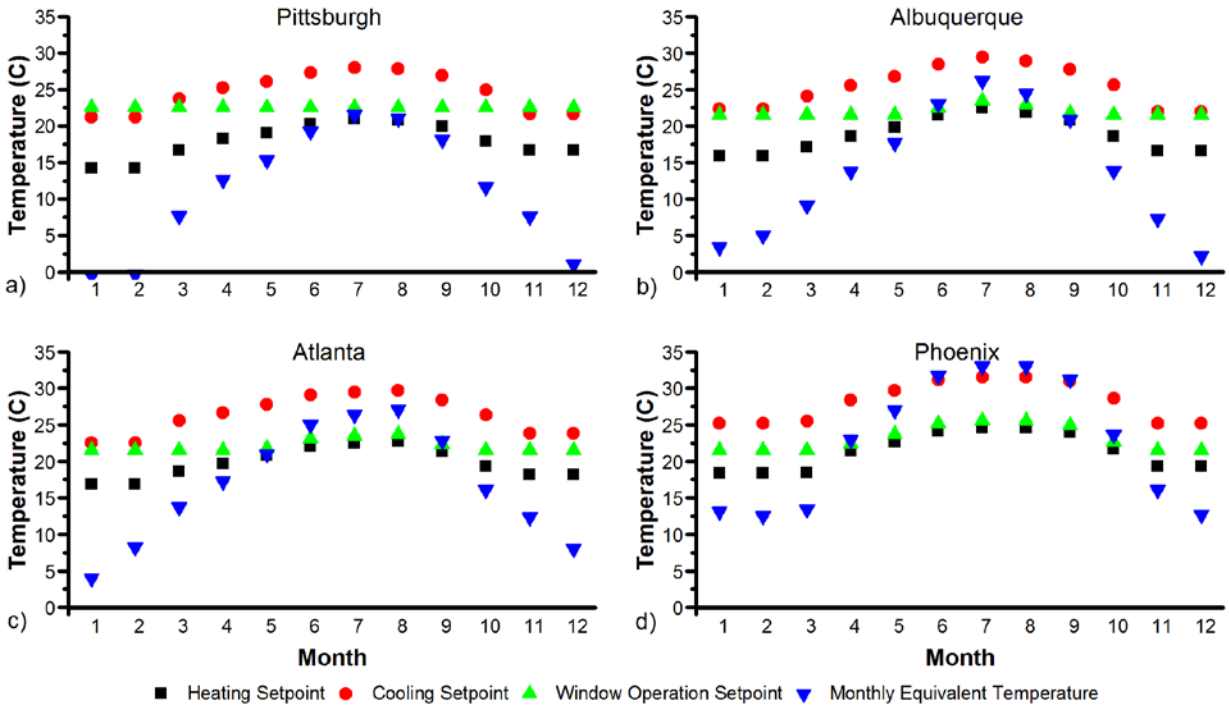

Figure 14: Monthly set points and equivalent exterior temperature for four climates

The window operation rules are intuitive and correspond to the behavior of a well informed occupant but the real occupant would inevitably make mistakes, fail to keep up with changes in the outside temperature or be out of the house at critical times, resulting in a decrease in ventilation performance. This problem could be solved with automated window operations or a system for reminding the occupant when to open and close windows. For this study, the results reflect the potential energy savings with ideal control of the windows.

2.2.3 Annual and Weekly Simulation Results

2.2.3.1 Performance Comparison to Baseline

This section discusses the results for the annual and monthly cooling load for each simulation case. The total annual cooling load by climate and case is shown in Figure 15. The results show

that in a high thermal mass home with ideal controls to maintain adaptive thermal comfort, cross and stack ventilation can remove most of the heat. This is true across the climates, but those techniques reduce the mechanical cooling load by a proportionally higher and quantitatively lower amount in cooler climates. Simply using cross ventilation and effective control of the windows reduces the load by approximately a factor of two in the three cooler climates and by 20% in Phoenix. Adding the ventilated roof technique to one face of the roof further reduces the load by up to 80% in Pittsburgh, and by up to 34% in Phoenix. In Pittsburgh, Albuquerque and Atlanta, clearing pathways for air to move through the house and properly controlling the windows reduces the cooling load by more than using high efficiency constructions and appliances. Compared to the base case, improving efficiency reduces the load by 30 to 35%, while using the ventilated roof techniques cuts it by 49 to 92%. Combining the two approaches results in reductions of over 70% in all four climates.

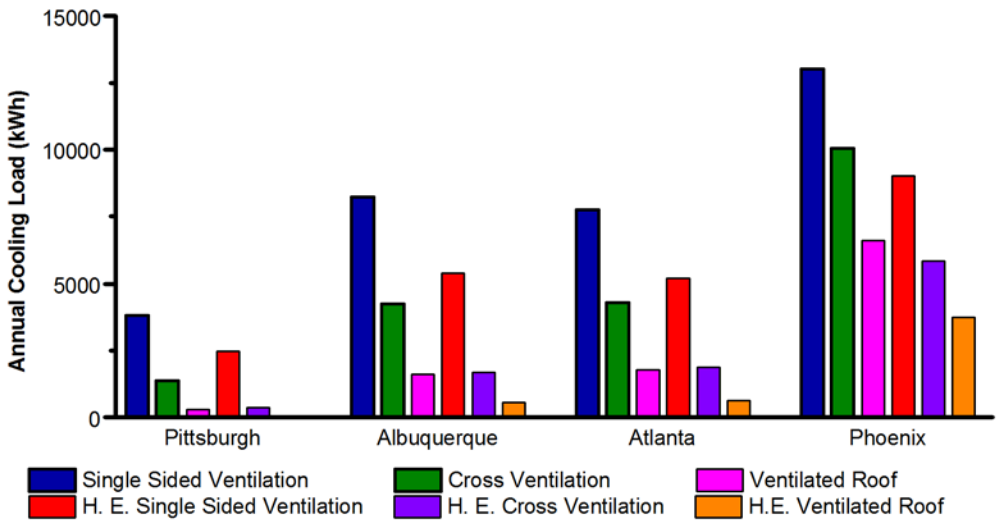

Figure 15: Annual cooling load by case and climate

A monthly breakdown of the cooling load for each climate is illustrated in Figure 16. In Pittsburgh and Albuquerque, the single sided ventilation cases have a cooling load even in some winter months. This indicates that the ideal control assumptions of the home in the model have an unrealistic effect on the results. In these climates, the adaptive cooling set-point standardized by ASHRAE would not be met during the heating season, and extra warming due to insolation during the day might be welcomed by the occupants.

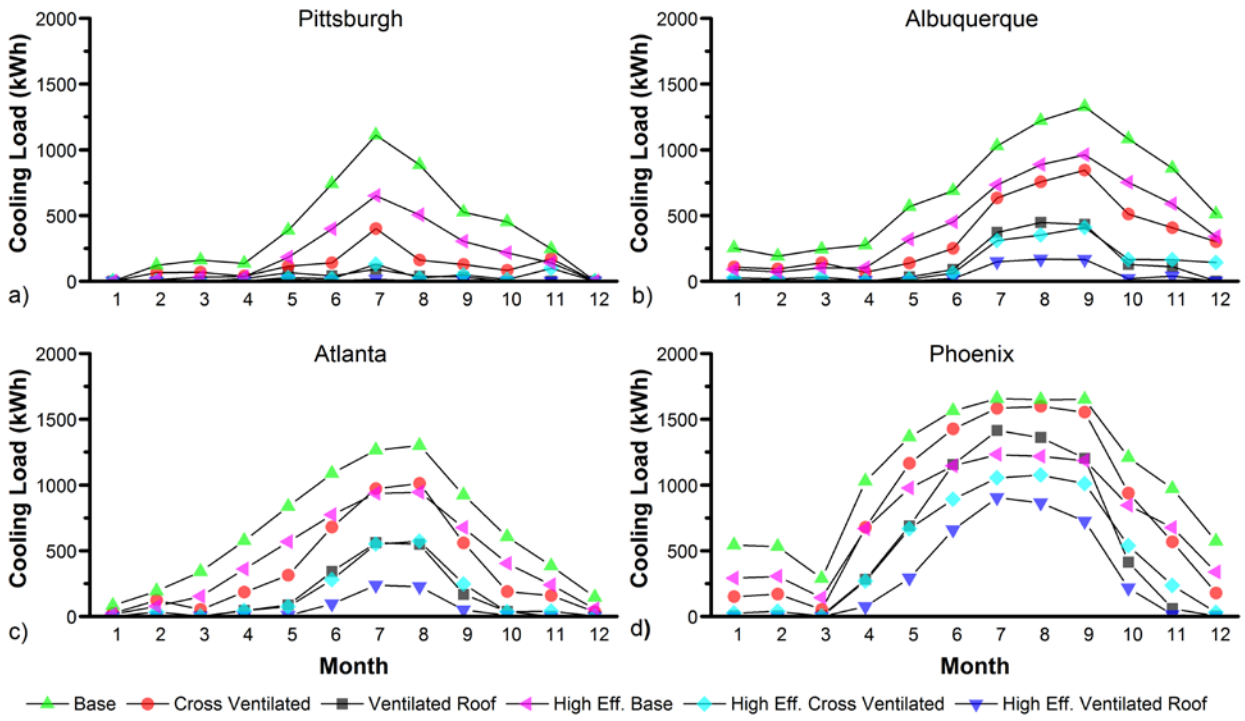

Figure 16: Monthly cooling load by case and climate

2.2.3.2 Ventilated Roof Performance Characteristics

This section describes the hourly simulation results in more detail, summarizing the operational characteristics of the ventilation systems. The airflow through the Ventilated Roof case with base

efficiency is examined in each season with seasonal typical weeks. As examples, the results for Albuquerque, a moderate climate, are shown here. The Spring Albuquerque results are compared to those in Phoenix, a much hotter climate.

The Spring and Fall Albuquerque weeks (Figure 17 and Figure 19) show very little mechanical cooling load. This is in opposition to the baseline case with single-sided ventilation, which has significant mechanical cooling load (see Section 2.2.3.1). There is ventilation flow through the roof throughout most of the week. The heat removed by the flow is not necessarily proportional to the flow rate because of the changing interior and exterior temperatures. The heat removal and mass flow tend to peak in the afternoon or evening when the exterior temperature falls below the inside temperature and the heat that has built up during the day is removed. There is flow throughout the day, however, because the ambient temperature remains lower than the inside temperature and buoyancy forces air from the room upward.

Conversely, Figure 18 shows operation in the summer when outside temperatures are warmer. The exterior temperature tends to be warmer than the interior temperature during the day, but cooler at night. During the day, when the outside temperature rises above the interior temperature, the ventilation is closed to prevent backflow as expected. Then in the evening when the outside temperature falls, free cooling begins. There is some mechanical cooling during the day but its magnitude is minimized by the heat removed through the ventilated roof.

The results for Spring in Phoenix are presented for comparison (Figure 20). Relative to Spring in Albuquerque, there is more mechanical cooling required, but the heat removed through natural ventilation is still much greater than that removed mechanically. There is a more consistent airflow in the warmer climate, and the flow does not need to be controlled to prevent overcooling.

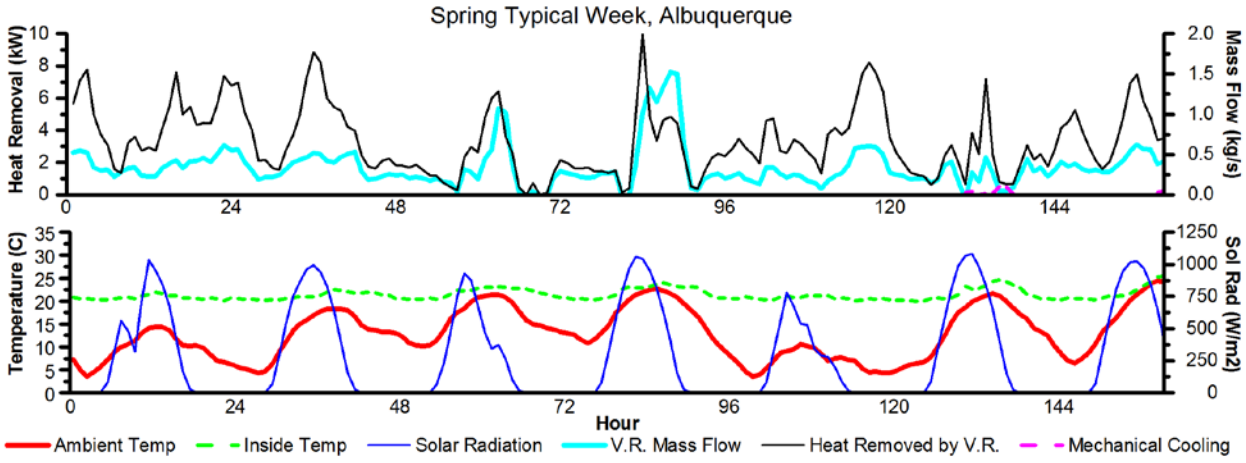

Figure 17: Hourly operation of the ventilated roof in Albuquerque for a typical spring week

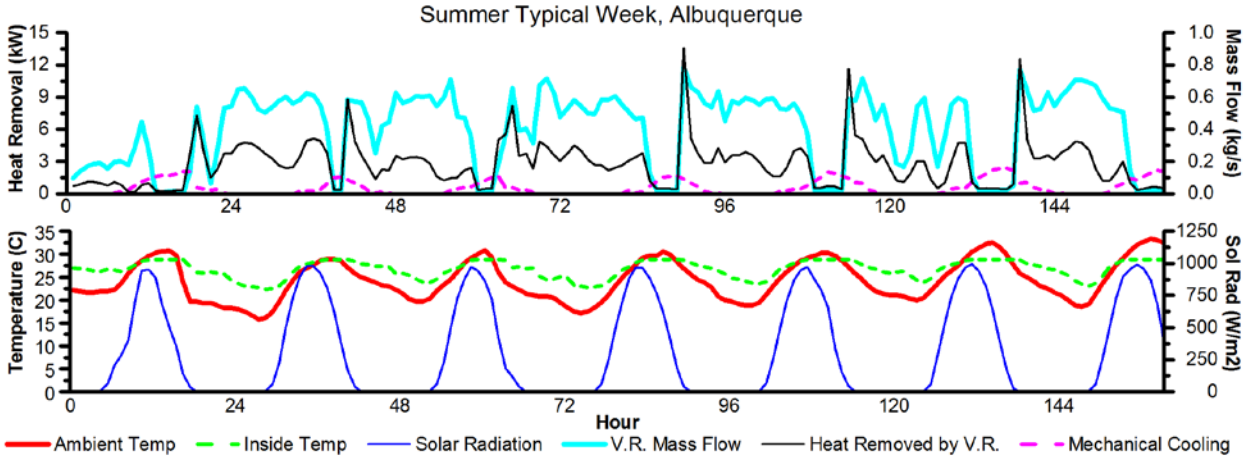

Figure 18: Hourly operation of the ventilated roof in Albuquerque for a typical summer week

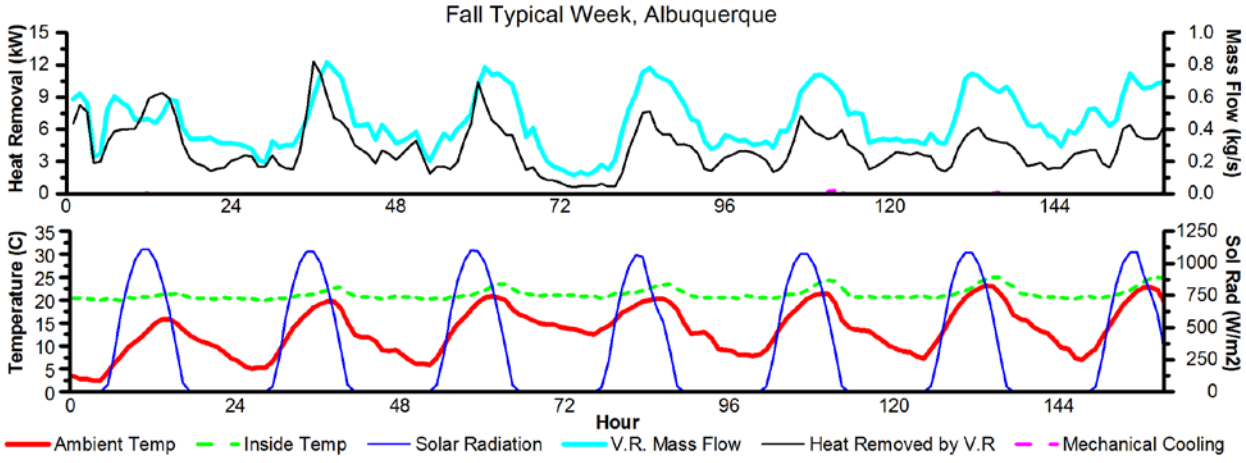

Figure 19: Hourly operation of the ventilated roof in Albuquerque for a typical fall week

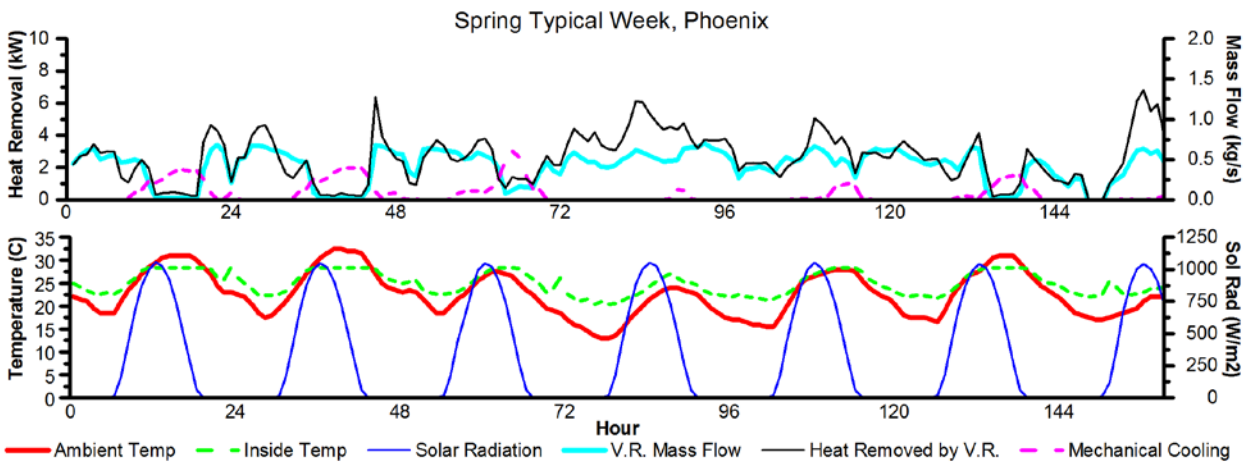

Figure 20: Hourly operation of the ventilated roof in Phoenix for a typical spring week

The ventilated roof acts primarily as a pathway for buoyant flow to remove the heat from internal and solar gains. Much of this free cooling occurs at night, and the "coolth" (thermal mass maintained at a temperature lower than ambient) is stored by the high thermal mass construction as thermal inertia. In many cases if the flow were not controlled, the temperature would actually fall below the heating set-point at night. During the day, even when flow stops because of the hot external temperature, the stored cooling reduces or eliminates the need for mechanical cooling.

By dividing the time steps into three types of flow, it is possible to quantify what role the ventilated roof plays in cooling the house. Time steps with little solar insolation, significant airflow and a positive temperature gradient between the chimney inlet and the peak outlet are defined as *Night Cooling*. Time steps for which there are flow, solar radiation, and the temperature of the flow inlet is lower or only slightly higher than the outside temperature are characterized as *Convective Flow*. The remaining time steps, when there is flow and there is both high solar radiation and a temperature differential aiding the flow are categorized as *Mixed*. Figure 21 shows the load for each season, in each climate. *Convective Flow* is the least significant of the types, being less than 10% in all simulations. Except in Phoenix in the

Summer, the mechanical cooling is a relatively small portion of the heat removed from the house. The remainder is split between *Mixed* and *Night Cooling*, both of which are driven by the temperature difference between the ambient and the house interior. This indicates that the difference between the inlet (interior) and outlet (outside) air temperatures is of primary importance for predicting the flow in a ventilated roof or roof solar chimney. This principle is key to the design and control of any solar chimney that has an inlet to a different space than the outlet.

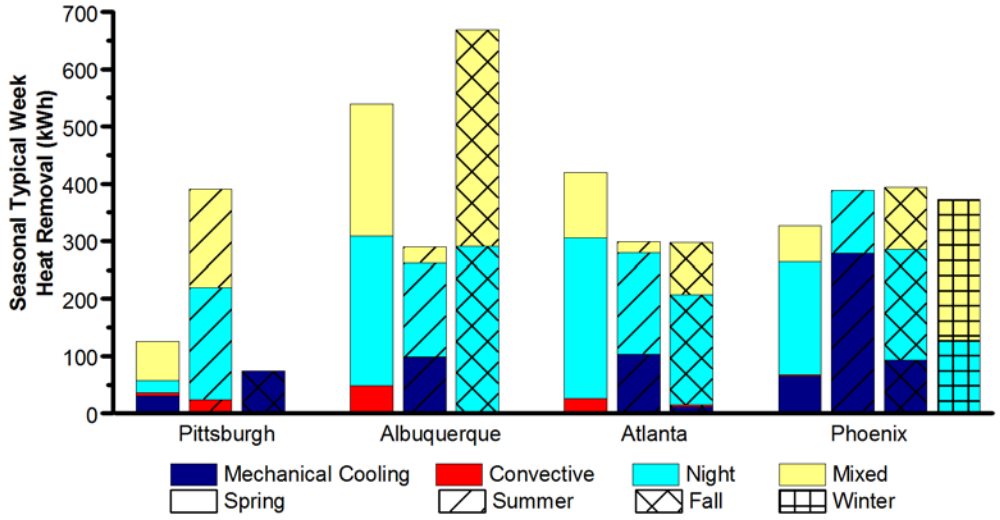

Figure 21: Cooling load by mode of operation, season, and week

The roof solar chimney design is most effective in terms of total energy saved in Phoenix. However, it may eliminate the need for mechanical cooling at all, in Pittsburgh. While hot climates should be a target market for the technique, the earliest adoption may take place in more mild climates. In addition to the cost savings of eliminating the need for a cooling system, fears about failure of the system components such as vent motors will be less significant because the climate is less extreme.

The RSC, which should be a product of thoughtful and detail-oriented home design, was a small-scale modeling problem that was successfully integrated into the larger framework of a full building model, thus improving the accuracy of the representation and evaluation of the technique and expanding the capabilities of building modeling. This aim of making building modeling responsive to user needs and ensuring accuracy was next expanded to look directly at the interplay between building occupants and modeling in the context of a larger, commercial building.

3.0 MODELING THE MASCARO CENTER

The MCSI BEM studies built upon the advanced modeling of passive cooling building components by expanding scope to focus on improving the representation of occupancy patterns in a detailed building model and representing to the occupants their options for making behavior interventions that improve energy efficiency. Detailed models need not only to represent physical phenomena accurately, but to affect the interaction between the building and the occupants. This relation is central to creating useful model outputs that accurately represent real-world building operation, and can be used to educate occupants on their role in the life of the building.

Many BEM practitioners see building modeling and calibration as an art, which often involves 'tuning' physical parameters based on experience or trial and error in order to achieve the desired results. This is beginning to change, however, as sensed data becomes more commonly available and evidence based calibration becomes the norm. A review by Reddy gives an overview of the literature relating to building model calibration. There are a number of approaches, and error in models calibrated by professionals is commonly in the range of 20% on a monthly time scale [7, 70].

A model is considered validated by ASHRAE if, for monthly observations, the coefficient of variation of the root mean square error (CVRMSE) is less than 15% and the normalized mean bias error (NMBE) is less than 5%. For hourly data those values for error in

total energy consumption should be 30% and 10%, respectively [71]. The CVRMSE is derived from the root mean square error (RMSE). The two measures of error are described by Equations 3.1 – 3.3:

$$RMSE = \sqrt{\frac{\sum_{i=1}^{n}(x_{1,i}-x_{2,i})}{n}} \quad (3.1)$$

$$CVRMSE = \frac{RMSE}{\bar{x}} \quad (3.2)$$

$$NMBE = \frac{\sum_{i=1}^{n}(x_{1,i}-x_{2,i})}{n} \quad (3.3)$$

In this case, x_1 is the observed energy consumption, x_2 is the simulated consumption, and n is the number of observations.

A detailed, structured approach to calibration was proposed by Raftery et al. The approach is shown graphically in Figure 22. Essentially, the process is a methodology for gathering data, using it to improve the model, and testing for accuracy and discrepancies. Because data sources are often conflicting, the data and evidence are ranked for reliability as follows: 1. data logged measurements; 2. spot measurement; 3. direct observation; 4. personnel interviews; 5. operation documents; 6. commissioning documents; 7. benchmark studies and best practice guidelines; 8. standards, specifications and guidelines; and 9. design stage information [72]. At the beginning of calibration, the MCSI building model used data from level 3 to 9 for different aspects of the building operation. By the end, the final model relied primarily on logged data, in addition to the construction documentation for materials.

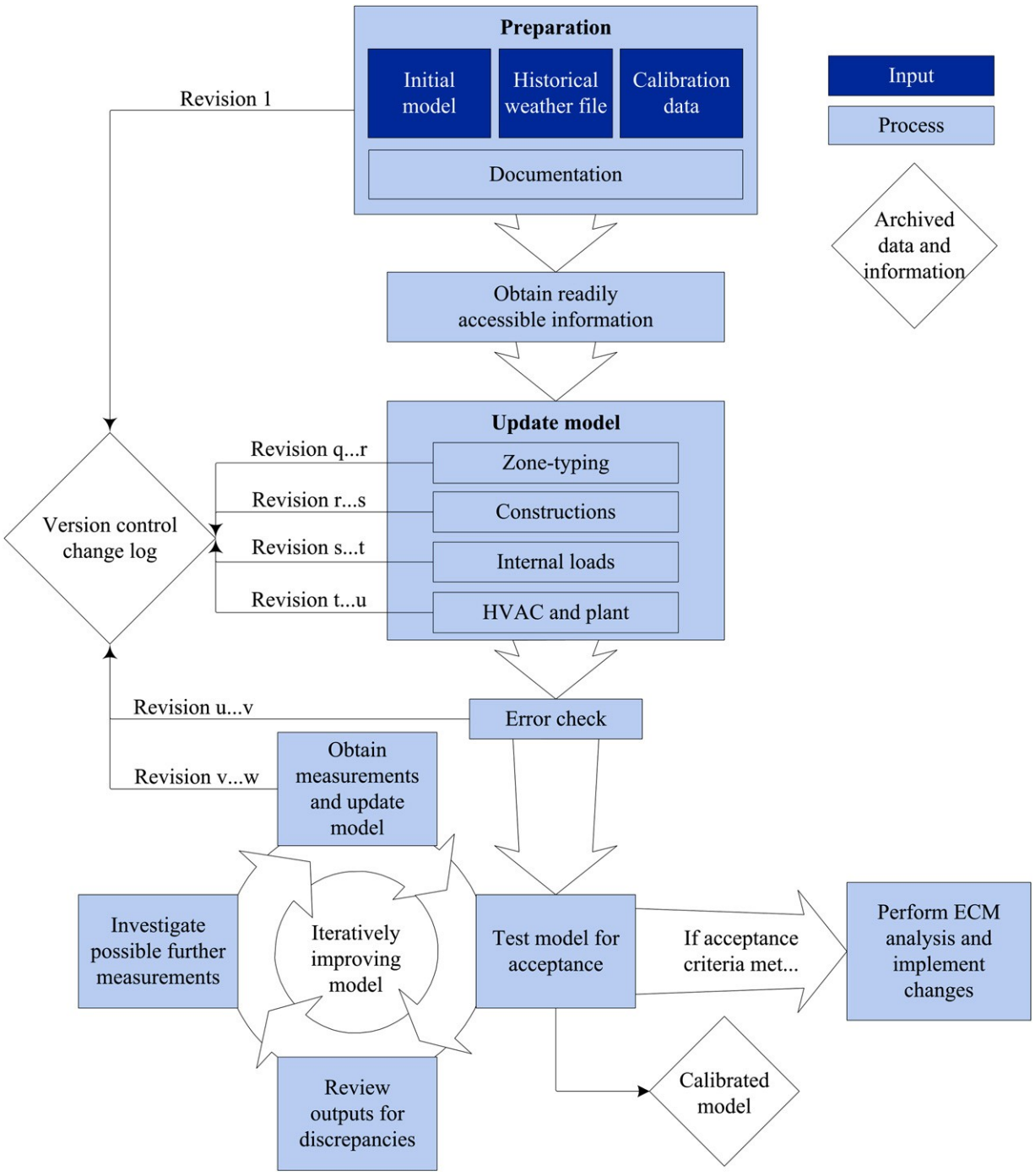

Figure 22: Model calibration process diagram [72]

3.1 MODEL DESCRIPTION

The building shown in Figure 23 is the annex portion of the MCSI building, connecting Benedum Hall and Engineering Auditorium. The MCSI building also includes the second floor of the Benedum tower. The scope of the model is these two buildings, and adjacency to the nearby buildings is treated adiabatically. This is justified because the space temperature set points in the other buildings are identical. The other buildings are too big to model in detail and only the MCSI building has the detailed sensed data available for calibration.

Figure 23: The MCSI annex

A brief description of the building follows. The first floor of the annex has a pedestrian area with stairs to the ground and second floors, and doors to the Engineering Auditorium building and the exterior. There is an office cluster with a reception area, conference room, offices and kitchen. The second floor continues this pedestrian area, which is open to the third floor and has vertical windows from floor to ceiling. There is an open office area, dry lab, and conference room on the second floor. There is a door to the second floor Benedum area, and an

open hallway to the second floor Engineering Auditorium building. The second floor Benedum space has a hallway connecting open student workspaces, offices, and a large wet-lab. The third floor annex has open office, conference, kitchen, and presentation areas.

The Mascaro Center is a LEED Gold building, with high efficiency constructions and low-gain windows. The interior spaces are largely open with moveable partitions for easy re-purposing. The floors are finished concrete and there are no drop ceilings, to save on materials and lower the occupants' exposure to manufactured surfaces that might emit harmful chemicals. The north-facing windows are sloped in order to improve day lighting and the south-facing façade has deep window dividers in order to provide some shading. There is a high albedo, reflective roof.

Figure 24 shows the DesignBuilder model of the MCSI. Preliminary simulation results were obtained for three HVAC configurations for this model using DesignBuilder: the actual variable air volume (VAV) system, a better controlled VAV system, and a constant volume (CV) system. The overall energy use per square meter (EUI) is shown in Figure 25. The benchmark values are from a survey of office buildings by the DOE. The MCSI extension has higher energy use than the benchmark buildings, despite being certified LEED Gold with many green features, because it is conditioned 24/7 and has different usage patterns than those of a typical office building. The comparison, therefore, may be a poor one. However, the office building baseline is the closest to the MCSI building in terms of occupancy density and plug loads. In addition to the annual energy usage, it is also instructive to view the results by end use and month, as shown in Figure 26.

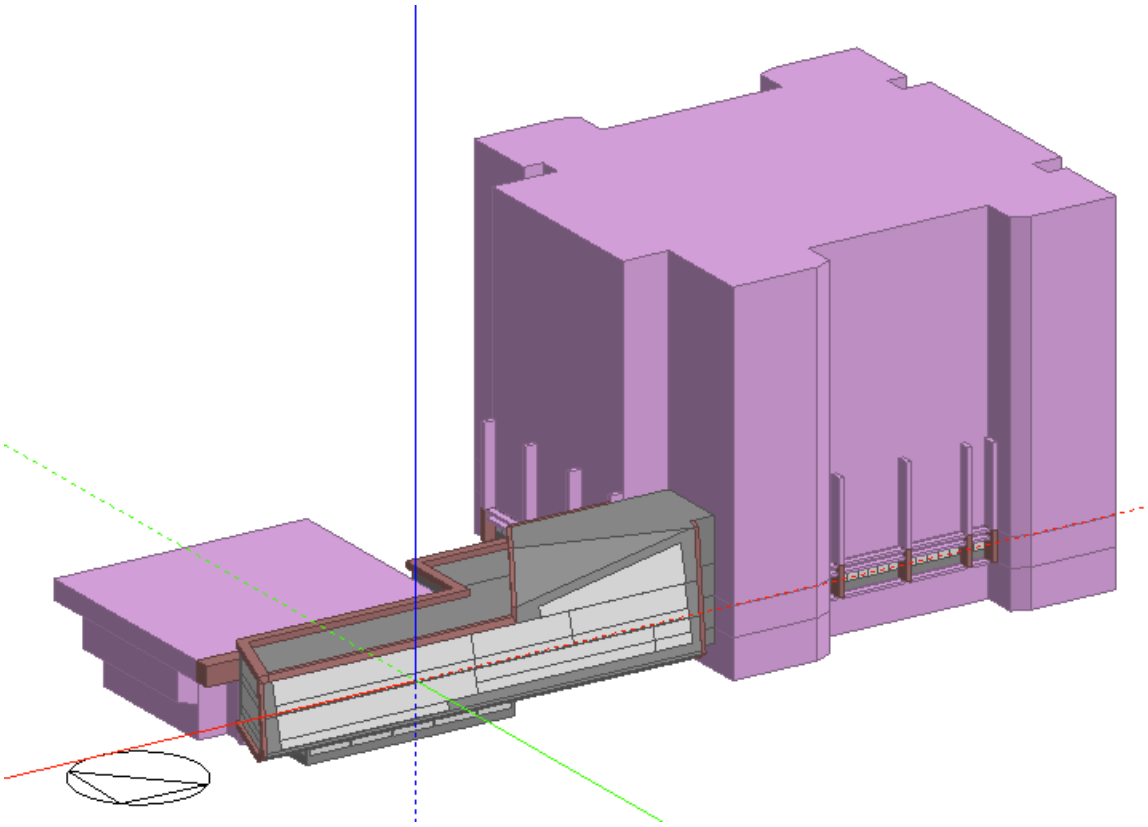

Figure 24: MCSI DesignBuilder model

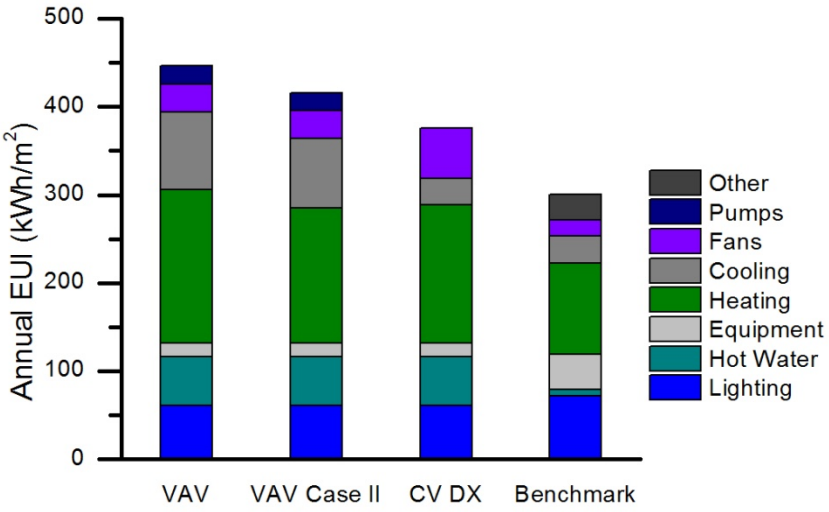

Figure 25: Preliminary annual energy use intensity by case

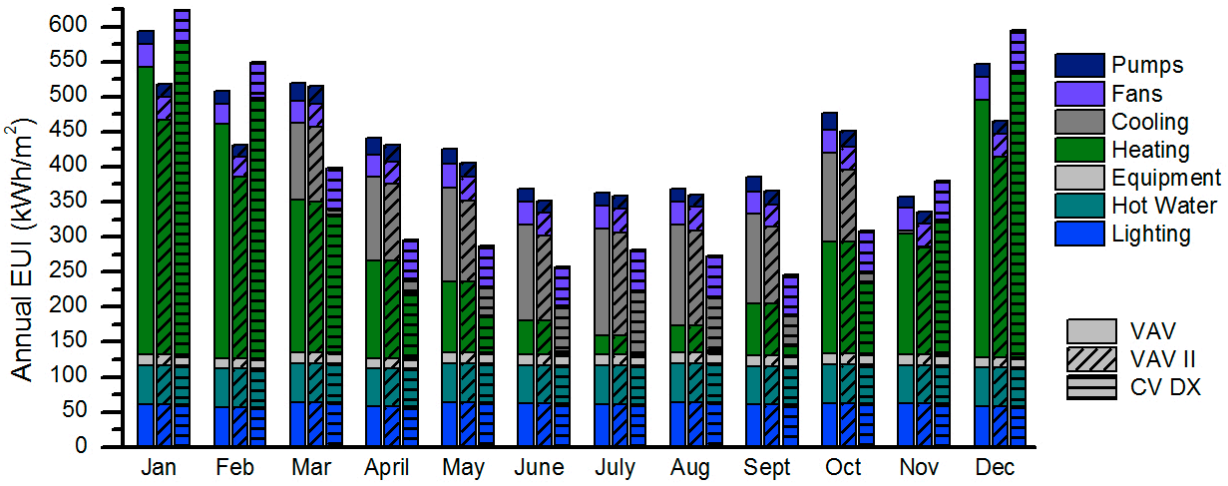

Figure 26: Preliminary energy consumption by end use

The results of the MSCI EnergyPlus model were compared to metered consumption data by Collinge et al. [73]. Figure 27 shows the results for heating and cooling consumption, which are proportional to the load measured and observed in the building. Figure 28 shows the estimated electricity consumption, compared to the modeled. In these figures, estimated energy consumption refers to data obtained by scaling building level meters by floor area. These data were preliminary and a higher resolution was available, so for the further calibration, the data were used directly rather than pro-rated from the total. Only the building annex was included in this preliminary study (not the second floor of Benedum) and the heating and electric data are based on an allocation of heating supplied to this portion. The data provide an indication of the starting point for the model, however. The CVRMSE for the heating and cooling energy use is 19.0% and the NMBE is 10.0%.

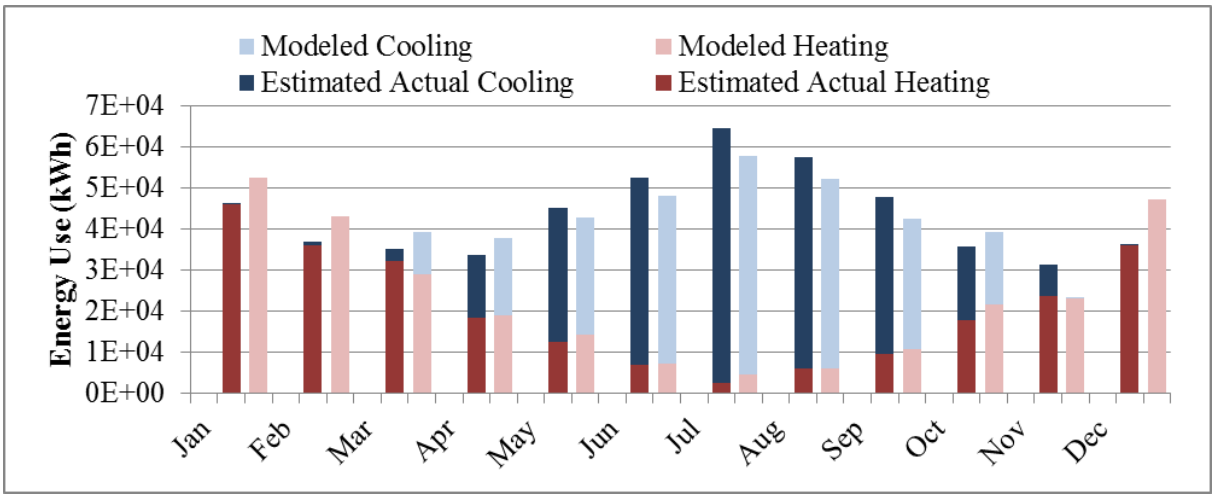

Figure 27: Preliminary MCSI modeled and estimated heating and cooling consumption [73]

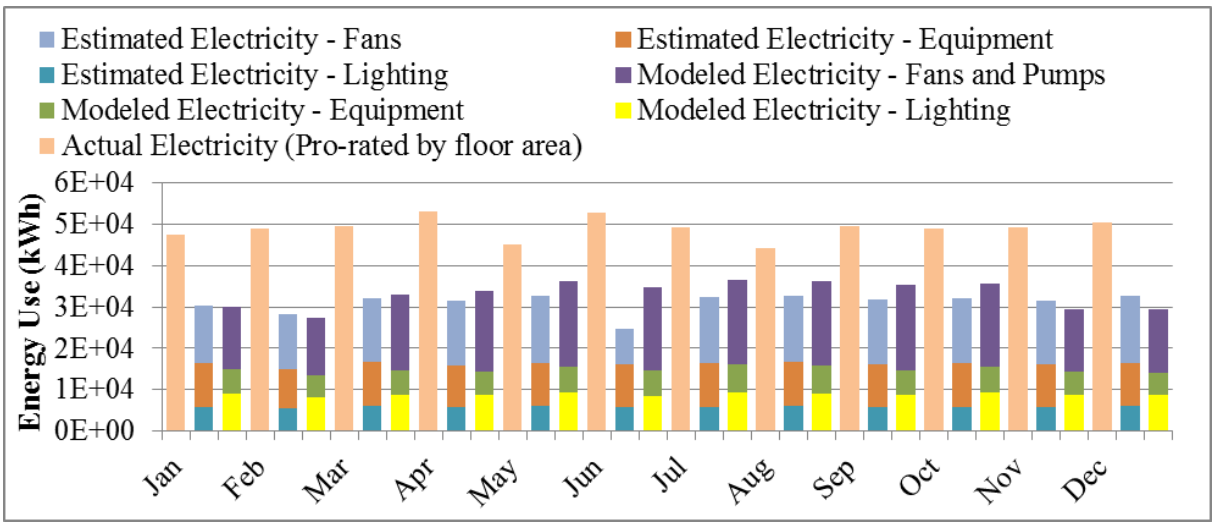

Figure 28: Preliminary MCSI modeled electric consumption by end use, compared to metered [73]

3.2 CALIBRATION

For calibration, the base geometry model was exported from DesignBuilder and edited using EnergyPlus IDF Editor. Three air loops were modeled to represent the three air systems in the MCSI, and this was a modeling capability that DesignBuilder did not include at the time. An

outside air system with heat recovery served the wet labs and fume hoods. An economizing system provided air for the other spaces. Both of these systems had variable frequency drives on the pumps and fans and supply reheat boxes with hot water reheat. A third loop recirculated air to supply cooling to the server rooms. A central plant provided the heating and cooling to the air handling units and reheat boxes. To model the district plant, a constant EER and boiler efficiency were applied to the total heating and cooling loads because no data was available for the plant performance.

The model calibration was an evidence-based process primarily drawing on data that was sensed by the building's building automation system (BAS) and stored in a central database. Other parameters were determined based on observations, construction documents, and personnel interviews, in that order. Recent hourly and sub-hourly data was used to calibrate components and test the performance of the model and controls.

Table 6 summarizes how the EMS data was used to calibrate the model. The majority of the HVAC system can be described with this data. It was understood in the context of observations and interviews of building personnel that were conducted regarding controls and operation such as the outside air settings, fan cycling, and nighttime set points. Two walk throughs of the facilities and air handling units were conducted with facilities staff during the process of energy modeling.

Table 6: Calibration sensor data points

Model Parameter	Sensor Data
Ventilation rates and schedules	Air flow rates through VAV branches
Outside air flow rate	Outside Air Valve % Supply Air CFM - Return Air CFM
Temperature set points	Space temperatures
Supply air temperatures and humidity	Supply air temperature and humidity
Discharge temperatures	Zone discharge temperatures
Cold and hot water supply temperatures	Cold and hot water temperature into AHUs
Fan operation	AHU power meters Electric breaker box meters Fan VFD speed meter

In EnergyPlus, the three internal gains categories, lighting, electric equipment and occupancy, are based on nominal capacities and scheduled percentage rates. The schedule can be defined by day type and season or a custom annual gains file can be chosen. Gains are more difficult to calibrate than HVAC settings because they are more unpredictable and don't operate based on control laws with a few inputs. The BAS and the Aircuity system, which monitors indoor environmental quality (IEQ), record indicators that can be used to estimate internal gains. Table 7 shows the sensor points that can be used to determine past gains patterns.

Table 7: Internal gains sensors

Model Input	Sensor Data
Electric load and schedule	Electric breaker box meters
Lighting load and schedule	Electric breaker box meters
Occupancy schedule	CO_2 level, supply air rate, return air rate

The best available method for determining occupancy levels was to calculate the rate CO_2 is exhausted from the space and divide that by the average human CO_2 exhalation rate. There are

several potential problems with this approach, such as the time delay in changing CO_2 concentrations and uncertainty in the amount of CO_2 produced by different people doing different activities [74]. For calibration, the actual recorded gains data from the calibration period were used as inputs to the model during the time period for which there was hourly data. Average diversity schedules for each day type were used to fill in gaps in the data. The impact of the uncertainty introduced by this variable is studied in depth in Section 3.3.

Fan performance and pressure drop, economizer controls, temperature set points and other controls parameters were confirmed or adjusted to match the data. As the calibration proceeded, the model results for 2012, run with the hourly occupancy and gains schedules and a weather file for Pittsburgh International Airport, converged to the energy consumption calculated from the BAS data for that year. Table 8 shows the calibration results. The model can be considered calibrated for both the hourly and monthly methods.

Table 8: MSCI model calibration results

Calibration Method	Normalized Mean Bias Error	Coefficient of Variation of the Root Mean Square Error
Monthly	1.30%	7.10%
ASHRAE Guideline 14 Limit	5.00%	15.00%
Hourly	1.20%	15.20%
ASHRAE Guideline 14 Limit	10.00%	30.00%

The end use energy consumption for the model and BAS data is shown in Figure 29.

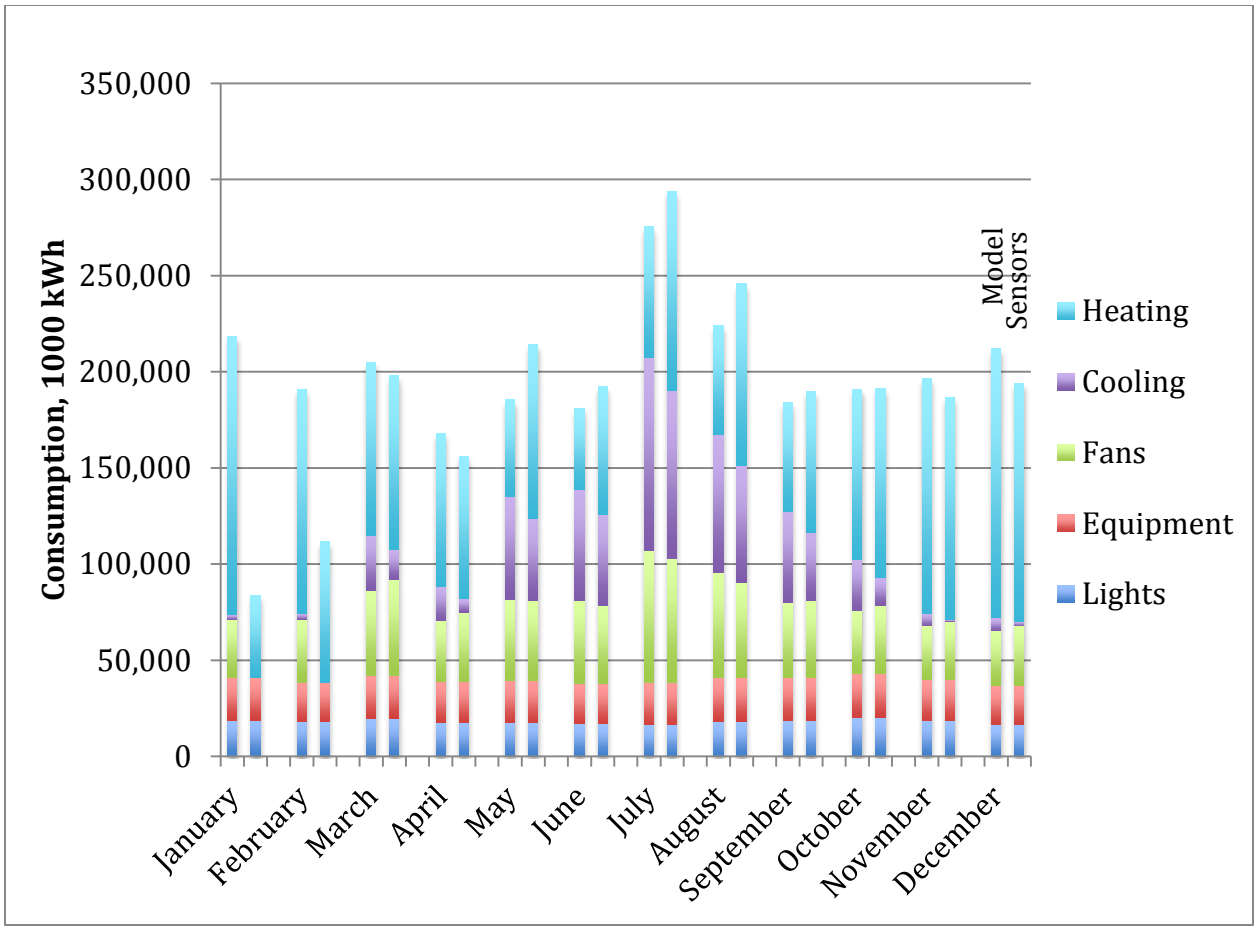

Figure 29: Calibrated monthly energy consumption by end use

The largest error comes from heating and cooling. The model tends to overestimate cooling and underestimate heating throughout the year. Equipment and lighting loads match exactly, because the BAS data for these end uses were directly input to the gains schedules. This figure demonstrates the close monthly calibration of 1.3% bias error and 7.1% coefficient of variation of the root mean square error. Note that the discrepancy in levels for January and February is due to a lack of data for those months.

Figure 30, the total hourly energy consumption for the model and sensed data, shows the hourly calibration. The jump in levels around hour 4,500 is due to a manual override of the fan flow rates in July for two weeks. The sensed data shows more variations from hour to hour than

the model data. However, the NMBE is only 1.2% and the CVRMSE is 15.2, well within the limits for confirming calibration.

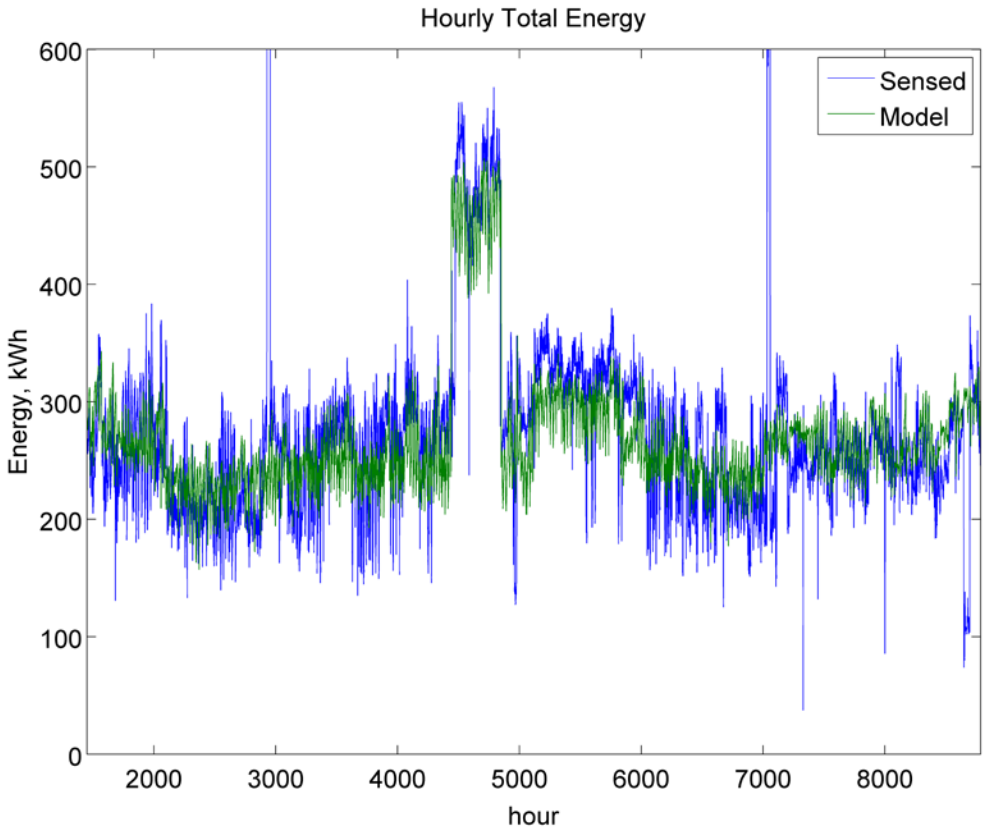

Figure 30: Calibrated hourly total energy consumption

Figure 31 shows the hourly total heating load for the model and actual building. The actual energy consumption is higher, especially in the summer. This indicates that the model does not completely capture the reheat energy expended. The reheat tends to operate in a less than ideal way, while the Energy Plus model has a more ideal set of control laws. The sensed data shows higher noise, or variations from hour to hour, while the model has a more smoothed curve. The model reacts to changes in weather and loads immediately, while in the actual

operation of the building, the controls do not operate as exactly but may overshoot set points and thermal loads. The space temperatures often fall outside of the temperature set points, and supply air temperatures vary by a degree or more.

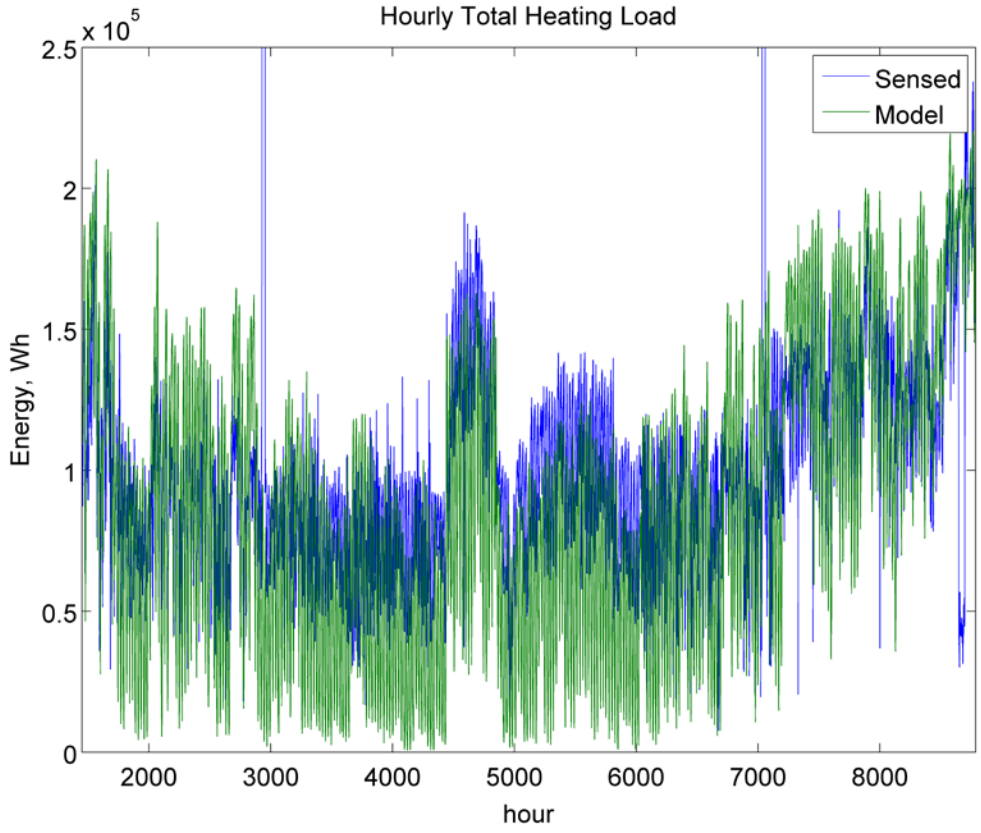

Figure 31: Calibrated hourly total heating load

The comparison between calibrated model and actual hourly cooling load is shown in Figure 32. Note that the model treats economization more ideally than the building actually operates, as indicated by the tendency of the model data to follow a horizontal line. Below the line, the simulated cooling load goes directly to zero. The actual building also economizes, but there is still a small cooling load for many of the hours. In general, the model overestimates the

cooling load. This could be due to a small error in supply air temperature and flow rate, or inaccuracy with the sensors.

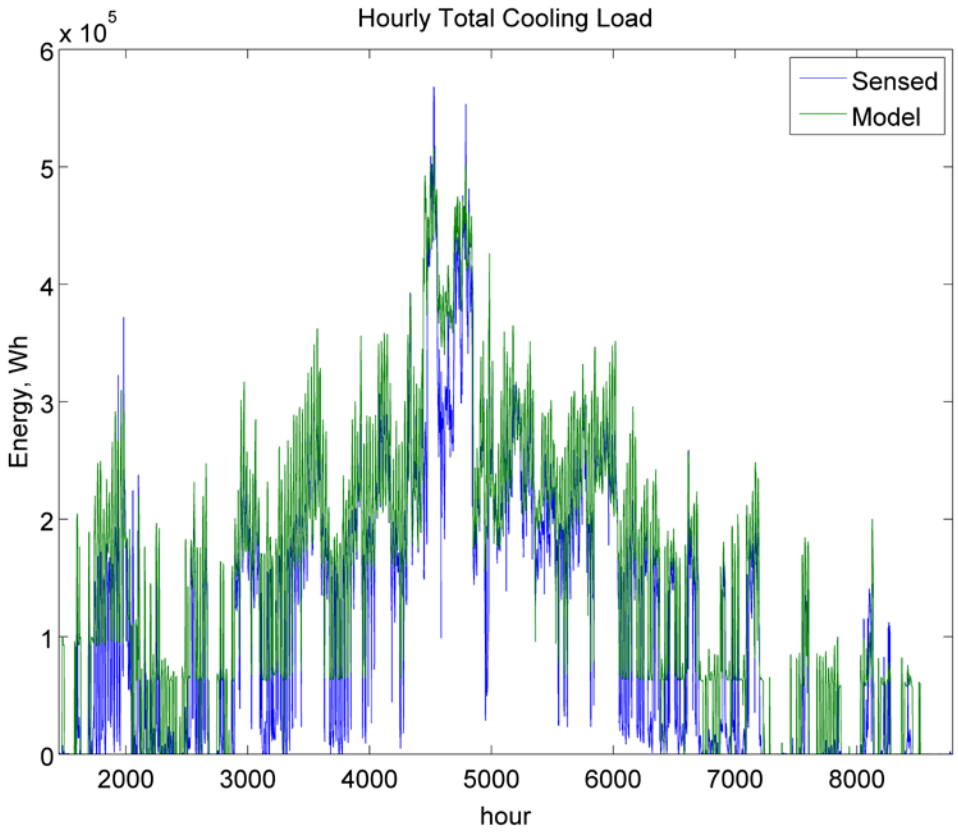

Figure 32: Calibrated hourly total cooling load

Figure 33 is an example of the calibration of one of the supply fans. The fan curve in the model was fit to match the sensed data. However, it is apparent that the model fan operates as a smooth variable frequency drive. While there was a variable frequency drive on the actual fan, actual data shows that the fan tends to operate at several specific flow rates. This is partly due to the manual override of the fan control settings by building maintenance staff. There also appears

to be some bad data included in this calibration. There are numerous outlying points and points for which the flow is positive but the power consumption is zero.

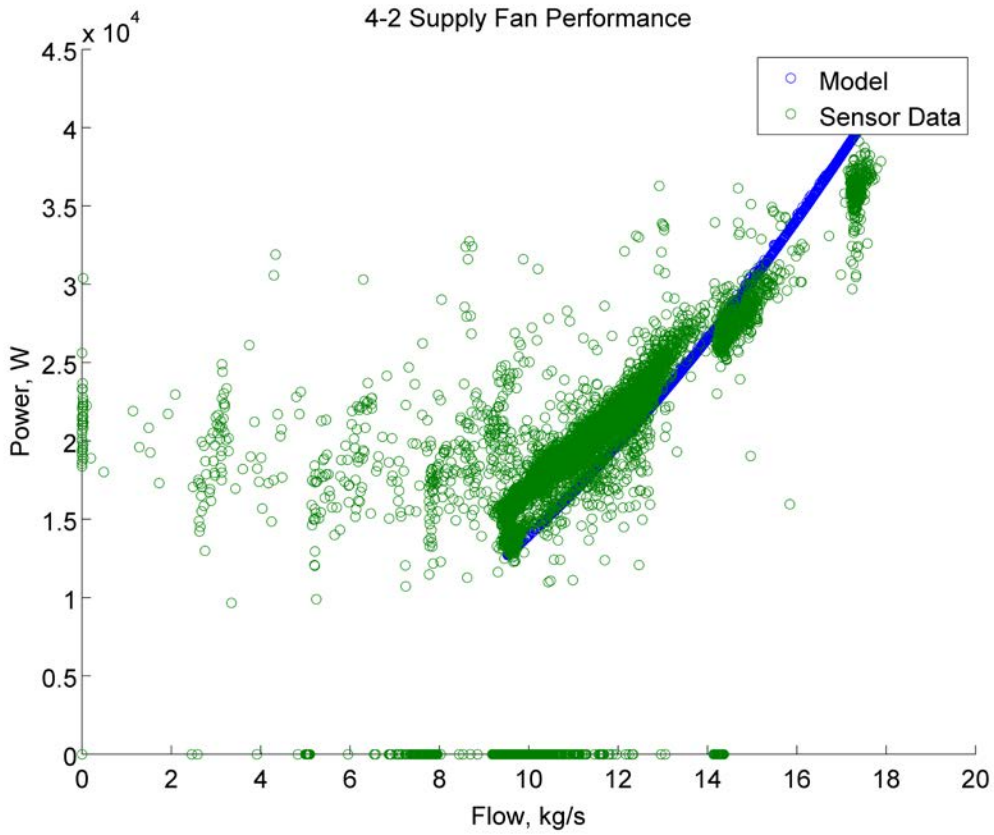

Figure 33: Calibrated annex supply fan performance

The manual override is clearly illustrated by Figure 34, which shows the hourly total fan energy consumption. As the seasons change and thermal comfort complaints are registered, the total air-flow rate seems to be set manually by the building staff. This was not indicated in interviews, however. For example, in the summer, more air is required to remove the excess heat. In the winter, a lower flow rate is needed to meet thermal comfort, in part because the temperature differential between space and supply air temperatures is greater. Ideally, the

minimum flow rate should be set based on outside air requirements by code, and the BAS should vary the flow rate above that automatically, as needed.

Again, the period of unusually high flow rate can be seen clearly, in July. The model matches the actual data because the minimum flow schedules were altered to match the flow rates recorded by the BAS.

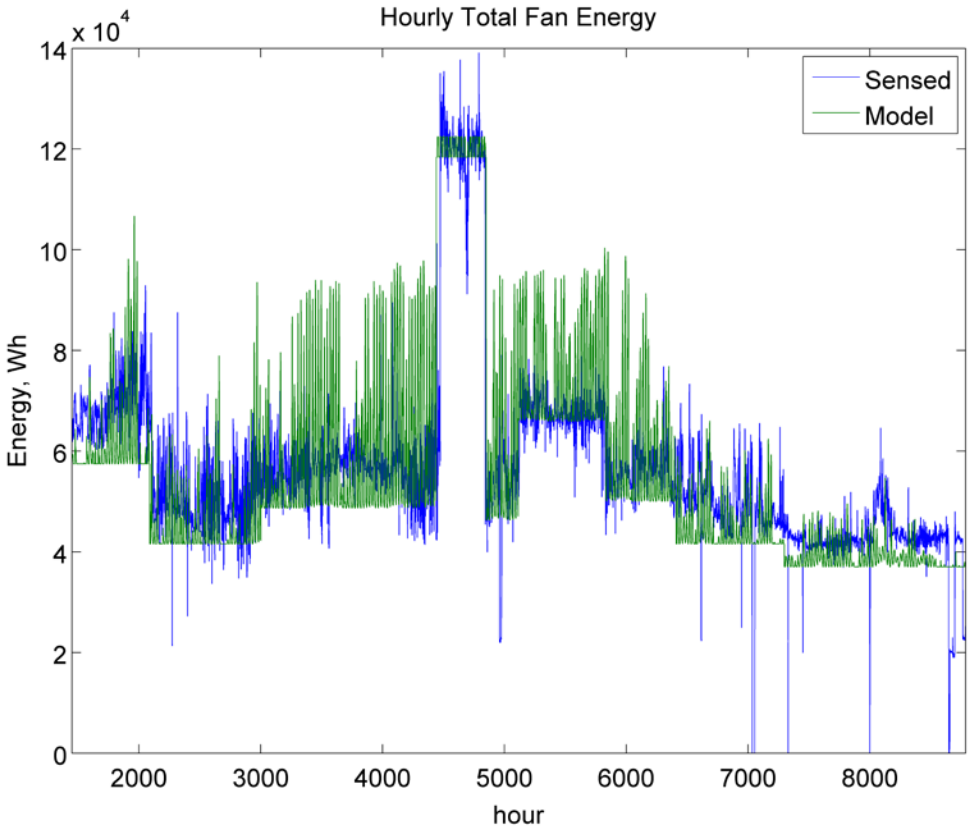

Figure 34: Calibrated hourly total fan energy

Figure 35 is the air flow rate for the AHU 2-1, or the air handler serving the wetlab. This is the air handler that experiences an unexplained spike in flow in July. The graph shows that the model tends to economize more, as can be seen by the blue peaks rising above the minimum air

flow rate. While there is no economizer unit on this fully outside air AHU, the flow rate is increased to provide free cooling in the model. The minimum flow rate for the model has been calibrated based on the sensed data.

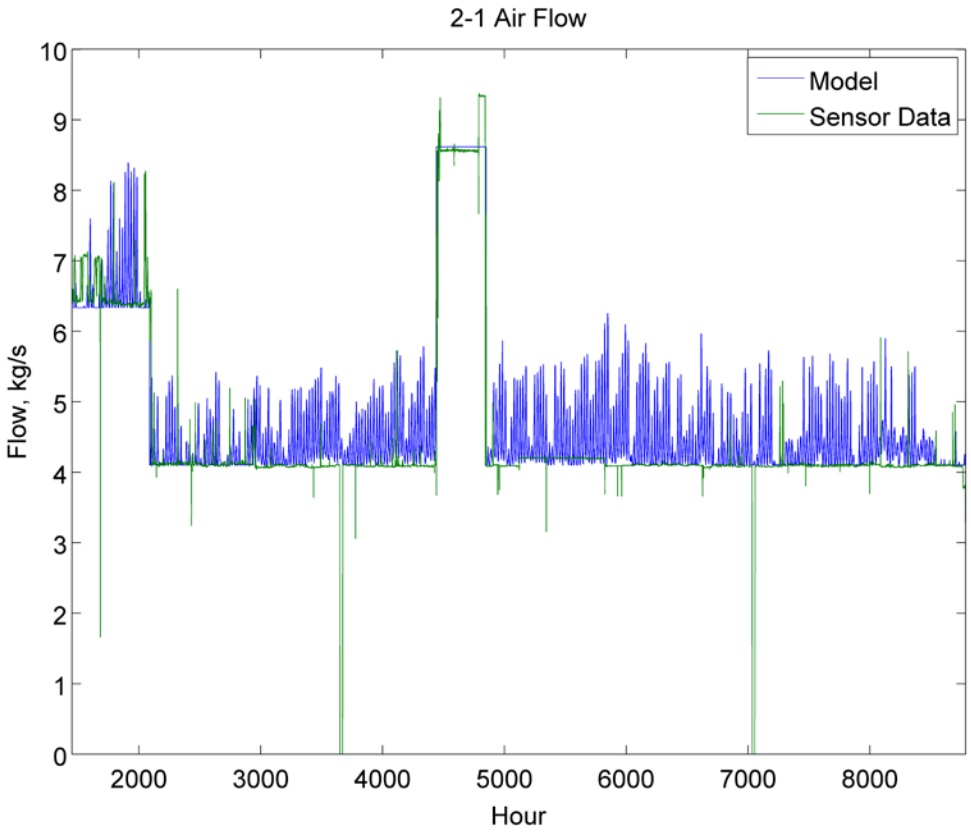

Figure 35: Calibrated hourly tower air flow rates

The same graph for AHU 4-2, or the handler serving the annex and office spaces, is shown in Figure 36. There is no spike in July, but there are floating arbitrary minimum flow rates. Again, the AHU's minimum flow schedule in Energy Plus was set based on the BAS data shown in this graph. Both model and sensor data match for the minimum and maximum flow

rates. Also, it can be seen that the economizing in both seems to match temporally, as there are certain days and weeks when the weather is ideal for economization.

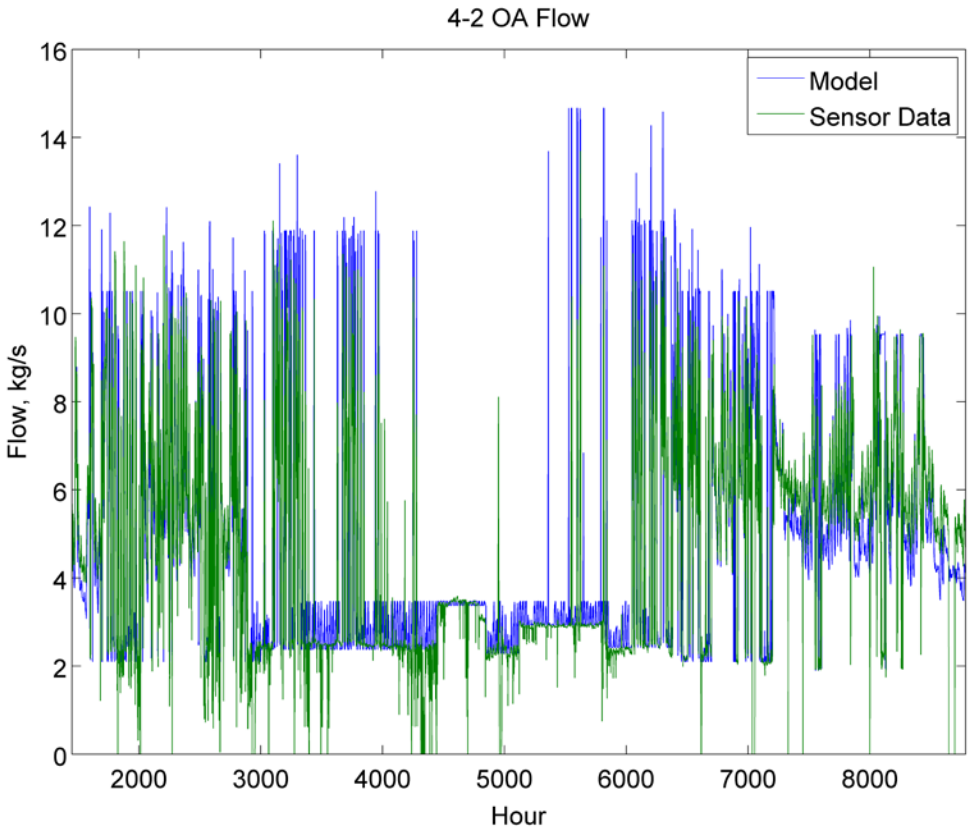

Figure 36: Calibrated hourly annex air flow rates

Finally, Figure 37 shows the occupancy rates for the year. Where there are no data, the levels look flat in the graph. This is because average schedules called diversity schedules were developed from the days with data, and substituted. The maximum occupancy for each section, wetlab and annex/offices, varies from 20 to over 70 people.

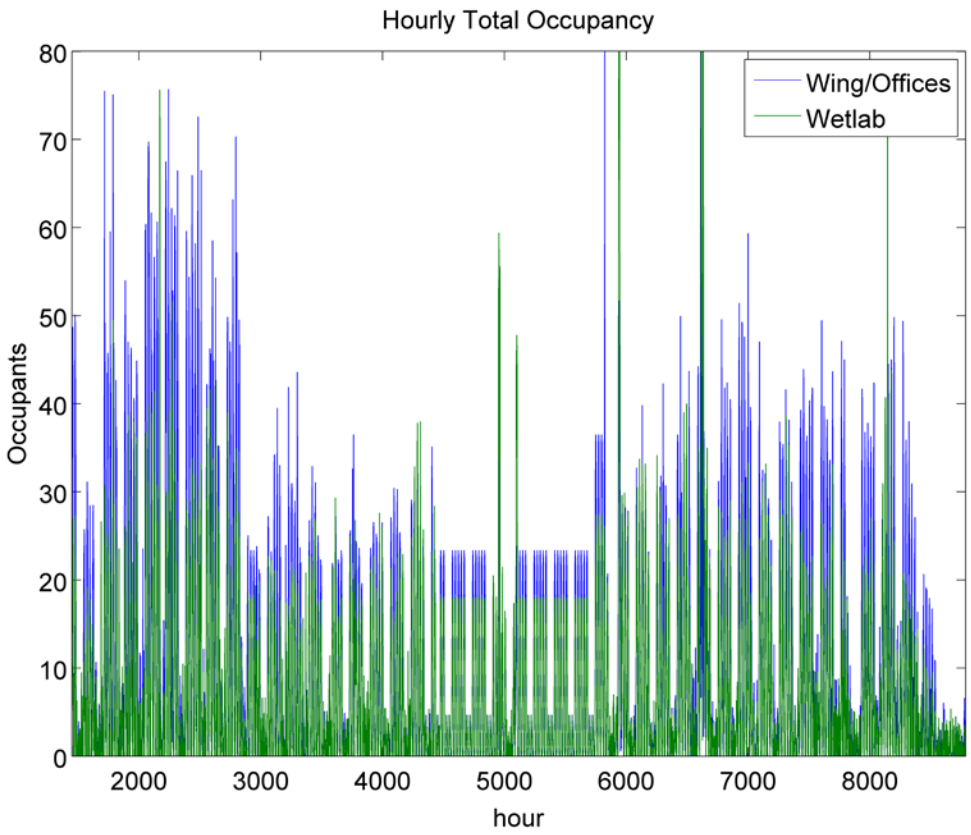

Figure 37: Hourly total occupancy rates

The occupancy data cannot be verified and the level of uncertainty is not apparent, and the use of diversity schedules for several weeks introduced further error. Section 3.3 explores the error introduced through the treatment of occupancy, and methods for representing occupancy stochastically instead of using diversity schedules.

3.3 OCCUPANCY STUDIES

Following the calibration of the model, the Monte-Carlo approach was used to study the effect of uncertainty and natural variation in gains levels on the model output. Monte-Carlo simulation

uses the probabilistic distribution of uncertain inputs to determine the distribution of the output of a complex function or model. Compared to other methods, it requires relatively few evaluations to resolve the output distribution even when there are many input variables. For a given number of runs, the convergence ratio of a Monte-Carlo simulation remains constant as the number of input variables increases. A parametric simulation that covers the input space deterministically must increase the number of runs exponentially to maintain convergence. To apply Monte-Carlo simulation, stochastic scheduling methods were developed as model inputs by scaling the daily diversity schedules and using random sampling from the recorded gains data.

3.3.1 Occupancy Data

The level of accuracy in the creation of internal gains schedules, as well as the validation of the calibrated model, was limited by the data available from the building automation system. Sixteen carbon dioxide (CO_2) sensors were spread throughout the building. Eight electric meters were installed on the circuit boxes for lighting and plug loads, and the system recorded each fan's electricity consumption. The metering of carbon dioxide and electricity consumption was coarser than the zoning in the model, so schedules overlapped several zoned spaces. There were gaps in the data due to changes in the larger building system and discrepancies between meter readings, which created uncertainty in calibration. In the creation of occupancy schedules, carbon dioxide levels and flow rates were used to create a balance and calculate the number of persons present. The difference in CO_2 ventilated in and out of the space, less the CO_2 stored in the space air volume, was divided by the average CO_2 exhaled per person. This method provided a rough estimate for occupancy, but was the best possible method with the available data. All of the final schedules are described in Table 9.

Table 9: Summary of the occupancy and gains schedules

Name	Type	Description	Area (m^2)
Wing Electric	Plug Load Electric	Electric plug load for open office, dry lab, conference and miscellaneous spaces	1,249
Tower Electric	Plug Load Electric	Electric plug load for tower wet lab, partitioned office, hallway and study area spaces	1,683
Fume Hood	Total Electric	Electric plug and lighting in four fume hoods located in the wet lab	150
Server Rooms	Total Electric	Electric plug and lighting in the wing server rooms	30
Wing Lighting	Lighting Load	Lighting load in the wing including open office, dry lab, conference and miscellaneous spaces	1,492
Tower Lighting	Lighting Load	Lighting load in the tower including wet lab, partitioned office, hallway and study area spaces	1,683
2^{nd} Floor Wing Occupancy	Occupancy	Occupancy schedule for the dry lab, open office and other spaces on the 2^{nd} floor of the wing	581
2^{nd} Floor Conference Occupancy	Occupancy	Conference room occupancy schedule	35
3^{rd} Floor Wing Occupancy	Occupancy	Occupancy schedule for the open office and gathering spaces on the 2^{nd} floor of the wing	500
3^{rd} Floor Conference Occupancy	Occupancy	Conference room occupancy schedule	30
Tower Offices Occupancy	Occupancy	Occupancy schedule for the tower partitioned office, student study, and meeting areas	616
Tower Wet Lab Occupancy	Occupancy	Occupancy Schedule for the tower Wet Lab and Fume Hoods	1114

As a first step in the study of occupancy and gains in the model, a sensitivity analysis was performed by uniformly scaling the schedules from 50% to 150% of their nominal values. As can be seen in Figure 38, an increase in gains results in reduced heating load, but increased overall energy consumption. An increase of 50% in overall gains results in approximately a 5% increase in energy consumption in the calibrated model, or more than 10% in the DCV model.

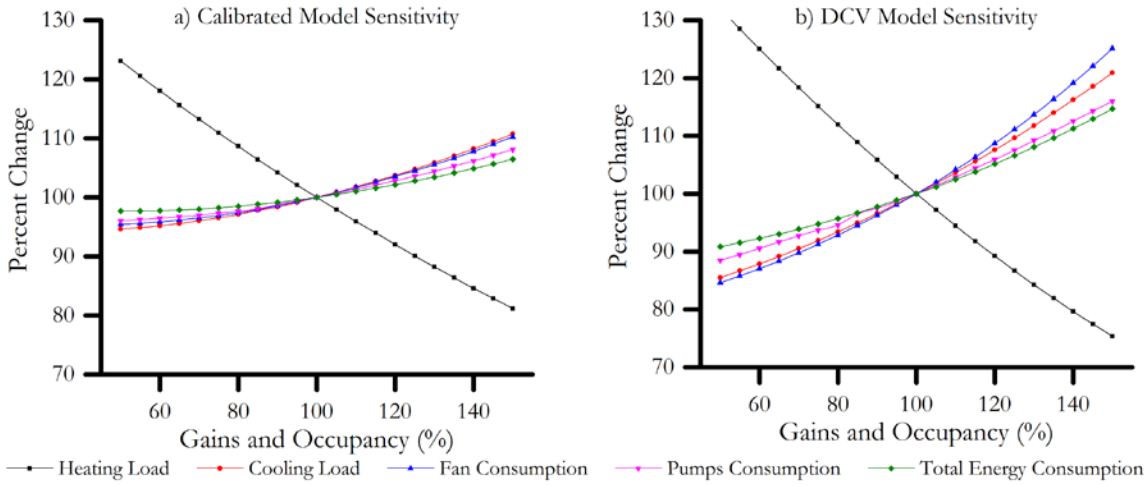

Figure 38: Model sensitivity to scaling of gains and occupancy

3.3.2 Schedule Statistics

Hourly calibrated schedules were created directly from the BMS data for each hour. Diversity schedules were used to fill the gaps in the data, which amounted to approximately 2,000 hours of the year. The diversity schedules were created for six day types: academic year weekdays, Saturdays, Sundays and holidays, and summer weekdays and weekends/holidays. The day types were chosen so that there were at least 20 complete days of data for each.

A closer study of the diversity schedules was necessary in order to determine the statistics relevant to a stochastic study of internal gains. The results are shown in Table 10. The best-fit distribution for electric gains was normal, while occupancy more closely resembled lognormal distributions. The means and scaling factors for each distribution are also shown in Table 10.

Table 10: Recorded data and schedule statistical characteristics for academic year day type

Name	Best-Fit Distribution	Area (m^2)	Daily Mean W/m^2 or People/10m^2	Daily Standard Deviation or Scaling Factor
Wing Electric	Normal	1,249	7.62	0.68
Tower Electric	Normal	1,683	7.67	0.35
Fume Hood	Normal	150	39.35	1.23
Server Rooms	Normal	30	46.59	5.72
Wing Lighting	Normal	1,492	6.21	0.46
Tower Lighting	Normal	1,683	11.29	0.66
2nd Floor Wing Occupancy	Lognormal	581	0.06	0.31
2nd Floor Conference Occupancy	Lognormal	35	0.11	0.75
3rd Floor Wing Occupancy	Lognormal	500	0.06	0.30
3rd Floor Conference Occupancy	Lognormal	30	0.02	0.83
Tower Offices Occupancy	Lognormal	616	0.11	0.73
Tower Wet Lab Occupancy	Lognormal	1114	0.09	0.40

The gains data are highly correlated. The levels of Pearson's correlation coefficient between occupancy schedules are up to 0.7, and the level of correlation between electric use and occupancy in separate zones is even as high as 0.4. This represented dependence in the levels between gains types and spaces, so in randomized generation of schedules the schedules could not be treated independently. It was important to keep this in mind when calculating the stochastic schedules, as explained further in Section 3.3.3.

3.3.3 Stochastic Simulations

Sample mean uncertainty was studied with the first set of Monte-Carlo simulations. A sample of thirty schedules was created with the statistics of the mean of the observed gains levels. For each day type, a vector of twelve standard normal random numbers was created, r. Then, the Cholesky decomposition, U, of the correlation matrix C, was found such that $U^T U = C$. The random numbers were correlated with Equation 3.3. The correlated vector of standard normal numbers

was used to create diversity schedules with Equation 3.4. Normality is assumed for the sample mean distribution because the sample size is greater than 20 for each day type and schedule. In Equations 3.3 and 3.4, i is the hour, while j is the day type and k is the schedule, with k = 1 to 12 representing each of the schedules in Table 10. $\bar{X}$ is the sample mean, S is the sample standard deviation, and n is the number of days in the sample.

$$\vec{v_j} = \vec{r_j}U \tag{3.3}$$

$$x_{i,j,k} = \left(v_j\right)_k * S_{i,j,k}/\sqrt{n_j} + \bar{X}_{i,j,k} \tag{3.4}$$

For the "population variance diversity schedules" set of simulations, the effect of uncertainty in the diversity schedule levels was expanded by using a sample size n = 1. This could be seen as the level of uncertainty that would result from using a one-day spot measurement as the diversity schedule level.

The "stochastic daily schedules" set of correlated stochastic schedules used the diversity schedule profile, but allowed each day's mean level to vary according to the population statistics by scaling the each day's schedules with a different vector of correlated random numbers, $\vec{v}$. For the gains, with normal distributions, the hourly levels were calculated with Equation 3.4 and n = 1 to represent the population statistics. The daily means and standard deviations are shown in the first six rows of Table 10. For the occupancy schedules, the lognormal distribution was used with Equation 3.5:

$$x_{i,j,k} = e^{\left(v_j\right)_k * \sigma_{i,j,k} + \mu_{i,j,k}} \tag{3.5}$$

The scaling, σ, and location, μ, factors are shown in rows 7-12 of Table 2.

The second method for representing the daily variation in gains levels was the random selection of profiles from the population of recorded days with complete data, called "random daily schedules," here. This method required no calculations other than the random selection

from the database of days. With this process, the correlation between schedules was naturally preserved. The distribution of the gains levels was also preserved. The profile of the schedule over the day, including arrival and departure times, became randomized according to the observed data rather than smoothed as in the case of a diversity schedule.

Finally, for a comparison between the effects on the model of variations in weather and gains, thirty years of weather data in the Pittsburgh region were simulated.

A set of thirty *.idf* EnergyPlus input files were created with hourly internal gains schedules for each of the above. The results of each batch of simulations show the degree of variation in model outputs that can be attributed to each variation in inputs. Figure 39 below shows the results for a summer day. The solid lines represent the calibrated gains taken directly from the data, the mean results for diversity schedules, the mean results for the random day method, and the mean results for the stochastic day method. The dotted lines represent the maximum and minimum outputs for each of the stochastic input sets. It can be seen that the variation in results due to variation in gains is significant. Each of the mean levels is close to the diversity schedule level, as could be expected because the diversity schedule is based on a mean of the data itself. The calibrated model, based on the actual data for the day, varies from the diversity schedule significantly, as do the maximum and minimum levels for the stochastic methods.

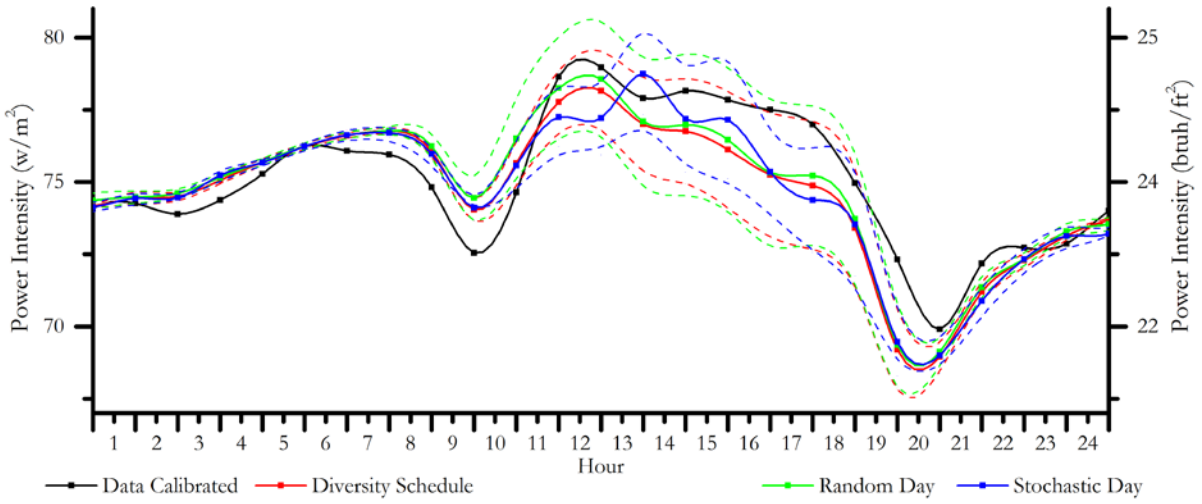

Figure 39: The energy consumption for different occupancy representations for the calibrated model

This shows that, as expected, the gains patterns can have a significant impact on the model output even when they are statistically representative of the data. Figure 40 shows the same day for the demand controlled ventilation case. For some time steps the model with data calibrated schedules falls outside the maximum and minimum for the stochastic methods, because the actual data deviated from the mean more than any of the schedules stochastically generated for this day.

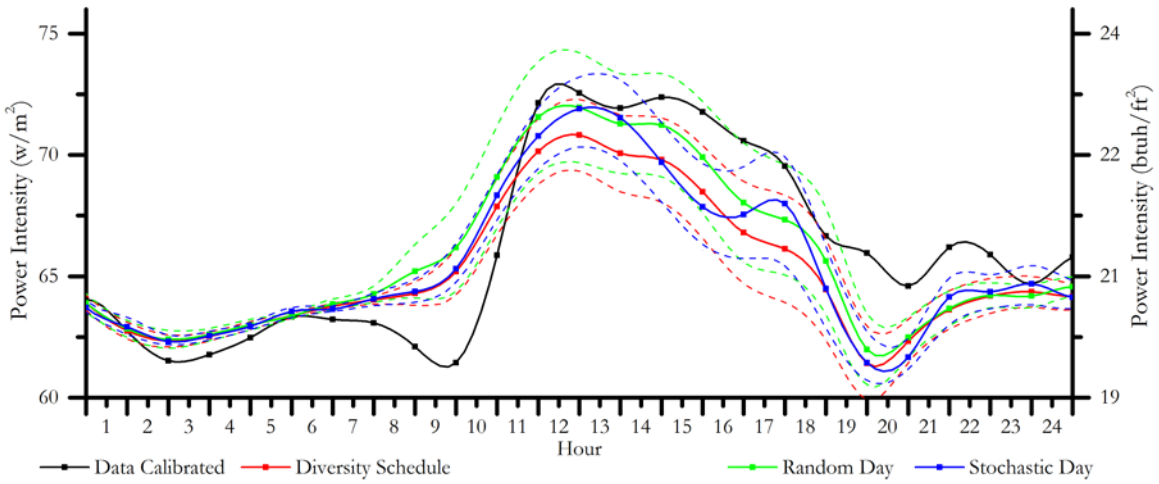

Figure 40: The energy consumption for different occupancy representations for the DCV case

Table 11 is a comparison of the results of the yearly simulation between the diversity schedule method and each of the stochastic methods. The mean bias error is the difference in total yearly energy use. These average values are small, which should be expected because the expected value of the magnitude of each input schedule is equal. The effects of randomness are demonstrated in the coefficient of variation of the root mean square error (CVRMSE) and the maximum and minimum bias errors. The input set with the highest uncertainty, population variance diversity schedules, shows yearly energy use from -0.45% to 0.85% from the mean. The CVRMSE represents the hour-by-hour difference between the outputs. The values range from 2 to 4%, a relatively small contribution to error but enough to make a difference in the calibration of the model. The minimum and maximum CVRMSE between the stochastic runs and the diversity schedule run are close together, indicating that variations in gains patterns have a uniform effect on this measure of error for this model. The DCV version of the model is about twice as sensitive to variations in gains as the standard version.

Table 11: Energy consumption comparison between stochastic representations and diversity schedules

Stochastic Representation	Statistic	Baseline Hourly NMBE	Baseline Hourly CVRMSE	DCV Hourly NMBE	DCV Hourly CVRMSE
Uncertain Sample Mean Diversity	Average	0.05%	1.47%	0.13%	2.94%
	Min	0.00%	1.45%	-0.05%	2.90%
	Max	0.14%	1.51%	0.29%	2.99%
Stochastic Daily Schedule	Average	0.33%	2.10%	0.01%	3.75%
	Min	0.30%	2.04%	-0.04%	3.66%
	Max	0.36%	2.17%	0.08%	3.87%
Random Daily Schedule	Average	0.02%	2.10%	0.08%	4.11%
	Min	-0.08%	1.90%	-0.06%	3.80%
	Max	0.09%	2.29%	0.28%	4.46%
Population Variance Diversity	Average	0.29%	2.09%	0.01%	3.73%
	Min	-0.45%	1.75%	-1.11%	3.21%
	Max	0.85%	2.42%	1.09%	4.53%
Thirty Year Weather	Average	-1.43%	9.73%	-0.41%	37.07%
	Min	-3.67%	0.00%	-4.58%	0.00%
	Max	0.00%	9.73%	5.29%	40.84%

The model is much more sensitive to weather data. The 2012 weather year was the most extreme simulated, and the difference between years was up to 3.6% in the base model and 5.3% in the DCV model. The variations in weather were enough to throw either model out of calibration – 10% in the base model and 40% for DCV.

Figure 41 compares the CVRMSE between the stochastic methods and the data calibrated model, with error bars for 95% confidence. The weather columns last bar is cropped for clarity in the scaling, with a value of 0.37 and interval of 0.14. These levels represent the hourly difference due to daily variations in gains levels not accounted for by day-type schedules. The levels range from 1.5% to 4%. There is a relatively small confidence interval for each method.

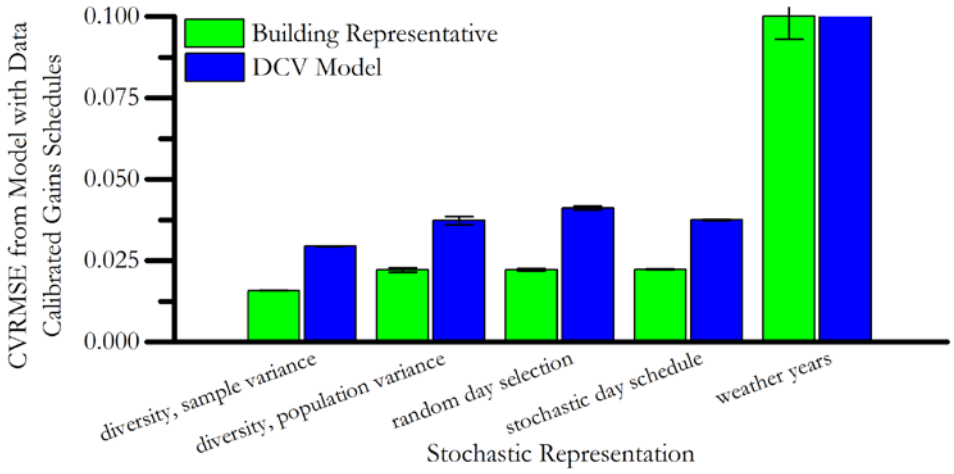

Figure 41: The mean coefficient of variation of each Monte-Carlo model run

4.0 REAL TIME ENERGY SAVINGS PREDICTIONS

The dashboard system at the MCSI was developed to show real-time feedback on the building's energy consumption, indoor environmental quality, and environmental impact. It combines wireless sensing and dynamic life cycle assessment (LCA). It gives an excellent, state of the art calculation of the running environmental impacts in several LCA categories, as well as total kilowatts. One goal of this project was to create the framework for implementing real-time energy modeling in conjunction with the other capabilities. Algorithms were developed for implementation in the dashboard that calculate the real-time energy impact of a number of scenarios. This would allow the user to see what the most energy efficient behaviors they could adopt are, and what the environmental impact of doing so would be. It would be both an educational tool and a practical way for occupants to reduce the building environmental footprint. The framework that is created can be used in conjunction with any detailed model, and could be implemented in the residential sector as well as the commercial. A different set of energy saving measures would be considered for a residential building, but there is great potential for the occupant to affect energy savings in this type of building.

A building dashboard application is a system that displays real-time building states such as energy consumption and comfort metrics. It often displays historical data and uses a graphical, user-friendly format, and may be internet based or developed for mobile devices. Some dashboards include energy targets or integrated remote controls. Much of the literature on these

systems focuses on the study of the disaggregation of energy consumption to end use or specific appliances, for display to the occupant. The ergonomics and layout of the systems are important in order for them to be adopted by and understandable to occupants, and this is also the subject of study. An ‘ecofeedback’ dashboard was developed for dormitory residents, and multiple variations of the application were tested, indicating a possible preference for consumption data that is disaggregated, and an easy view of historical consumption data [75]. Another study of a residential dashboard showed that a simpler form with dollar-feedback and appliance specific data was preferred [76]. One dashboard used a virtual environment combined with physical sensors to display energy consumption [77]. The display of real time energy data alone can result in a 2% to 11% reduction in consumption [78].

4.1 SCENARIOS

Using the calibrated model as a baseline, eleven alternative models were created to represent the scenarios in Table 12. These include six occupant behaviors or choices such as changing the shading or temperature set point. The other five scenarios are operational characteristics of the HVAC system or changes to the physical building, including night setback, demand control ventilation, and insulation levels. The scenarios were chosen to provide a range of understandable options to the dashboard user for exploration. They include hands-on measures that a building occupant can control independently, and aspects of the green building and systems of which the user may be less aware.

Table 12: Behavior and operations scenarios

Scenario	Description
Shading	Interior roll blinds, 20% transparent, rolled down over sun-facing windows
Shading 50%	Interior roll blinds, 40% transparent, rolled down over sun-facing windows
Temperature Decrease	Interior space temperature set-points decreased by 1 °C
Temperature Increase	Interior space temperature set-points increased by 1 °C
Widen Temperature Band	Upper set-point increased and lower decreased by 1 °C
Decrease Plug Load	10% reduction in space electrical loads, not including server room equipment
Night Temp Setback	2° C setback from 9 PM to 7 AM
Less Reflective Roof	Roof material with 50% increased absorptance
Increase Insulation	Insulation with 50% increase in thickness
Daylight Dimming	Continuous dimming in office, open office and dry lab spaces
Demand Control Ventilation	Demand controlled ventilation in office, open office, dry lab, and wet lab spaces.

The shading scenarios were created by applying partially translucent roll down blinds to the large windows of the wet lab, offices, and conference rooms. Many of these rooms already have similar blinds that are infrequently adjusted. There were two shading scenarios – one with 20% transparency and one with 40% transparency, to represent a case where the blinds are only half way down. The second set of scenarios regarded temperature set points. One scenario increased all temperature set points by 1 °C, one decreased the temperature by the same amount, and one widened the set point band by 1 °C in each direction. These two sets of scenarios, shading and space temperature set points, were regarded as the most practical behavioral changes by occupants. The MCSI building has very few features that allow interaction between the occupant and the interior environment. There are, however, thermostats and blinds. The other scenarios are more hypothetical changes for education and demonstration.

Decreasing the plug load is also theoretically under the control of the occupant, although it might require the purchase of new appliances. This scenario was modeled by decreasing the space plug loads, excluding the server rooms, by 10% throughout the building. This might be achieved through Energy Star appliances or by using sleep mode and power strips more

effectively. Night temperature setback is not under the control of the occupant in this building, however it is an important energy saving scenario, which is not implemented in the current building control scenario. All temperature set points were set back by 2° C from 9 PM to 7 AM. The building is open during these hours, but there are few occupants.

Finally, several design scenarios were considered. The roof reflectance was considered. Currently there is a high albedo roof installation, which is considered green. The alternative scenario is a less reflective roof with 50% increased absorptance. Increased insulation is another scenario, with the thickness of the exterior insulation layer increased by 50%. The daylight dimming scenario uses the illuminance calculations of light entering the spaces through windows to automatically dim the lights. The amount of power consumed by lighting diminishes linearly with the amount of exterior light reaching the center of the spaces. Finally, demand controlled ventilation was a scenario because this is a widely used, highly energy efficient control strategy. This strategy monitors CO_2 levels in the building and adjusts the outside air rate to keep the indoor concentration of CO_2 below a predetermined level. For the implementation in Energy Plus, the minimum outside air rate for each space is the sum of the per-area code requirement for the space type and the per-person amount multiplied by the occupancy rate. This is an ideal simulation of demand controlled ventilation, because CO_2 levels are not simulated directly.

A survey conducted by the BUILD group shed light on the willingness of some occupants to undertake behavior interventions and building changes. Occupants were asked to respond, on a scale of one to seven, how several hypotheticals would affect their productivity. A higher score indicated a perceived positive change. There were 48 respondents in the MCSI. Increasing the summer temperature received a mean score of 4.6, indicating that the space is over-cooled and occupant control would both save energy and result in a more comfortable space. Decreasing the

winter temperature received a score of 2.9, indicating little receptivity to the idea. Increasing the amount of daylighting received a score of 5.3 and using automatic lighting controls received a score of 4.1, indicating slightly positive reactions to both [79].

Figure 42 shows the average energy savings or cost for each scenario compared to the baseline, calibrated model. The shading scenarios actually add to the total energy consumption, by increasing the need for reheat, although there are many times for which shading is preferable. This is the type of scenario that requires occupant education on when to use it. The biggest energy saver is the demand controlled ventilation, because of the reduced flow rates associated with it.

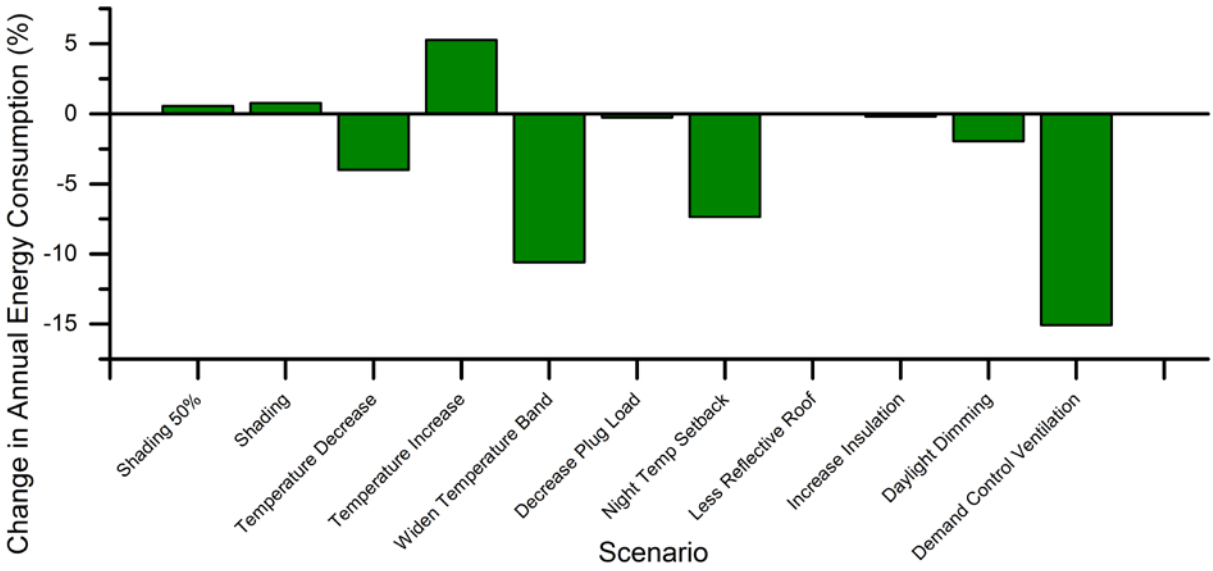

Figure 42: Average energy savings for each scenario compared to the baseline

4.2 NEAREST NEIGHBOR APPROACH

The first attempt at predictive modeling took a unique approach that can be referred to as a nearest neighbor search. A database of entries was created from the sensed data and the corresponding time steps for the calibrated model and each scenario. For a given time step and set of data obtained by the dashboard, the database would be searched for the closest corroborating model time steps. The savings for that time step would be considered to be similar to the savings for the nearest fitting model time steps. This would eliminate the need for full modeling of each time step in real time, but introduce computational intensity through the search algorithm.

Further, rather than simply looking at the potential savings for the immediate adoption of a scenario, the method would use the nearest neighbor time step and the two following it to make a prediction of the trend in energy consumption for the baseline and the scenario over the next three hours.

The database was an aggregation of the time-step results of the parametric building modeling. Each parametric run was divided into entries with initial times offset by one hour and including 3 hours of outputs. The entry fields were the set of initial conditions for the first time step and the set of outputs for the following time steps. The initial condition variables included weather and building conditions: outside temperature and relative humidity; wind speed; wind direction; diffuse and direct solar radiation; time; day of year; day type; occupancy level; and electric and lighting gains. The outputs included: electric consumption by end use; chilled water consumption; hot water consumption; and total energy use, although primary concern was given to the total energy use. The outputs for each entry were repeated for the baseline and for each parametric ECM run.

The prediction algorithm was a simple process of first disqualifying entries that did not meet minimum constraints for the initial condition variables, and then ranking the remaining entries based on a linear function of the difference in each variable (equation 4.1):

$$z_j = \sum_{i=1}^{n} w_i \left| x_{0,i} - x_{j,i} \right| \quad (4.1)$$

For the database entry j, the indicator of the match with current conditions is z_j, the database entry initial variables are $x_{j,i}$ for variable i from 1 to n, the measured state of the building is $x_{o,i}$, and the weighting factor for the initial condition i is w_i. When the several top ranking entries have been chosen, the average for each time step was the single output prediction profile for display on the Dashboard.

The algorithm was optimized for the weighting factors w_i. This optimization problem was attempted in Matlab. The objective was to minimize the CVRMSE of the error between the algorithm-predicted output and the simulated output for each time step in the prediction. The output for this optimization was the difference in energy consumption.

The large amount of simulated results data was used for the optimization. A Matlab function selected n time steps at random from the simulation results and ran the search and regression algorithm for each. The CVRMSE over the time period will be calculated for each prediction (i = 1 to n) and the cost function will be the root mean square of these errors, as shown by equation 4.2.

$$min \sqrt{\frac{1}{n} \sum_{i=1}^{n} CVRMSE_i^2} \quad (4.2)$$

s.t. $w_i \geq 0$

The Matlab optimization toolbox was first used to find the weighting factors. A number of approaches were taken, including the genetic algorithm, interior point, and trust region reflexive methods. Because each search took on the order of one second, and many searches

were required to find the cost function, each optimization required over 24 hours to run and still did not meet the standard convergence criteria. One attempt at a custom optimization method was completed, with a Matlab script. The approach was to evaluate the gradient of the cost function in each dimension, and move in the dimension with the highest negative change. When no direction was negative, the interval was decreased. Each method resulted in a different set of weighting factors, but with a similar cost.

When evaluating the resulting weighting factor sets, they did not meet basic criteria for accuracy. When the predictions using any set of weighting factors was compared to real data, it was found that predicting no change was more accurate than the predictions obtained with the nearest-neighbor approach. This was despite an overall error of around 5%. After numerous attempts at improving the weighting factors, adjusting the amount of data used, and changing the initial conditions used in the search, the method was abandoned.

It appears that despite the large number of instantaneous initial conditions used in the search, there were too many unpredictable variables that affected the energy consumption to allow for prediction using this simple method. Not least of these variables was likely the weather, which cannot be predicted with this limited data. Also, there are transient effects in the building dynamics and occupancy that were not accounted for.

The goal of making a dynamic prediction was abandoned at this point, and a simpler approach of making an instantaneous estimate of the energy savings for each scenario was attempted. This could be done by creating a function fit to the model data based on the same initial variables. A polynomial fit to this high-dimension, non-linear model was not sufficient, so neural networks were used.

4.3 NEURAL NETWORK APPROACH

As the first step in creating the inputs for training neural networks, each model was simulated for three sample years. These were the weather years from 2010 to 2012. Different hourly electric, lighting and occupancy schedules were developed for each year, based on the gains data recorded by the building automation system (BAS). Days of recorded schedule data were divided into day types. Then, each new stochastic annual schedule was created by randomly assigning data days to each day of the simulation year, according to day type. This method preserved the statistical properties of the gains data while also representing random variations present in occupancy and building use and creating three unique schedules. Each model was simulated for the three sample years and the results were integrated by the hour. The first two simulation years were used for training neural networks, and the third only for validation.

The network architecture was feedforward backpropagation, with the Levenberg-Marquardt training algorithm [80]. Artificial neural networks (ANNs) consist of multiple layers of nodes, connected with weighting factors and biases. In a feed-forward, back-propagation ANN, there is an input layer, one or more hidden layers, and an output layer. For a three layer, single output network the output of each hidden layer node is given by Equation 4.3:

$$y_{1,i} = \frac{2}{1-e^{-2(a_{1,ij}x_j+b_{1,i})}} - 1 \qquad (4.3)$$

Here, $y_{1,i}$ is the output of hidden layer node i, $a_{1,ij}$ is the first weighting factor for node i, input j, x_j is the input j, and $b_{1,i}$ is the second weighting factor for hidden node i. The output layer, which in this case consists of a single node, is represented by Equation 4.4:

$$y_2 = \frac{2}{1-e^{-2(a_{2,i}y_{1,i}+b_2)}} - 1 \qquad (4.4)$$

Here, y_2 is the output, $a_{2,i}$ is the first weighting factor for the input from hidden node i, and b_2 is the second weighting factor for the output layer.

The artificial neural network is characterized by the architecture, the number of nodes and layers, and the weighting factors. The weighting factors can be chosen by one of a number of training algorithms using sample data. The Levenberg-Marquardt algorithm was used in this study. This algorithm minimizes the root mean square error in the outputs of the ANN for the training data set, compared to the actual training outputs. It interpolates between the Gauss-Newton algorithm and the method of gradient descent.

Each time step formed an input-target pair, with the inputs being: outside air dry bulb temperature, outside air relative humidity, wind speed, wind direction, diffuse radiation, direct radiation, occupancy, day of the year, hour of the day, plug load, lighting load, fans consumption rate, heating load, cooling load, and total energy consumption. Each of these is monitored by a weather station and the MCSI BAS. The targets for training the networks were the total and individual end use energy consumption savings ratios. This ratio is the difference between the baseline and scenario energy consumption for the given hour divided by the baseline consumption.

The training module randomly divided the two years of training inputs into 80% training entries, 10% validation entries, and 10% test entries. It stopped training when a mean square error of the test data started to record an increasing level of error, thereby preventing overtraining. To find the optimal number of nodes, parametric runs for two to forty nodes were completed as shown in Figure 43. For each model, twenty was found to be an adequate hidden layer size. Adding multiple hidden layers did not increase the accuracy of the fit to the data.

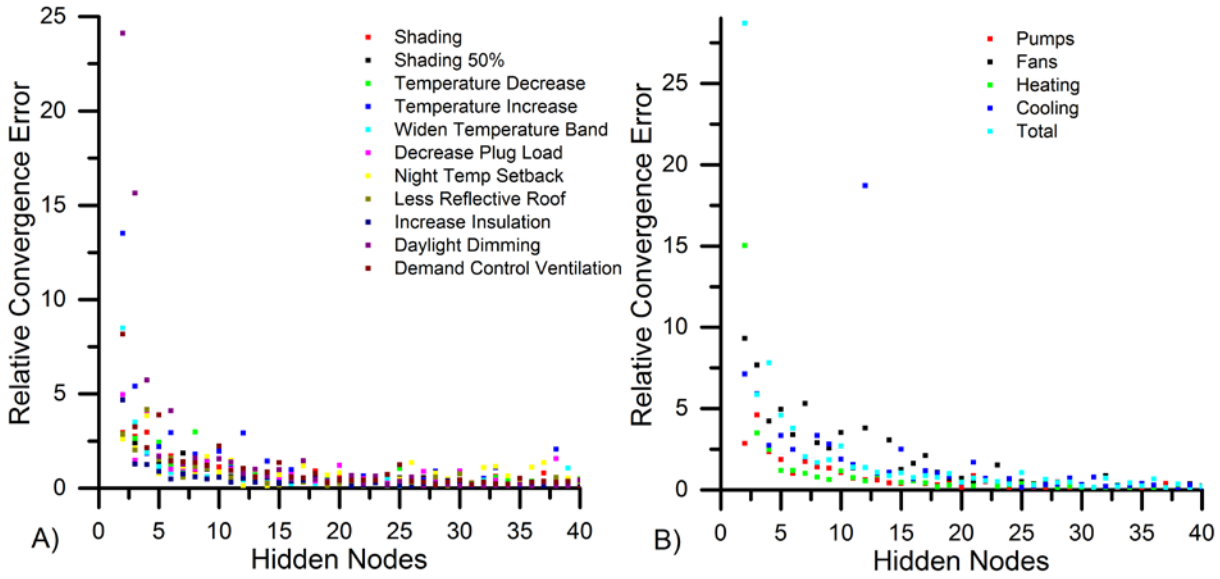

Figure 43: Error as a function of the number of hidden nodes for a) each scenario, and b) each end use in the day light dimming sample scenario

Finally, the neural networks were run for the entire third year of input data and the resulting outputs were compared to the simulated savings for each hour. This comparison of an entire year of simulation data was used to estimate the CVRMSE and bias error, normalized to the average savings ratio.

4.3.1 Results

The neural network fits to the model output of total energy consumption were tested for an entire simulation year not used in training, and the results are shown in Figure 44. The mean bias error for the neural network approach was less than 6% for all of the scenarios tested. This indicates that on average, the functions estimate the savings for each scenario well. The CVRMSE is calculated by normalizing with the average energy savings, which is relatively small in some cases, and indicates a higher degree of uncertainty for some of the scenarios. Demand controlled

ventilation and the temperature set point changes have a low CVRMSE, indicating a close fit over most of the time steps. Increasing insulation, daylight dimming, and decreasing the plug load have slightly higher CVRMSE of approximately 20%. The networks don't fit to the night temperature setback as well as the other temperature scenarios because the neural networks have trouble discriminating between night and day time steps with high precision. The effects of insulation and wall thickness are highly dynamic, and therefore may not be approximated by the static fit as easily. Shading has a higher CVRMSE because of the complicated solar angle and dynamic building interactions, as well as a relatively low normalizing factor. The scenario with a normal roof rather than the high albedo green roof also has a very low normalizing energy savings ratio.

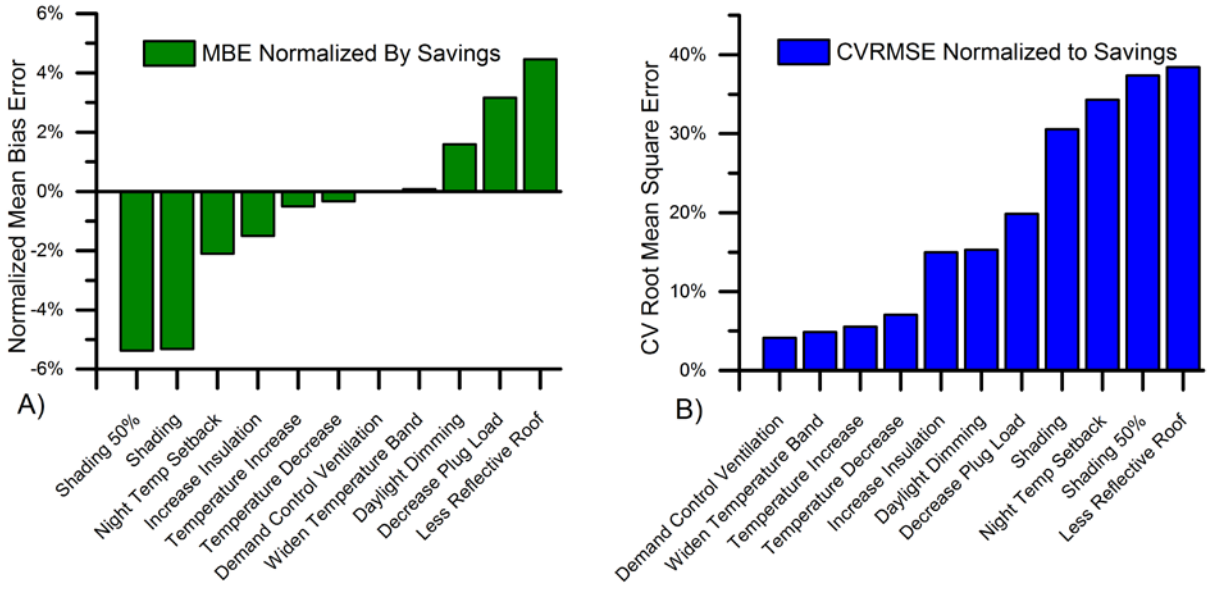

Figure 44: Error for an annual test of the neural networks for each scenario

Figure 45 shows the breakdown of networks trained to each energy end use for the daylight dimming scenario, which had a medium overall error. The largest level of energy savings is in

the lighting category, and the smallest normalized errors are in this category. This indicates that the network predicts the sunlight levels and resulting lighting energy savings with good accuracy. The higher normalized errors are in the secondary energy categories. There is a higher level of interactions in these categories, in addition to lower normalizing savings ratios. The highest NMBE and CVRMSE are for pumps, which are a small proportion of the energy savings. The fans and cooling also have high levels of error, and are secondary energy impacts of the measure. The heating level is more predictable, probably because the reheat, which constitutes the majority of heating consumption, is more directly related to the level of energy spent on lighting in the spaces. The total errors are calculated separately, and are relatively small because the largest component is the more predictable lighting system.

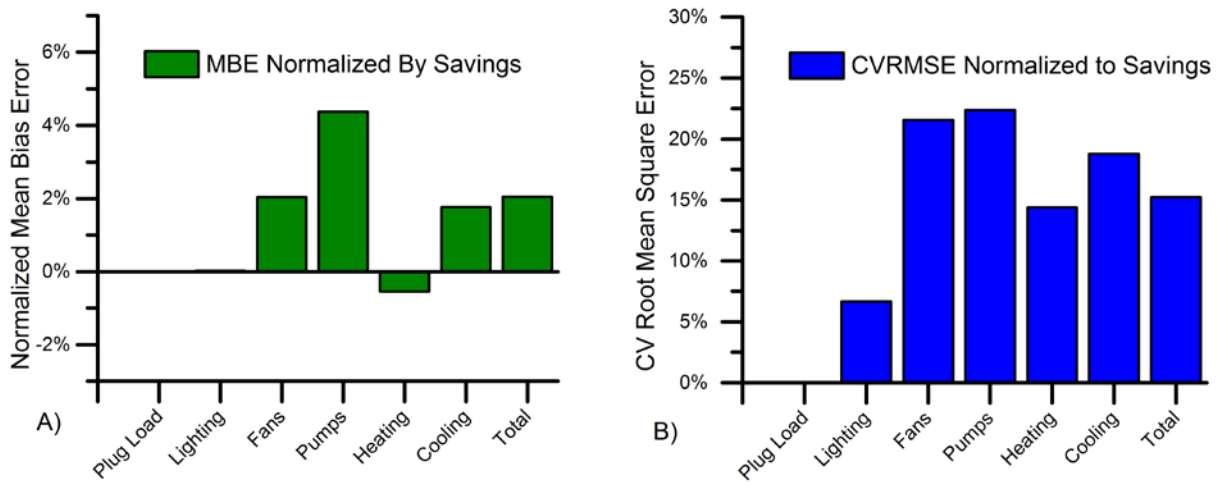

Figure 45: Error for an annual test of the neural networks for each end use in the daylight dimming scenario

The R-squared values were calculated for each input to explore the impact of each on the prediction capability of the neural networks. A single input neural network was trained for each input, and the R-squared value for each and for the combination of all inputs is shown in Table

13. Dry bulb temperature, solar radiation, hour of the day, and heating and cooling loads have high R-quared values. The wind speed and direction, relative humidity, and plug and lighting consumption have lower R-squared and may be unnecessary as inputs. Some inputs are only useful in predicting savings for certain scenarios, such as day of the year and increasing insulation.

Table 13: R-Squared values for individual inputs

	Shading 50%	Shading	Temperature Decrease	Temperature Increase	Widen Temperature Band	Decrease Plug Load	Night Temp Setback	Less Reflective Roof	Increase Insulation	Daylight Dimming	Demand Control Ventilation
Dry Bulb	.27	.39	.55	.55	.72	.54	.02	.42	.88	.42	.66
Relative Humidity	.03	.03	.16	.13	.05	.19	.01	.14	.03	.15	.03
Wind Speed	.01	.01	.02	.02	.03	.01	.02	.01	.03	.01	.02
Wind Direction	.03	.02	.02	.03	.05	.01	.02	.02	.04	.01	.04
Diffuse Rad.	.29	.20	.35	.27	.02	.34	.57	.32	.12	.50	.01
Direct Rad.	.28	.27	.43	.36	.04	.38	.36	.37	.11	.54	.01
Occupancy	.19	.14	.31	.27	.03	.30	.21	.20	.02	.34	.07
Day of the Year	.10	.14	.07	.04	.59	.18	.01	.07	.72	.13	.35
Hour of the Day	.25	.15	.34	.29	.04	.30	.82	.32	.03	.39	.05
Plug Consumption	.17	.13	.24	.22	.05	.25	.17	.13	.04	.27	.09
Lighting Consumption	.22	.15	.34	.30	.04	.31	.28	.24	.03	.36	.09
Fan Consumption	.40	.49	.65	.61	.47	.60	.10	.59	.60	.61	.23
Pump Consumption	.30	.43	.52	.53	.68	.51	.07	.39	.86	.45	.61
Heating Load	.33	.46	.69	.60	.54	.71	.07	.57	.70	.65	.43
Cooling Load	.26	.38	.46	.46	.69	.49	.03	.34	.87	.42	.63
Total Power	.10	.16	.16	.20	.16	.12	.02	.13	.12	.11	.33
Total Combined	.90	.93	.99	.99	.96	.98	.97	.87	.97	.99	.97

Sample time steps were chosen for winter and summer afternoons to explore the impact of uncertainty on the results and possible display methods for the dashboard user interface. Figure 46 is a bar graph comparing the total energy consumption for each scenario for the two time

steps. The error bars indicate the 75% confidence intervals. The uncertainty range is very large for the night temperature setback scenario, but for most of the models, uncertainty is small compared to the energy savings. Implementing demand controlled ventilation is by far the most energy-saving measure for both winter and summer time steps and its confidence interval is large in magnitude. This figure mimics one possible mode of data presentation on the dashboard device: total magnitude of energy consumption for a variety of different scenarios. Only the real-time data set would be displayed, or the real-time data and annual consumptions for each scenario.

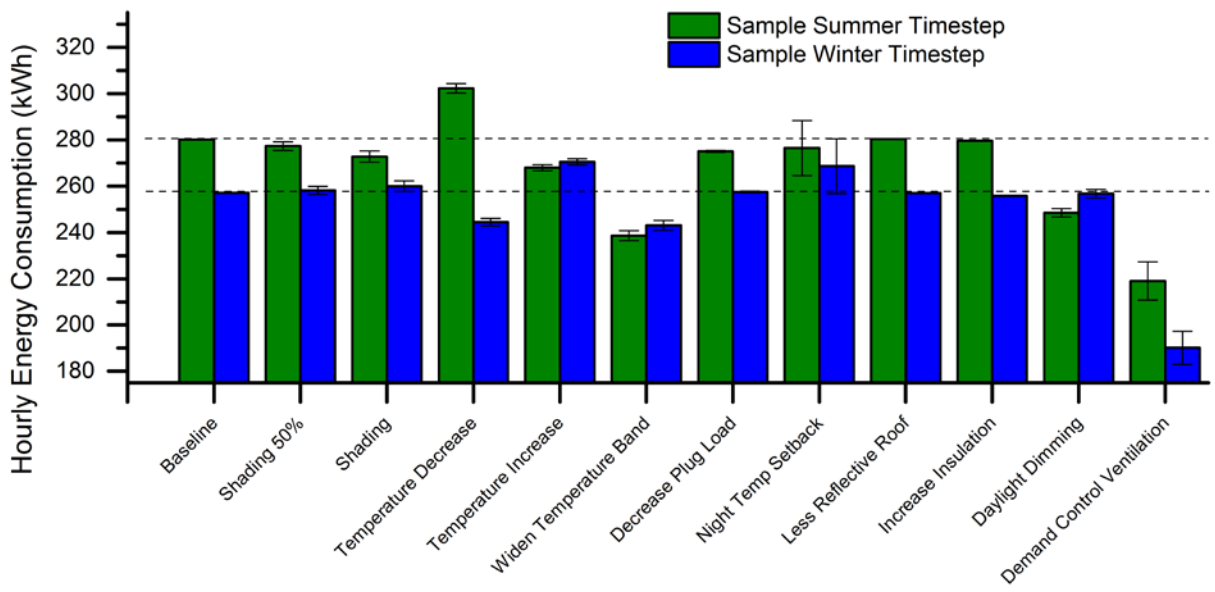

Figure 46: Hourly end use energy for each scenario for sample summer and winter time steps

Figure 47 shows a more in-depth look at the two time steps for the daylight dimming scenario. Again, error bars represent the confidence intervals. There is no change or uncertainty in the plug load, which is unaffected by lighting. There are significant lighting savings in both winter and summer. In summer, the reduction in internal loads results in lower cooling load and a lower

ventilation rate, reducing the consumption for fans and pumps. The reheat is higher, because of the fixed supply air temperature, minimum ventilation rate, and significant reduction in internal gains. For the winter, there is a similar reduction in lighting consumption, a small relative increase in heating consumption and a large relative increase in cooling consumption. To meet the increased heating load, a higher ventilation rate is required. The cooling is negligible in the winter but the small relative increase in heating load negates most of the energy savings from lighting for this time step.

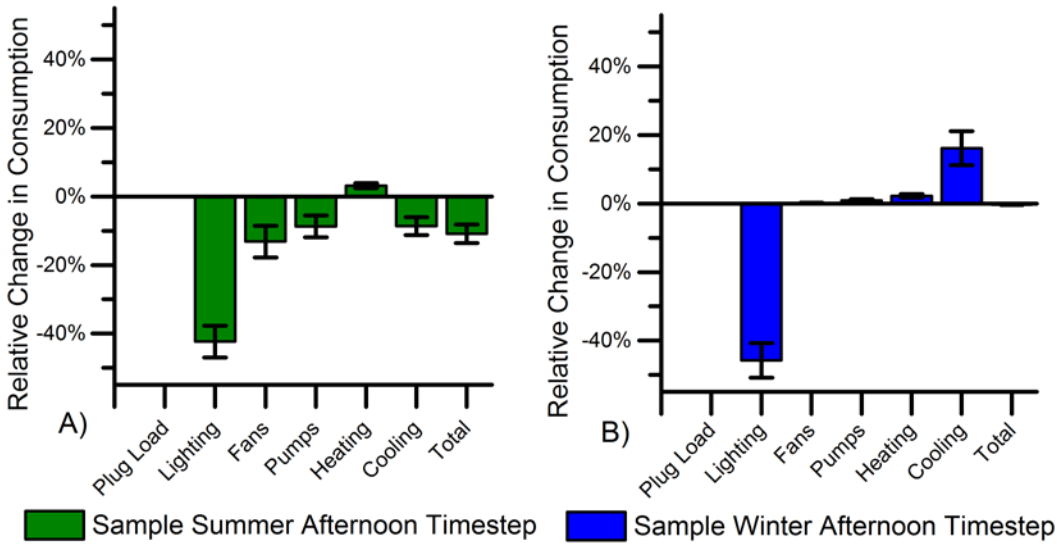

Figure 47: Relative change in end use consumption for the daylight dimming scenario in a) summer afternoon and b) winter afternoon time step

Each display has its advantages, but both provide both an overview of the energy savings due to behavior and operational changes, and an opportunity for more in-depth study of the building dynamics. The uncertainty ranges are not large enough to obscure the meaning of the results. However, in creating a real-time function to evaluate the measures that does not rely on co-simulation, the dynamic aspects of building systems interactions were lost. The 20-node neural

networks are comparatively simple functions that can be implemented in most programming languages. The modeling and training process was not computationally intensive, and can be repeated for any dashboard of a building with an up to date building model.

4.3.2 User Interface

An outline of the proposed dashboard user interface is shown in Figure 48. The first step is choosing the scenario or scenarios for comparison. This is followed by the option to display real time or annual data. The annual data is for a typical year, and shows the average effectiveness of each scenario, while the real time shows the instantaneous effectiveness for the current conditions, as calculated by the neural network algorithms.

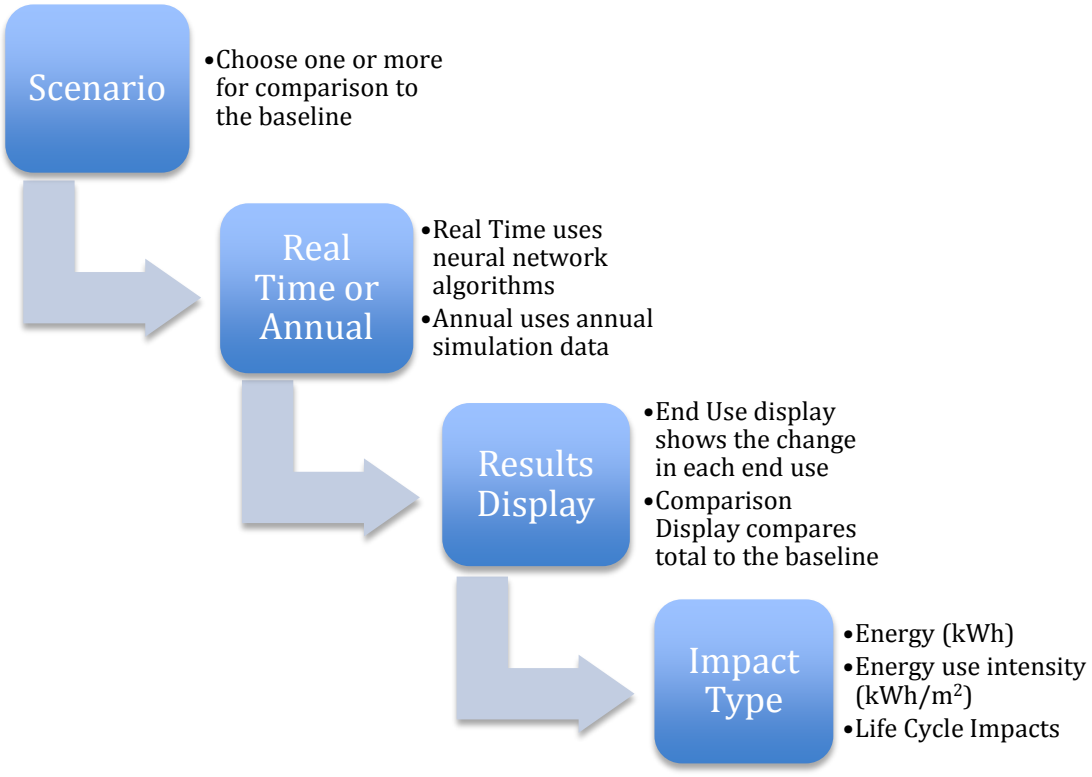

Figure 48: User interface flow diagram

Next, there are several options for the display of results. First there is the choice of end-use display, as exemplified in Figure 47. The other option is the total energy display, as was shown in Figure 46. Finally, there is a choice of units. The total energy consumption can be displayed in kWh or normalized by floor space. In keeping with the dashboard project's theme of life cycle assessment, the energy calculations can be integrated with impact factors and dynamic life cycle assessment to determine the life cycle impacts for the building under each scenario.

The user interface and algorithms have not been applied to the dashboard at this point. There is no direct link between the dashboard and the BAS, although the dashboard application framework is in place. This is due to permission issues with data sharing and transfer. This programming aspect of the dashboard project is beyond the scope of this particular work. However, the algorithms and framework here are ready for installation and can be repeated for any building with a calibrated building model.

4.4 CO-SIMULATION

4.4.1 Dashboard-Informed User Behavior Algorithms

Using MLE+, described in Section 1.2.5, it was possible to simulate the behavior of a building occupant using the dashboard. For every time step, EnergyPlus was configured to output all of the inputs required by the dashboard algorithms as well as the occupancy and thermal comfort levels. A Matlab script read them, and decided to change certain actuators based on the simulated actions of the occupants. These actuators were the shading and temperature set points, to examine the use of the dashboard with the corresponding scenarios.

For temperature setback, the control rules were as follows. If the thermal comfort was projected to be acceptable to over 80% of the occupants and the dashboard showed that energy would be saved by changing the temperature by one degree in any direction, the occupant did this. If at any time the thermal comfort left the acceptable range, the set-point temperature reverted to the default. The occupants only made changes when the occupancy level was above five people in the whole building. For shading, the rules were similar. If the dashboard indicated that changing the shading would save energy, the occupant did so.

For each of these scenarios, the perfect occupant control was for every timestep. There were twelve time steps per hour, so this meant that the occupant would be checking the dashboard every five minutes. To see the impact of different frequencies of occupant attention, first, regular intervals from 1 to 4 hours were simulated. Then, sets of random frequencies with average interval times from 1 to 4 hours were simulated.

4.4.2 Analysis of Results

For the regular decision intervals, it can be seen that the effectiveness of the dashboard for temperature changes becomes slightly lower with a higher decision interval (Figure 49). The energy savings is on the same order for each season, but the summer both has the most energy saving potential, and is the most sensitive to decision interval. Spring most likely has the lowest energy savings due to its mild conditions, and use of economization to achieve thermal comfort rather than mechanical heating and cooling. Note that each time step is five minutes, and the intervals start at midnight.

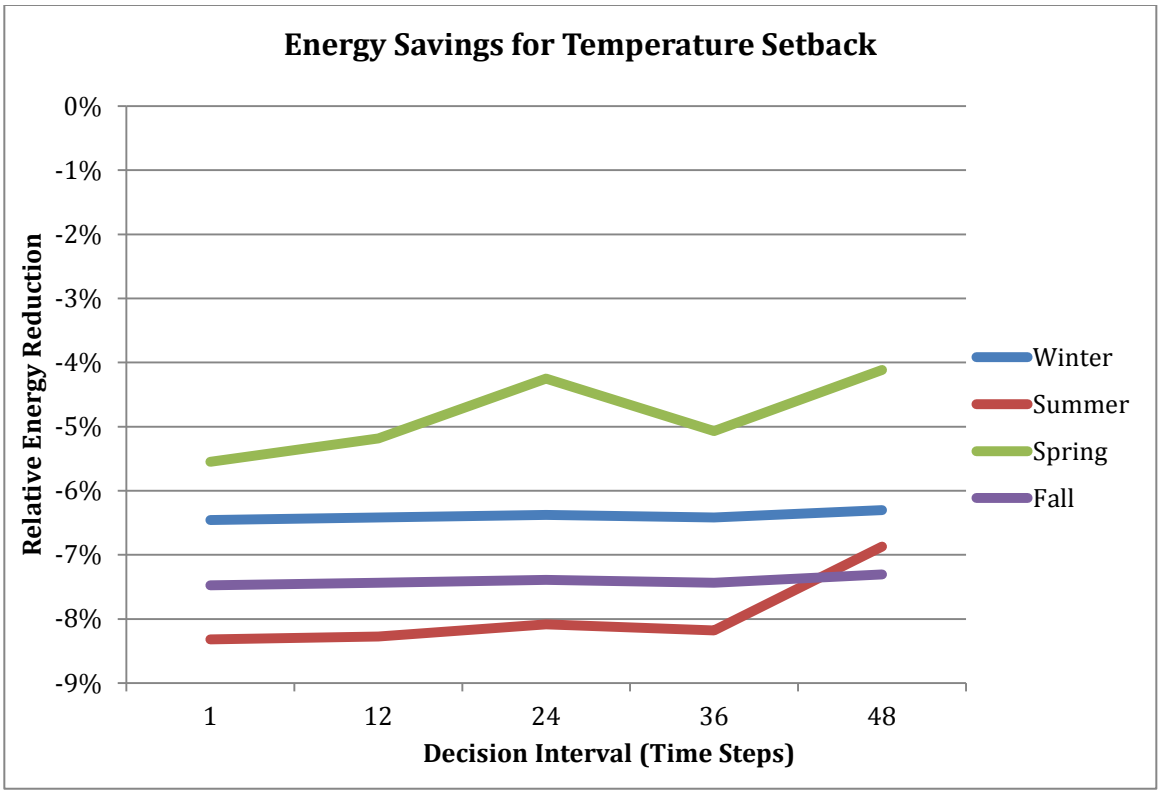

Figure 49: Co-simulation results of temperature setback by regular decision interval

Figure 50 shows the corresponding time intervals for shading. There is no clear trend in the data. This may be because of the interaction between the building schedules and the intervals, which start at midnight. The spring is the only season with clear energy savings. This is counterintuitive, but not entirely unexpected since the shading scenarios result in an overall increase in energy consumption when shading was applied for the whole year (Figure 42). It does indicate that the dashboard does not function optimally, however. Ideally, the change should be zero but never positive because shading should not be implemented if the dashboard indicates a positive change in energy consumption. The positive increase could be because at a particular decision interval, shading was effective, but it quickly became ineffective before the next interval, wasting energy. More likely, it could also be because of error in the dashboard

algorithms resulting in poor occupant decisions. The very small margins of energy savings may contribute to the frequency of these errors.

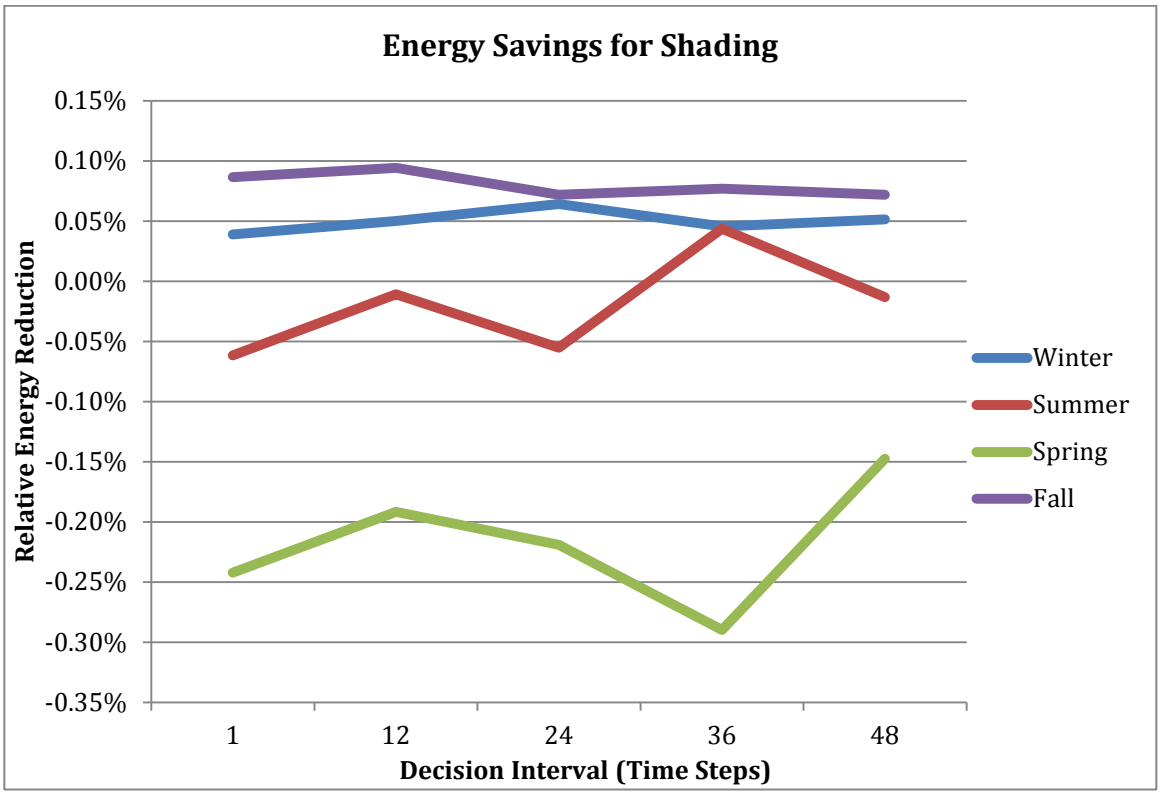

Figure 50: Co-simulation results of shading by regular decision interval

To better simulate the actual behavior of occupants, the models were run stochastically with set probabilities of an occupant looking at the dashboard for any given step. This approximates an exponential distribution. The average interval is on the x-axis of Figure 51. This figure shows the shading scenario in the spring. Note that the green point is the building operation with shades down for the whole week. The red is the average of each set of simulations. There is no clear trend, but it is clear that the use of the dashboard is what allows the

shading to save energy – without intelligent use of the shades, they actually cost the building energy.

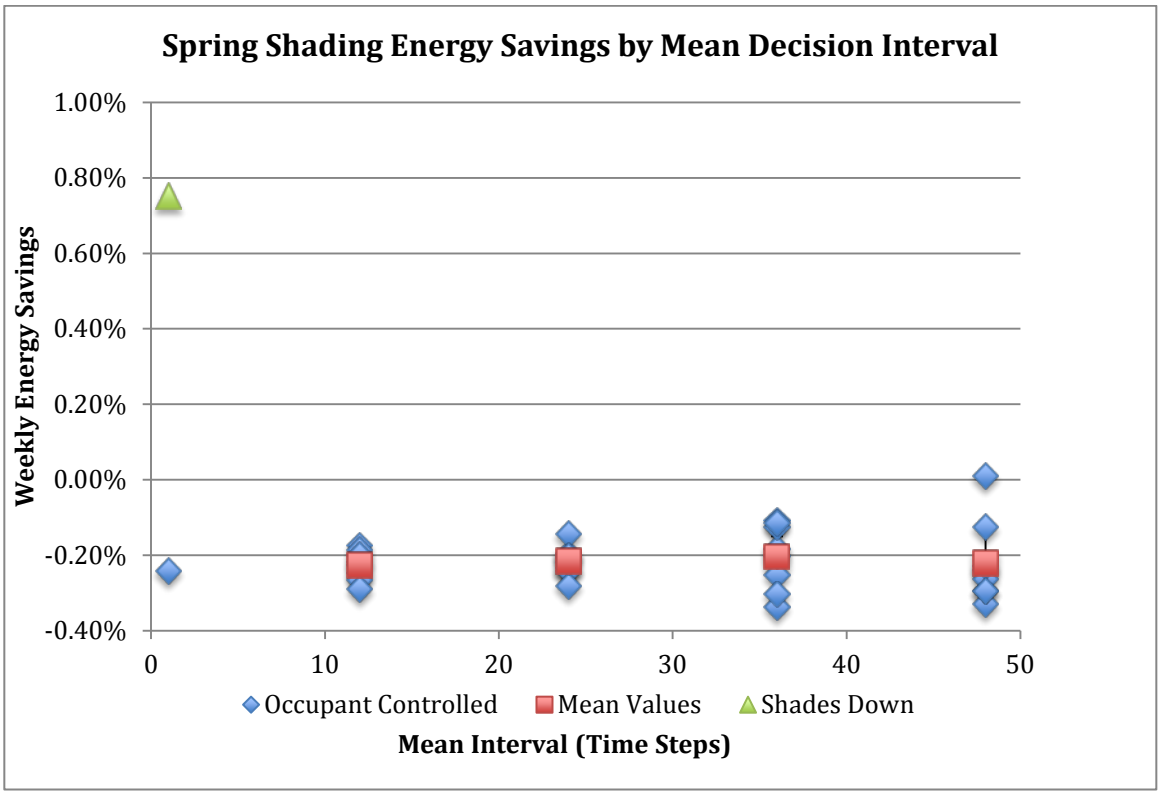

Figure 51: Spring co-simulation results of shading for stochastic decision intervals

Figure 52 shows the same graph for the summer. The only energy saving operation of the shades is the perfect use of the dashboard every five minutes. Less frequent use costs energy, although there is no clear trend with increased interval. Keeping the shades down all week has the highest energy consumption, so infrequent dashboard use is an improvement over this option. There is very little difference in energy consumption, however, with all scenarios under 1% difference.

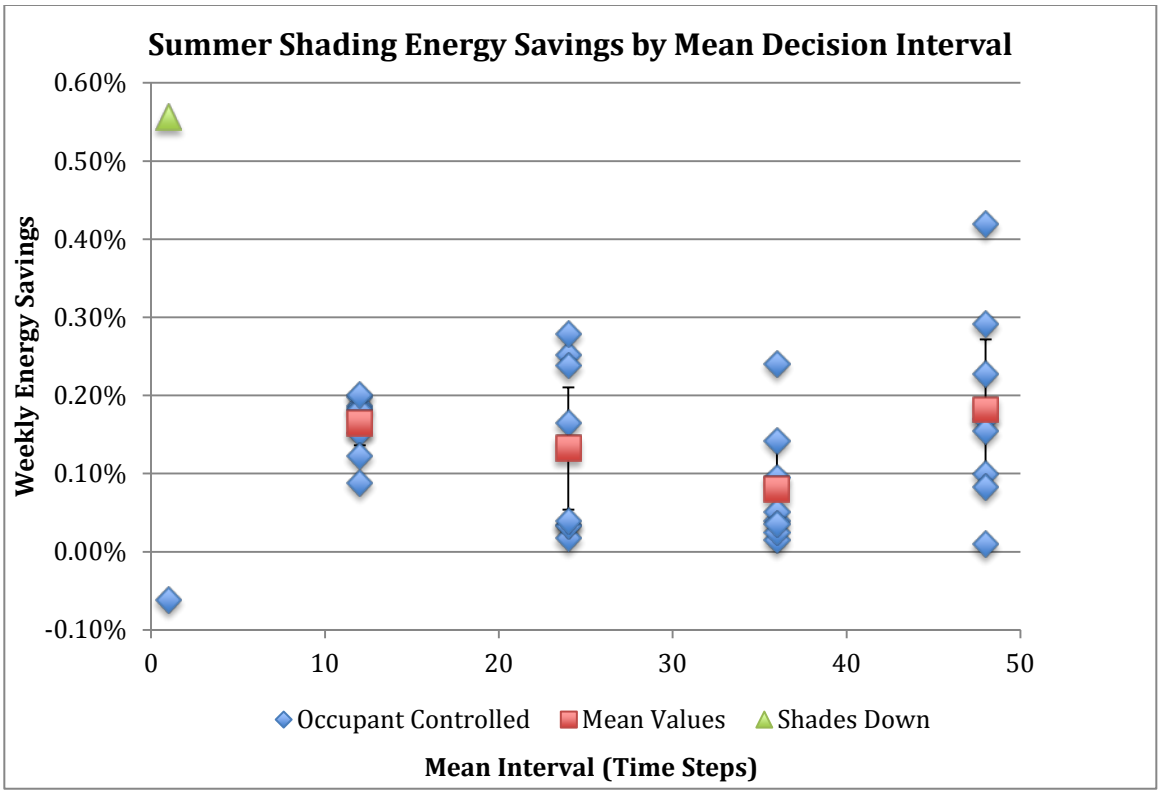

Figure 52: Summer co-simulation results of shading for stochastic decision intervals

The results show that for a scenario such as shading, with complicated interactions between the heating and cooling systems of the building, the dashboard can result in energy savings. In the spring there is no significant sensitivity to the interval at which the dashboard is used, at least under four hours. In the summer, when there is very little energy to be saved, the only way to use it effectively is to check the dashboard at every time step. For temperature setback, it is clear that there is less sensitivity to the decision interval. There is also a much greater margin of energy savings, with savings in every season.

5.0 CONCLUSIONS AND FUTURE WORK

5.1 CONCLUSIONS

This work studied the advancement of building energy modeling to improve the accuracy of the simulation of energy conserving concepts. The study started with the small scale simulation of a roof solar chimney, validating it with corresponding mathematical and computational fluid dynamics models. The model was then expanded to simulation in a whole building, so that interactions with the rest of the building could be studied, and occupant thermal comfort and control could be simulated. On the building scale, the behavior of the occupant has an important impact on the model outputs, so the interplay between occupancy and modeling was studied in the context of a larger, commercial building. The uncertainty introduced by scheduling occupancy patterns was studied and a framework for using BEM to educate occupants on energy efficient behavior was developed. As diagramed in Figure 1, none of the research directions and improvements to model accuracy was a stand-alone issue. Modeling small scale phenomena and the behavior of occupants accurately is necessary for reliable model outputs. To save energy, it is necessary to both create efficient buildings and educate occupants to create efficient behaviors.

5.1.1 Discretized Zonal Modeling of a Roof Solar Chimney

The research began by modeling a passive solar technique which has proven problematic to accurately simulate. A new method for modeling a roof solar chimney was developed and verified using computational fluid dynamics and a numerical model. Three sources of uncertainty were explored and minimized. The treatment of convection from the RSC walls was calibrated using CFD, as was the air flow loss coefficient. The model discretization was explored, until convergence was reached at twelve segments. Finally, a sensitivity analysis quantified the uncertainty in model outputs attributed to the error in the treatment of convection.

Combining the methods of modeling showed that the proposed roof solar chimney design provides ventilation flow through most of the day, both due to the convection from the hot external surface and buoyant forces from inlet to outlet. The flow can be grouped into three modes of operation with similar characteristics: convection driven flow, nighttime free cooling driven solely by buoyancy, and mixed daytime flow. The flow rate is largest when free cooling occurs and the ambient temperature is less than the room temperature. This temperature difference is the parameter to which the RSC flow rate is most sensitive in all modes of operation. Over two sample days, the RSC operated in primarily convection driven flow for less than 18% of the time steps. In the convective flow mode, there is a high sensitivity to a number of other inputs, including solar insolation, thermal resistance of the roof, and the convection coefficient.

Comparing the results of the convection correlation in the BEM program to results calculated numerically with CFD, it is concluded that the natural convection correlation selected for the walls of the channel worked well for flow driven by natural convection, but poorly for other flow modes. However, there is little sensitivity to the uncertainty in the convection

coefficient in these modes. There is a difference of less than 3.5% in the mass flow rate and 3% in the surface temperature, but a much higher difference of up to 60% in the conduction heat transfer through the insulated surface of the chimney to the attic. The RSC can operate as a solar chimney with heat collected by the roof driving convection flow, but the magnitude of the flow is smaller and the flow is highly sensitive to several parameters as compared to operation as a channel for free cooling [81].

5.1.2 Control and Performance of a House Integrated Roof Solar Chimney

The scale of the model was then increased to consolidate the improvement in accuracy of RSC modeling to the whole building scale. The unique RSC configuration was modeled in the context of a home, for both high efficiency and standard constructions. This was the first annual simulation of a similar passive technique in the literature. The simulations were run for four climates to determine the performance in hot and cold parts of the United States. The ventilation configuration with a roof solar chimney and cross ventilation was compared to standard single sided ventilation and cross ventilation, for both standard efficiency and high efficiency building constructions. In addition, the modes of operation were compared, to determine if the RSC was operating as a true solar chimney or a path for buoyant flow.

The amount of heat removed by the solar chimney effect of the roof configuration was shown to be negligible, while effective free cooling and stack ventilation were predicted consistently. In the moderate climates, using cross ventilation and window control was more effective than adding insulation to the walls, using state of the art windows, reducing infiltration, and using high efficiency lighting and appliances combined. In a more extreme climate such as Phoenix, it is nearly as effective. Cooling load reductions with cross ventilation were from 23%

(Phoenix) to 64% (Pittsburgh), and ventilated roof savings from 49% to 92%. Incremental improvements in efficiency alone saved 35% in Pittsburgh to 30% in Phoenix. Using advanced natural ventilation significantly reduced the cooling load in the high efficiency home as well as in the base efficiency home. With the techniques combined, load reductions of over 70% are possible in all climates.

The effectiveness of the advanced natural ventilation strategies is enhanced by the high thermal mass construction of the house. All of the cases simulated were for high thermal mass constructions with ideal control. During the summer, over a third of US homes have centralized HVAC systems that run in air conditioning mode 24 hours a day [5]. These homes might especially benefit from a new, passive ventilation and control strategy [82].

5.1.3 Stochastic Methods for Occupancy Simulation

Just as a whole building model is required to estimate occupant comfort and energy consumption performance of a smaller model component, the representation of occupancy in that model should be well developed to obtain accurate results. Monte Carlo simulations were run to explore the effect of the representation of occupancy schedules on model outputs. Occupancy statistics were calculated from the sensed building automation system data. Then, the model runs with compiled diversity schedules were compared to runs with the actual data and three Monte Carlo sets of stochastic schedules.

It was shown that when calibrating a building model of a multipurpose green university building, having the actual gains and weather data corresponding to the calibration period helped validate calibration. However, this research showed that, for most purposes of predictive modeling, simply obtaining the mean gains levels and diversity schedules will be sufficient.

There was a several percent difference in hourly calibration CVRMSE by using the actual data. The impact on long-term energy consumption was not significantly affected by variations in the gains data. This is the more important output when evaluating energy conservation measures, but for controls optimization, a close calibration to operations profiles is important. It was even more important to use the corresponding weather data to the specific time period that was modeled. The variations between weather years caused significant long-term variation in energy consumption, and verification of hourly calibration would have been very difficult without the actual weather data [83].

5.1.4 Real-Time Prediction of Energy Savings

After exploring how to accurately capture random occupancy trends in a building model, a study was completed with the complementary objective of using building modeling to improve the energy efficiency of occupant behaviors. A framework for the real-time analysis and display of green behaviors and operation scenarios on a mobile dashboard was proposed. The method, based on neural networks trained with model data, can be applied to a mobile application and does not require co-simulation. It does, however, neglect the dynamic interactions between building systems. The energy use and savings can be displayed to the dashboard user as consumption or savings in net energy or by end use. The 20 node triple layer feedforward backpropagation neural network was shown to have less than 6% bias error for all scenarios and end uses. The CVRMSE ranged from 5% to 40%, depending on the scenario. The uncertainty intervals were demonstrated to be tight enough to allow the use of the data for demonstrative and educational purposes. This framework expands the capability of a building dashboard beyond

displaying sensed and historical data to informing the occupant of the quantitative energy savings or cost of individual, everyday decisions.

5.2 FUTURE WORK

The future work should continue to improve model accuracy, starting at the small scale and with a focus on occupant comfort and behavior. The RSC work can be improved experimental work on a RSC segment. The resulting improvement can be studied with co-simulation of a whole building. Then, the impact of occupancy at this level should be represented even more accurately. Finally, the framework developed in this work should be implemented to the MCSI dashboard to help the occupant understand the impact of their behavior. This research direction is a cohesive thrust towards improving modeling accuracy from the small scale modeling of physical phenomena upward. The behavior of air flows and natural convection should be studied with as much detail as the behavior of occupants, and the work should be consolidated with the application of the results to a dashboard for occupant education.

Small-scale uncertainty exists with regard to the flow patterns and CFD calculations. Future work should include experiments to validate the CFD and BEM. At the small scale, this could be in the form of a roof section with highly controlled boundary conditions, and corresponding model. Increasing in scale, it could also be done by applying the technique to a test house and measuring performance over a test period. The same time period and corresponding weather data would then be simulated to confirm the model accuracy.

To better implement these developments in experimental work and make comparisons, efforts should enhance the simulation of the entire home. This can be achieved by co-simulation,

linking computational fluid dynamics and zonal building energy modeling directly. For each timestep, the convective heat transfer coefficient should be calculated directly via CFD from the space temperatures and flow rates. Optimally, the two programs would iterate between each other until the flow rate and wall temperatures converge, because they are each dependent on the heat transfer coefficient. The problem with this approach is the computational intensity of any simulation of significant length. MLE+ and a Matlab script that calls ANSYS Fluent from the command line could be used to implement this simulation strategy.

A building scale model also requires accurate input on occupancy to have reliable model outputs. When developing occupancy schedules for the MCSI model, the method used to calculate occupancy levels was subject to error because it was based solely on the carbon dioxide levels. The method is sensitive to error in the CO_2 concentration and flow rates. It assumes perfect pollutant mixing in the space and neglects the dynamic aspects of changing concentrations. To improve the study of building occupancy and its representation in building modeling, more accurate methods could be used. These could include occupancy sensors, manual counts, or devices worn by occupants to record their locations. Using extensive sensors is expensive and still subject to error because sensors typically can't distinguish between multiple occupants. Manual counts are intrusive and time intensive, but might be effective to validate another method. Electronic monitoring devices, which could be cell phone applications, that record location may be seen as an invasion of privacy but could be anonymized. The data gained by one of these advanced occupancy counts would make for more accurate assessments of the statistical properties of occupancy patterns.

Developments can also be made in how occupancy and gains patterns are represented in building energy modeling programs, so the random properties of occupancy are included in all

simulations. Rather than using diversity schedules, input parameters for variance could be used to create stochastic schedules automatically. In addition, with more information on specific occupants and spaces, agent-based modeling could be built into BEM programs. The preliminary work in this study should be implemented in BEM tools to provide a range of model outputs depending on the uncertain occupancy and gains parameters, rather than a single output that could be misleading.

Key to tying together the research on improving the accuracy of the representation of occupancy and the work on educating occupants regarding their behavior is the implementation of the dashboard's connection to real-time data so that the algorithms and user interface can be tested by occupants. There is work ongoing on this part of the project. When the dashboard has been made available to occupants, researchers can seek feedback on the user interface. It is important to make sure it is understandable and manageable for the user. Measurements of the interval of usage would also be informative, as well as the frequency of usage of each feature and scenario. A combination of surveys and records of dashboard usage would make an important contribution to understanding how occupants like to view data and how to improve their level of effort towards green behaviors.

APPENDIX A

STOCHASTIC DIVERSITY SCHEDULES WITH POPULATION MEAN UNCERTAINTY

```
function [ X ] = stdivsch( schedHr,schedules2,avg,stdev,cor,j1,j2,linenum,fle )
% Copies mcsi.idf to mcis_i.idf with stochastic diversity schedules
% schedHr: sensed data for 8760 hours
% schedules2: diversity schedules
% avg: average levels/location factor for each day type
% stdev: standard deviation/scaling factor of daily levels for each day type
% cor: correlation matrices for each day type
% j1, j2: start and stop number (ie 1 to 30 for 30 random schedules)
% linenum: idf line at which to insert schedules
% fle: idf file name

for a = j1:1:j2

   %create 'mult' correlated random multipliers for diversity schedules (6x12)
   mult = zeros(6,12);
   for i = 1:1:6
         u = normrnd(0,1,1,12);
         u1 = u*chol(cor(:,:,i));%correlated random variables
      for j = 1:1:12
         mult(i,j)=max(0,1+u1(j)*stdev(i,j)/avg(i,j));%multiplier
      end
   end

   A=zeros(8760,18);

   % create 'A' Matrix - hourly levels
   for i = 1:1:8760
      d = schedHr(i,21);
      A(i,1:5) = schedHr(i,1:5);
      A(i,7:12)=schedules2(schedHr(i,4),1:6,d).*exp(mult(d,1:6));%occupancy schedules
```

```
   A(i,13:18)=schedules2(schedHr(i,4),7:12,d).*mult(d,7:12);%gains schedules
end

% create new file
data = textread([fle '.idf'],'%s','delimiter','\n');
nm = [fle '_div_' int2str(a) '.idf'];
f = fopen(nm,'wt');
fprintf(f,'%s\n',data{1:linenum}); % Write first 'line' lines

%write diversity schedules
for n = 1:1:12
   switch n
      case 1
         name = 'Wetlab Occ people/10m2';
         id = '10008';
      case 2
         name = 'Tower Occ people/10m2';
         id = '10009';
      case 3
         name = 'DryLab Occ people/10m2';
         id = '10011';
      case 4
         name = '2 Conf people/10m2';
         id = '10012';
      case 5
         name = 'Open Office people/10m2';
         id = '10013';
      case 6
         name = '3 Conf people/10m2';
         id = '10015';
      case 7
         name = 'Wing Electric w/m2';
         id = '10002';
      case 8
         name = 'Tower Electric w/m2';
         id = '10005';
      case 9
         name = 'Fume hoods electric w/m2';
         id = '10007';
      case 10
         name = 'idf w/m2';
         id = '10003';
      case 11
         name = 'wing light w/m2';
         id = '10004';
      case 12
```

```
            name = 'tower light w/m2';
            id = '10006';
        end
            fprintf(f,'\n!Schedule: %s\n',name);
            fprintf(f,'Schedule:Compact,\n');
            fprintf(f,'    %s,\n',id);
            fprintf(f,'    Any Number,\n');
        for i = 1:24:8760
            fprintf(f,'    Through: %02i/%02i,\n',A(i,2),A(i,3));
            fprintf(f,'    For: AllDays,\n');
            for j = 0:1:23
                fprintf(f,'    Until: %02i:00,\n',A(i+j,4));
                fprintf(f,'    %f',A(i+j,n+6));
                if i+j==8760
                    fprintf(f,';\n');
                else
                    fprintf(f,',\n');
                end
            end
        end
    end
    fprintf(f,'\n%s\n',data{linenum+1:end}); % Write remaining lines
    fclose(f);
end
X=1;
end
```

APPENDIX B

STOCHASTIC DIVERSITY SCHEDULES WITH POPULATION VARIANCE

```
function [ X ] = stdivsch_var( schedHr,schedules2,loc,scl,cor,j1,j2,linenum,fle )
% Copies mcsi.idf to mcis_i.idf with stochastic diversity schedules with
% population variance
% schedHr: sensed data for 8760 hours
% schedules2: diversity schedules
% loc: average levels/location factor for each day type
% scl: standard deviation/scaling factor of daily levels for each day type
% cor: correlation matrices for each day type
% j1, j2: start and stop number (ie 1 to 30 for 30 random schedules)
% linenum: idf line at which to insert schedules
% fle: idf file name

for a = j1:1:j2
   A=zeros(8760,18);
   % create 'A' Matrix - hourly levels

      %create 'mult' correlated random multipliers for diversity schedules (6x12)
      mult = zeros(6,12);
      for k = 1:1:6
            u = normrnd(0,1,1,12);
            u1 = u*chol(cor(:,:,k));%correlated random variables
         for j = 1:1:12
            mult(k,j)=max(0,1+u1(j)*scl(k,j)/loc(k,j));%random multiplier
         end
      end

      for i = 1:1:8760
         d = schedHr(i,21);
         A(i,1:5) = schedHr(i,1:5);
         A(i,7:12)=schedules2(schedHr(i,4),1:6,d).*exp(mult(d,1:6));%occupancy schedules
```

```
   A(i,13:18)=schedules2(schedHr(i,4),7:12,d).*mult(d,7:12);%gains schedules
end

% create new file
data = textread([fle '.idf'],'%s','delimiter','\n');
nm = [fle '_stdivvar_' int2str(a) '.idf'];
f = fopen(nm,'wt');
fprintf(f,'%s\n',data{1:linenum}); % Write first 'line' lines

%write diversity schedules
for n = 1:1:12
   switch n
      case 1
         name = 'Wetlab Occ people/10m2';
         id = '10008';
      case 2
         name = 'Tower Occ people/10m2';
         id = '10009';
      case 3
         name = 'DryLab Occ people/10m2';
         id = '10011';
      case 4
         name = '2 Conf people/10m2';
         id = '10012';
      case 5
         name = 'Open Office people/10m2';
         id = '10013';
      case 6
         name = '3 Conf people/10m2';
         id = '10015';
      case 7
         name = 'Wing Electric w/m2';
         id = '10002';
      case 8
         name = 'Tower Electric w/m2';
         id = '10005';
      case 9
         name = 'Fume hoods electric w/m2';
         id = '10007';
      case 10
         name = 'idf w/m2';
         id = '10003';
      case 11
         name = 'wing light w/m2';
         id = '10004';
      case 12
```

```
                name = 'tower light w/m2';
                id = '10006';
            end
                fprintf(f,'\n!Schedule: %s\n',name);
                fprintf(f,'Schedule:Compact,\n');
                fprintf(f,'    %s,\n',id);
                fprintf(f,'    Any Number,\n');
            for i = 1:24:8760
                fprintf(f,'    Through: %02i/%02i,\n',A(i,2),A(i,3));
                fprintf(f,'    For: AllDays,\n');
                for j = 0:1:23
                    fprintf(f,'    Until: %02i:00,\n',A(i+j,4));
                    fprintf(f,'    %f',A(i+j,n+6));
                    if i+j==8760
                        fprintf(f,';\n');
                    else
                        fprintf(f,',\n');
                    end
                end
            end
        end
        fprintf(f,'\n%s\n',data{linenum+1:end}); % Write remaining lines
        fclose(f);
    end
    X=1;
end
```

APPENDIX C

STOCHASTIC DAILY SCHEDULES

```
function [ X ] = stdaysch8( schedHr,schedules2,loc,scl,cor,j1,j2,linenum ,fle)
% Copies mcsi.idf to mcis_i.idf with stochastic diversity schedules
% different for each day
% schedHr: sensed data for 8760 hours
% schedules2: diversity schedules
% loc: average levels/location factor for each day type
% scl: standard deviation/scaling factor of daily levels for each day type
% cor: correlation matrices for each day type
% j1, j2: start and stop number (ie 1 to 30 for 30 random schedules)
% linenum: idf line at which to insert schedules
% fle: idf file name

for a = j1:1:j2
   A=zeros(8760,18);
   % create 'A' Matrix - hourly levels
   for i = 1:1:8760

      %create 'mult' correlated random multipliers for diversity schedules (6x12)
      mult = zeros(6,12);
      for k = 1:1:6
            u = normrnd(0,1,1,12);
            u1 = u*chol(cor(:,:,k));%correlated random variables
         for j = 1:1:12
            mult(k,j)=max(0,1+u1(j)*scl(k,j)/loc(k,j));%daily multiplier
         end
      end

      d = schedHr(i,21);
      A(i,1:5) = schedHr(i,1:5);
      A(i,7:12)=schedules2(schedHr(i,4),1:6,d).*exp(mult(d,1:6));%occupancy schedules
```

```
    A(i,13:18)=schedules2(schedHr(i,4),7:12,d).*mult(d,7:12);%gains schedules
end

for n = 1:1:12
    switch n
        case 1
            name = 'Wetlab Occ people/10m2';
            id = '10008';
        case 2
            name = 'Tower Occ people/10m2';
            id = '10009';
        case 3
            name = 'DryLab Occ people/10m2';
            id = '10011';
        case 4
            name = '2 Conf people/10m2';
            id = '10012';
        case 5
            name = 'Open Office people/10m2';
            id = '10013';
        case 6
            name = '3 Conf people/10m2';
            id = '10015';
        case 7
            name = 'Wing Electric w/m2';
            id = '10002';
        case 8
            name = 'Tower Electric w/m2';
            id = '10005';
        case 9
            name = 'Fume hoods electric w/m2';
            id = '10007';
        case 10
            name = 'idf w/m2';
            id = '10003';
        case 11
            name = 'wing light w/m2';
            id = '10004';
        case 12
            name = 'tower light w/m2';
            id = '10006';
    end

    % create new file
    nm = [id '_' fle '.csv'];
    f = fopen(nm,'wt');
```

```
        %write diversity schedules (CSV)
        for i = 1:24:8760
            for j = 0:1:23
                fprintf(f,'    %f,\n',A(i+j,n+6));
            end
        end
    end
    fclose(f);
end
X=1;
end
```

APPENDIX D

RANDOM DAILY SCHEDULES

```
function [ X ] = rnddaysch8( schedHr,hrlist,j1,j2)
% Copies mcsi.idf to mcis_i.idf with schedules randomly selected from
% sensed data days with the same day type and complete data
% schedHr: sensed data for 8760 hours
% hrlist: list of complete days of data (schedHr without incomplete data
% days)
% j1, j2: start and stop number (ie 1 to 30 for 30 random schedules)

rand('twister',.5);

% Copies mcsi.idf to mcis_i.idf with deterministic diversity schedules inserted in row 'line'
l = hrlist(1,1,:);
for a = j1:1:j2
   A=zeros(8760,18);
   % create 'A' Matrix - hourly levels
   for i = 1:1:365

      %create 'mult' correlated random multipliers for diversity schedules (6x12)
      d = schedHr(1+(i-1)*24,21);%day type
      rint = randi([1 l(d)]);
      for k = 1:1:24
         A((i-1)*24+k,1:5) = schedHr((i-1)*24+k,1:5);
         A((i-1)*24+k,7:12)=max(0,hrlist(1+(rint-1)*24+k,7:12,d));
         A((i-1)*24+k,13:18)=max(0,hrlist(1+(rint-1)*24+k,13:18,d));
      end
   end

   for n = 1:1:12
      switch n
         case 1
```

```
        name = 'Wetlab Occ people/10m2';
        id = '10008';
    case 2
        name = 'Tower Occ people/10m2';
        id = '10009';
    case 3
        name = 'DryLab Occ people/10m2';
        id = '10011';
    case 4
        name = '2 Conf people/10m2';
        id = '10012';
    case 5
        name = 'Open Office people/10m2';
        id = '10013';
    case 6
        name = '3 Conf people/10m2';
        id = '10015';
    case 7
        name = 'Wing Electric w/m2';
        id = '10002';
    case 8
        name = 'Tower Electric w/m2';
        id = '10005';
    case 9
        name = 'Fume hoods electric w/m2';
        id = '10007';
    case 10
        name = 'idf w/m2';
        id = '10003';
    case 11
        name = 'wing light w/m2';
        id = '10004';
    case 12
        name = 'tower light w/m2';
        id = '10006';
end

% create new file
nm = [id '_' int2str(a) '.csv'];
f = fopen(nm,'wt');
%write diversity schedules (CSV)
for i = 1:24:8760
    for j = 0:1:23
        fprintf(f,'    %f,\n',A(i+j,n+6));
    end
end
```

```
    end
    fclose(f);
end
X=1;
end
```

BIBLIOGRAPHY

1. *Table 2.1a Energy Consumption Estimates by Sector, Selected Years, 1949-2010,* in *Annual Energy Review, 2010*2010, U.S. Energy Information Administration.

2. *Table 1.3 Primary Energy Consumption Estimates by Source, Selected Years, 1949-2010,* in *Annual Energy Review 2010*2010, U.S. Energy Information Administration.

3. US Census Bureau, *New Residential Construction: New Privately Owned Housing Units Completed in the United States, by Intent and Design*, 2009, US Census Bureau.

4. US Energy Information Administration, *Annual Energy Review*, 2009, U.S. Department of Energy.

5. U.S. Energy Information Administration, *Residential Energy Consumption Survey*, 2011, Department of Energy: Washington, DC.

6. Ryan, E.M. and T.F. Sanquist, *Validation of building energy modeling tools under idealized and realistic conditions.* Energy and Buildings, 2012. **47**(0): p. 375-382.

7. Reddy, A., *Literature review on calibration of building energy simulation programs : Uses, problems, procedures, uncertainty, and tools*. Vol. 112. 2006, New York, NY, ETATS-UNIS: American Society of Heating, Refrigerating and Air-conditioning Engineers. XXXVI-780 ; 816 p.

8. Crawley, D.B., et al. *EnergyPlus, A New-Generation Building Energy Simulation Program*. in *Renewable and Advanced Energy Systems for the 21st Century*. 1999. Lahaina, Maui, Hawaii.

9. Strachan, P.A., G. Kokogiannakis, and I.A. Macdonald, *History and development of validation with the ESP-r simulation program.* Building and Environment, 2008. **43**(4): p. 601-609.

10. Clarke, J. and J.L.M. Hansen, *An Approach to the Simulation of Coupled Heat and Mass Flows in Buildings.* Int. J. Indoor Air Quality and Climate, 1991. **1**: p. 283-96.

11. Beausoleil-Morrison, I., *The Adaptive Coupling of Heat and Air Flow Modelling within Dynamic Whole-Building Simulation*, in *Department of Mechanical Engineering*2000, University of Strathelyde: Glaskow UK.

12. *EnergyPlus Engineering Reference*, EnergyPlus, Editor 2010, Ernest Orlando Lawrence Berkeley National Laboratory.

13. Henninger, R.H. and M.J. Witte, *EnergyPlus Testing with AHSRAE 1052-RP Toolkit-Building Fabric Analytical Tests*, 2012, U.S. Department of Energy: Washington, D.C.

14. Henninger, R.H. and M.J. Witte, *EnergyPlus Testing with Building Thermal Envelope and Fabric Load Tests from ANSI/ASHRAE Standard 140-2011*, 2012, U.S. Department of Energy: Washington D.C.

15. Bertagnolio, S. and V. Lemort, *Simulation assisted audit & Evidence based calibrated methodology.* 2012.

16. *Design Building Made Easy*. DesignBuilder 2012 [cited 2012 8/13/12]; Available from: http://www.designbuilderusa.com.

17. Bernal, W., et al., *MLE+: A Tool for Integrated Design and Deployment of Energy Efficient Building Controls*, in *4th ACM Workshop On Embedded Sensing Systems for Energy-Efficiency in Buildings*2012: Toronto, Canada.

18. Meyers, S., et al., *Impacts of US federal energy efficiency standards for residential appliances.* Energy, 2003. **28**(8): p. 755-767.

19. Mills, B. and J. Schleich, *Residential energy-efficient technology adoption, energy conservation, knowledge, and attitudes: An analysis of European countries.* Energy Policy, 2012. **49**(0): p. 616-628.

20. Audah, N., N. Ghaddar, and K. Ghali, *Optimized solar-powered liquid desiccant system to supply building fresh water and cooling needs.* Applied Energy, 2011. **88**(11): p. 3726-3736.

21. Buonomano, A., F. Calise, and A. Palombo, *Solar heating and cooling systems by CPVT and ET solar collectors: A novel transient simulation model.* Applied Energy, 2013. **103**(0): p. 588-606.

22. Khanal, R. and C. Lei, *Solar chimney,ÄîA passive strategy for natural ventilation.* Energy and Buildings, 2011. **43**(8): p. 1811-1819.

23. Aboulnaga, M.M., *A roof solar chimney assisted by cooling cavity for natural ventilation in buildings in hot arid climates: An energy conservation approach in Al-Ain city.* Renewable Energy, 1998. **14**(1-4): p. 357-363.

24. Santamouris, M., A. Sfakianaki, and K. Pavlou, *On the efficiency of night ventilation techniques applied to residential buildings.* Energy and Buildings, 2010. **42**(8): p. 1309-1313.

25. Brecha, R.J., et al., *Prioritizing investment in residential energy efficiency and renewable energy‚ÄîA case study for the U.S. Midwest.* Energy Policy, 2011. **39**(5): p. 2982-2992.

26. Sadineni, S.B., T.M. France, and R.F. Boehm, *Economic feasibility of energy efficiency measures in residential buildings.* Renewable Energy, 2011. **36**(11): p. 2925-2931.

27. Beerepoot, M. and N. Beerepoot, *Government regulation as an impetus for innovation: Evidence from energy performance regulation in the Dutch residential building sector.* Energy Policy, 2007. **35**(10): p. 4812-4825.

28. Fong, K.F. and C.K. Lee, *Towards net zero energy design for low-rise residential buildings in subtropical Hong Kong.* Applied Energy, 2012. **93**(0): p. 686-694.

29. Munari Probst, M. and C. Roecker, *Towards an improved architectural quality of building integrated solar thermal systems (BIST).* Solar Energy, 2007. **81**(9): p. 1104-1116.

30. Brinkworth, B.J., *Estimation of flow and heat transfer for the design of PV cooling ducts.* Solar Energy, 2000. **69**(5): p. 413-420.

31. Hirunlabh, J., et al., *New configurations of a roof solar collector maximizing natural ventilation.* Building and Environment, 2001. **36**(3): p. 383-391.

32. Biwole, P.H., M. Woloszyn, and C. Pompeo, *Heat transfers in a double-skin roof ventilated by natural convection in summer time.* Energy and Buildings, 2008. **40**(8): p. 1487-1497.

33. Costa, A., et al., *Key factors methodology‚ÄîA novel support to the decision making process of the building energy manager in defining optimal operation strategies.* Energy and Buildings, 2012. **49**(0): p. 158-163.

34. de Wilde, P., W. Tian, and G. Augenbroe, *Longitudinal prediction of the operational energy use of buildings.* Building and Environment, 2011. **46**(8): p. 1670-1680.

35. Hoes, P., et al., *User behavior in whole building simulation.* Energy and Buildings, 2009. **41**(3): p. 295-302.

36. Wang, L., P. Mathew, and X. Pang, *Uncertainties in Energy Consumption Introduced by Building Operations and Weather for a Medium-Size Office Building.* Energy and Buildings, 2012(0).

37. Kwok, S.S.K. and E.W.M. Lee, *A study of the importance of occupancy to building cooling load in prediction by intelligent approach.* Energy Conversion and Management, 2011. **52**(7): p. 2555-2564.

38. Kwok, S.S.K., R.K.K. Yuen, and E.W.M. Lee, *An intelligent approach to assessing the effect of building occupancy on building cooling load prediction.* Building and Environment, 2011. **46**(8): p. 1681-1690.

39. May-Ostendorp, P., et al., *Model-predictive control of mixed-mode buildings with rule extraction.* Building and Environment, 2011. **46**(2): p. 428-437.

40. Oldewurtel, F., et al., *Use of model predictive control and weather forecasts for energy efficient building climate control.* Energy and Buildings, 2012. **45**(0): p. 15-27.

41. Platt, G., et al., *Adaptive HVAC zone modeling for sustainable buildings.* Energy and Buildings, 2010. **42**(4): p. 412-421.

42. Goyal, S. and P. Barooah, *A method for model-reduction of non-linear thermal dynamics of multi-zone buildings.* Energy and Buildings, 2012. **47**(0): p. 332-340.

43. Kumar, R., R.K. Aggarwal, and J.D. Sharma, *Energy analysis of a building using artificial neural network: A review.* Energy and Buildings, 2013. **65**(0): p. 352-358.

44. Boithias, F., M. Mankibi, and P. Michel, *Genetic algorithms based optimization of artificial neural network architecture for buildings‚Äì indoor discomfort and energy consumption prediction.* Building Simulation, 2012. **5**(2): p. 95-106.

45. Ferreira, P.M., et al., *Neural networks based predictive control for thermal comfort and energy savings in public buildings.* Energy and Buildings, 2012. **55**(0): p. 238-251.

46. Leung, M.C., et al., *The use of occupancy space electrical power demand in building cooling load prediction.* Energy and Buildings, 2012. **55**(0): p. 151-163.

47. Fonseca, R.W.d., E.L. Didoné, and F.O.R. Pereira, *Using artificial neural networks to predict the impact of daylighting on building final electric energy requirements.* Energy and Buildings, 2013. **61**(0): p. 31-38.

48. Mathur, J., S. Mathur, and Anupma, *Summer-performance of inclined roof solar chimney for natural ventilation.* Energy and Buildings, 2006. **38**(10): p. 1156-1163.

49. Lai, C.-m., J.Y. Huang, and J.S. Chiou, *Optimal spacing for double-skin roofs.* Building and Environment, 2008. **43**(10): p. 1749-1754.

50. Susanti, L., et al., *A laboratory experiment on natural ventilation through a roof cavity for reduction of solar heat gain.* Energy and Buildings, 2008. **40**(12): p. 2196-2206.

51. Wei, D., Y. Qirong, and Z. Jincui, *A study of the ventilation performance of a series of connected solar chimneys integrated with building.* Renewable Energy, 2011. **36**(1): p. 265-271.

52. Maerefat, M. and A.P. Haghighi, *Passive cooling of buildings by using integrated earth to air heat exchanger and solar chimney.* Renewable Energy, 2010. **35**(10): p. 2316-2324.

53. Maerefat, M. and A.P. Haghighi, *Natural cooling of stand-alone houses using solar chimney and evaporative cooling cavity.* Renewable Energy, 2010. **35**(9): p. 2040-2052.

54. Walton, G.N., *Thermal Analysis Research Program Reference Manual*, 1983, National Bureau of Standards.

55. Ansys, I., *Ansys Fluent 12 User's Guide*, 2009.

56. Cable, M., *An Evaluation of Turbulence Models for the Numerical Study of Forced and Natural Convetive Flow in Atria*, in *Mechanical and Materials Engineering*2009, Queen's University: Kingston, Ontario, Canada.

57. Gharbi, N.E., et al. *Effect of near-wall treatments on airflow simulations*. in *International Conference on Computational Methods for Energy Engineering and Environment*. 2009. Sousse, Tunisia.

58. Baharvand, E., *How to model a wall solar chimney?*, in *Department of Architecture*2010, Eindhoven University of Technology. p. 120.

59. Jiru, T.E. and F. Haghighat, *Modeling ventilated double skin faÁade--A zonal approach.* Energy and Buildings, 2008. **40**(8): p. 1567-1576.

60. Bar-Cohen, A. and W.M. Rohsenhow, *Thermally Optimum Spacing of Vertical Natural Convection Cooled Parallel Plates.* Journal of Heat Transfer, 1984. **106**(1984).

61. Stavrakakis, G.M., et al., *Natural cross-ventilation in buildings: Building-scale experiments, numerical simulation and thermal comfort evaluation.* Energy and Buildings, 2008. **40**(9): p. 1666-1681.

62. Awbi, H.B., *Air movement in naturally-ventilated buildings.* Renewable Energy, 1996. **8**(1,Äì4): p. 241-247.

63. Zhai, Z., M.-H. Johnson, and M. Krarti, *Assessment of natural and hybrid ventilation models in whole-building energy simulations.* Energy and Buildings, 2011. **43**(9): p. 2251-2261.

64. Jiang, Y., et al., *Natural ventilation in buildings: measurement in a wind tunnel and numerical simulation with large-eddy simulation.* Journal of Wind Engineering and Industrial Aerodynamics, 2003. **91**(3): p. 331-353.

65. Chan, H.Y., S.B. Riffat, and J. Zhu, *Review of passive solar heating and cooling technologies.* Renewable & Sustainable Energy Reviews, 2010. **14**(2): p. 781-789.

66. Susanti, L., H. Homma, and H. Matsumoto, *A naturally ventilated cavity roof as potential benefits for improving thermal environment and cooling load of a factory building.* Energy and Buildings, 2011. **43**(1): p. 211-218.

67. Hendron, R. and C. Engebrecht, *Building America House Simulation Protocols*, 2010, National Renewable Energy Laboratory: Oak Ridge, TN.

68. *2009 International Energy Conservation Code*, 2009, International Code Council: Country Club Hills, IL. p. 97.

69. American Society of Heating Refrigeration and Air Conditioning Engineers, *Standard 55-2010: Thermal Environmental Conditions for Human Occupancy*, 2010.

70. Haberl, J.S. and T.E. Bou-Saada, *Procedures for calibrating hourly simulation models to measured building energy and environmental data*. 1998, New York, NY, ETATS-UNIS: American Society of Mechanical Engineers. 82.

71. ASHRAE, *Measurement of Energy and Demand Savings*, in *ASHRAE Guideline 14-2002*2002.

72. Raftery, P., M. Keane, and A. Costa, *Calibrating whole building energy models: Detailed case study using hourly measured data.* Energy and Buildings, 2011. **43**(12): p. 3666-3679.

73. Collinge, W.O., et al., *Measuring Whole-Building Performance with Dynamic LCA: A Case Study of a Green University Building*, in *International Symposium on Life Cycle Assessment and Construction*2012: Nantes, France.

74. Dong, B., et al., *An information technology enabled sustainability test-bed (ITEST) for occupancy detection through an environmental sensing network.* Energy and Buildings, 2010. **42**(7): p. 1038-1046.

75. Jain, R.K., J.E. Taylor, and G. Peschiera, *Assessing eco-feedback interface usage and design to drive energy efficiency in buildings.* Energy and Buildings, 2012. **48**(0): p. 8-17.

76. Krishnamurti, T., et al., *Creating an in-home display: Experimental evidence and guidelines for design.* Applied Energy, 2013. **108**(0): p. 448-458.

77. Alahmad, M., et al., *Integrating physical and virtual environments to conserve energy in buildings.* Energy and Buildings, 2011. **43**(12): p. 3710-3717.

78. Martinez, K., K.A. Donnelly, and J.A. Laitner, *Advanced Metering Initiatives and Residential Feedback Programs: A Meta-Review of Household Electricity-Saving Opportunities,* 2010, American Council for an Energy-Efficient Economy.

79. Collinge, W.O., *A dynamic life cycle assessment framework for whole buildings including indoor environmental quality impacts,* 2013, University of Pittsburgh: Ann Arbor. p. 192.

80. Levenberg, K., *A Method for the Solution of Certain Non-Linear Problems in Least Squares.* Quarterly of Applied Mathematics, 1944. **2**: p. 164-168.

81. DeBlois, J.C., M.M. Bilec, and L.A. Schaefer, *Design and zonal building energy modeling of a roof integrated solar chimney.* Renewable Energy, 2013. **52**(0): p. 241-250.

82. DeBlois, J., M. Bilec, and L. Schaefer, *Simulating home cooling load reductions for a novel opaque roof solar chimney configuration.* Applied Energy, 2013. **112**(0): p. 142-151.

83. DeBlois, J., et al., *Modeling a Multi-Purpose Public Building with Stochastic Gains and Occupancy Schedules*, in *ASHRAE Winter Conference*2014: New York City.